ON THE DESIGN OF ENERGY STORAGE SYSTEMS FOR THE SMOOTHING AND DISPATCH PLANNING OF LARGE-SCALE WIND POWER GENERATION

LI MENGTING

School of Electrical and Electronic Engineering

A thesis submitted to the Nanyang Technological University
in partial fulfillment of the requirement for the degree of
Doctor of Philosophy

2016

Acknowledgements

My greatest thanks go to my supervisors, Professor Choi San Shing, Associate Professor Tseng King Jet and Assistant Professor Zhao Jiyun, for their constant guidance and encouragements. Their dedication to scientific research would continue inspiring me in my future career. What I learnt from them is not only in the academic aspect, their value of life, ways of thinking and behaving has greatly influenced me. My future career and life would benefit from their suggestions and advices on me.

I greatly appreciate Dr Yao Dailin for her support, cooperation and suggestions on my research. I also would like to thank Dr Wee Kok Woei, Dr Li Yang, Dr Nima SAADAT, Dr Wu Si, Dr Xian Liang, Dr Wei Feng, Dr Hu Xiaolei, Dr Li Song and Dr Sun Chengchen for their valuable suggestions and help. I also thank all my good friends for their friendship, understanding and encouragement.

Research scholarship granted by Nanyang Technological University is sincerely appreciated.

I wish to thank the staff in the electric power research laboratory, namely Mr Lim Kim Peow and Madam NG-TAN Siew Hong, Jennifer, for their concern and kind assistance. I also thank Madam CHEW-SIM Annie for all her help during my PhD study.

Lastly, my great thanks go to my grandma, my parents and my husband, Mr Zhang Weiwei, for their everlasting love and support.

Table of Contents

Summary

The demand on energy supply increases continuously as economies develop and world population grows. Most of the energy in the world comes from the fossil fuels and the increase in energy demand accelerates the rate of depleting the fossil fuel resources. As fossil fuel is finite and also due to the environmental considerations, renewable energy (RE) resources have been actively developed as the alternative sources for electricity generation. Renewable sources used for large-scale electricity production can include wind, photovoltaic (PV), waves and so on. Among all the RE resources, wind power generation is witnessing rapid developments in recent years.

Unfortunately, wind tends to be unsteady. The fluctuating and uncertain output powers from wind farms can be problematic, especially if there is a high penetration level of the renewable source in a grid system. The fluctuations may lead to excessive voltage variations and unacceptable degree of frequency deviations. Moreover, the unsteady and uncertain input wind power can cause firm power dispatch commitment from wind farms a difficult task. Expensive generation reserves have to be provided for grid system to ensure adequate level of system security and reliability is guaranteed. In fact, power generation from wind farms has often been excluded in the dispatch planning of the grids. Unless other viable techniques can be found, the above issues can constitute major impediment to the successful large-scale integration of wind power generation into grid systems.

In this connection, the use of energy storage system (ESS) is one possible solution to mitigate the negative impacts of the unsteady wind power on electricity supply systems and to improve on the dispatchability of the wind power. In this investigation, in order to smoothen the fluctuations in the wind and to realize the dispatch planning of the wind power in a way similar to that of conventional generators, it is proposed that a three-level ESS is incorporated in a large-scale wind power generation scheme.

In essence, at cluster-level of wind turbine generators (WTG), the solution involves having the high- and mid-frequency components of the aggregated wind power routed to supercapacitors (SC) and battery banks respectively of a battery-supercapacitor hybrid energy storage system (BSHESS) by a high-pass filter (HPF) and a band-pass filter (BPF). It then results in the smoothening of the wind power harnessed by the cluster. In this thesis, the BSHESS control scheme to reduce the wind power perturbations has been shown. A statistical method is also developed to determine the capacities of the minimum-cost BSHESS to meet the power smoothing objective at pre-specified probability level. Application of the proposed design approach is demonstrated using data obtained from an existing wind farm.

As for dispatch planning, attention is to use a low-pass filter (LPF) to extract the low-frequency intrinsic mode and residue functions of wind power. The relatively slow-changing characteristics of the low-frequency wind power components, which contain most of the energy in the wind power, allow accurate forecasts of the power components to be obtained using artificial neural network (ANN). Dispatch planning of the wind power is then realized through buffering the low-frequency power fluctuations by a proposed power flows control strategy applied to a pumped hydroelectric storage (PHS) system. Focusing on low-frequency wind power for dispatch planning is a distinct advantage over the dispatch planning methods proposed by other researchers. Furthermore, a statistical method to determine the power and energy capacities of the PHS is included. The efficacy of the developed approach to dispatch planning is again illustrated based on data obtained from an existing wind farm.

In all the above works, suitable cut-off frequencies for the HPF, BPF and LPF are derived based on the developed concept of minimum overlap energy and the outcome of empirical mode decomposition (EMD) analysis. EMD method is used to gain insights into the frequency-time characteristics of wind power. In this manner, the wind power can then be grouped into high-, mid- and low-frequency bands.

List of Figures

List of Tables

List of Abbreviations

AA-CAES	Advanced Adiabatic CAES
AGC	Automatic Generation Control
AI	Artificial Intelligence
ANN	Artificial Neural Network
AR	Autoregressive
ARIMA	Autoregressive Integrated Moving Average
ARMA	Autoregressive Moving Average
BESS	Battery Energy Storage System
BKF	Basic Kalman Filter
BP	Back-propagation
BPF	Band-pass Filter
BSHESS	Battery-supercapacitor Hybrid Energy Storage System
CAES	Compressed Air Energy Storage System
CDF	Cumulative Distribution Function
CDF	Cumulative Density Function
DFIG	Doubly Fed Induction Generator
DoD	Depth of Discharge
EDLC	Electrochemical Double Layer Capacitor
EMA	Energy Market Authority
EMD	Empirical Mode Decomposition
EOF	Empirical Orthogonal Function
ESS	Energy Storage System
FIT	Feed-in-Tariff
HPF	High-pass Filter
IEA	International Energy Agency
IMF	Intrinsic Mode Function
IPCC	Intergovernmental Panel on Climate Change
LPF	Low-pass Filter

LVRT	Low-voltage-ride-through
MA	Moving Average
MPPT	Maximum Power Point Tracking
NWP	Numerical Weather Prediction
PCC	Point of Common Coupling
PCU	Power Conditioning Unit
PDF	Probability Density Function
PHS	Pumped Hydroelectric Storage
PMSG	Permanent Magnet Synchronous Generator
PSO	Particle Swarm Optimization
PV	Photovoltaic
PWM	Pulse Width Modulation
R&D	Research and Development
RE	Renewable Energy
RES	Renewable Electricity Standard
RPS	Renewable Portfolio Standard
RSC	Rotor Speed Control
SC	Supercapacitors
SMES	Superconducting Magnetic Energy Storage System
SOC	State of Charge
SVM	Support Vector Machines
TES	Thermal Energy Storage System
t.o.e	Tonne Oil Equivalents
T&D	Transmission-Distribution
UPS	Uninterruptible Power Supply
VSC	Voltage Source Converter
WTG	Wind Turbine Generators
WWEA	World Wind Energy Association

List of Symbols

a	Cost/MW of the BESS
b	Cost/MWh of the BESS
c	Cost/MW of the SC
C	Capacitance of SC
c_B	The capital cost of the BESS
c_i, $c_i(t)$	IMF
C_p	Turbine-rotor-power coefficient
C_{p_opt}	Optimum value of turbine-rotor-power coefficient
c_S	The capital cost of the SC
d	Cost/MWh of the SC
$d_{B,max}$	Maximum depth of discharge of BESS
$d_{P,max}$	Maximum depth of discharge of PHS
$d_{S,max}$	Maximum depth of discharge of SC
e	Scale factor of wind speed distribution
$e(t)$	The forecast error in $P_L(t)$
$E_{B,r}$	The rated energy capacity of the BESS
E_d	The energy equaled to the shaded area
E_i	Overlap energy
$E_{o\ min,\ i}$	Minimum overlap energy for the set $c_i(t)$ and $c_{i+1}(t)$
$E_{o\ min,\ j}$	Minimum overlap energy for the set $c_j(t)$ and $c_{j+1}(t)$
$E_{P,r}$	The rated energy capacity of the PHS
$E_{S,r}$	The rated energy capacity of the SC
$\overrightarrow{E_S}$	The source voltage of Thevenin equivalent of the upstream grid system

$F(P_w)$	Cumulative distribution function of P_w
$f(v_w)$	Probability density function of wind speed v_w
$F(v_w)$, $F(v_{w1})$, $F(v_{w2})$	Cumulative distribution function of wind speed v_w, v_{w1}, v_{w2}
f_{ac}, $f_{ac,i}(t)$	Cycle frequency
f_l	Lower cutoff frequency of BPF
$f_{l,Eo\ min,\ i}$	The lower cutoff frequency of BPF with minimum overlap energy for the set $c_i(t)$ and $c_{i+1}(t)$
$f_{l,Eo\ min,\ I}$	The lower cutoff frequency of BPF with minimum overlap energy
$f_{l,max}$	The upper bound on f_l
$f_{l,min}$	The lower bound on f_l
f_u	Upper cutoff frequency of BPF
$f_{u,Eo\ min,\ j}$	The upper cutoff frequency of BPF with minimum overlap energy for the set $c_j(t)$ and $c_{j+1}(t)$
$f_{u,Eo\ min,\ J}$	The upper cutoff frequency of BPF with minimum overlap energy
$f_{u,min}$	The lower bound on f_u
g, k, m, n, s	Number
H	The inertia constant
H'	Hidden variable set of a three-layer BP network
h_1, h_2,…, h_m	Hidden variables of a three-layer BP network
h_{1k}	The difference between the data set and the mean in the (k+1)th sifting process
$\overrightarrow{I_L}$	The current to the load
$\overrightarrow{I_s}$	The current from the upstream grid system
$\overrightarrow{I_w}$	Injected current from the wind farm
k	Shape factor of wind speed distribution

m_{1k}	The mean of the upper and lower envelops in the (k+1)th sifting process
p_1, p_2	Probabilities
p_B	The probability $P_{MF}(t)$ is within the BESS power capacities
$P_{B\ ref,\ i}(t)$	The reference signals for the PCU of the BESS in the BSHESS of the i^{th} WTG group
$P_{B,i}(t)$	The output powers of the BESS installed at the group level of the i^{th} WTG group
$p_{B,min}$	Minimum value of p_B
$P_{B,r}$	The rated power capacity of the BESS
$P^B_{c,max}$	Charging power capabilities of BESS
$P^B_{d,max}$	Discharging power capabilities of BESS
P_E	Active power from the energy storage system
$P_G(t)$	The net dispatched power from the n groups of the WTG-ESS to the grid system
$P_{G,ref}(t)$	The reference for the planning of the dispatch power flows $P_G(t)$
$P_{HF}(t)$	High-frequency component of $P_w(t)$
P_L	Active power of load
$P_L(t)$	Low-frequency components of wind power
$P_L^*(t)$	Forecast of $P_L(t)$
$P_{L,i}(t)$	The difference between the wind power and the BSHESS power of the i^{th} WTG group
$P_{MF}(t)$	Mid-frequency component of $P_w(t)$
p_P	The probability $\|P_P(t)\|$ is within the PHS power capacities
$P_P(t)$	The power flows to the PHS
$P_P^*(t)$	The estimated output power of the PHS
$P_{P,r}$	The rated power capacity of the PHS

P_R	The power stored in the rotating mass
p_S	The probability $P_{HF}(t)$ is within the SC power capacities
P_s	Active power from the upstream grid system
$P_{S\ ref,\ i}(t)$	The reference signals for the PCU of the SC in the BSHESS of the i^{th} WTG group
$P_{S,i}(t)$	The output powers of the SC installed at the group level of the i^{th} WTG group
$p_{S,min}$	Minimum value of p_S
$P_{S,r}$	The rated power capacity of the SC
$P^S_{c,max}$	Charging power capabilities of SC
$P^S_{d,max}$	Discharging power capabilities of SC
P_T	The power from the hydro/steam turbine
P_w	The active power harnessed by wind turbine
$P_w(t)$	Long-term historical wind power data
$P_{w,i}(t)$	Wind power output from the i^{th} WTG group
$P_{w,r}$	The wind turbine rated power
P_{w_opt}	Maximum wind power
Q_E	Reactive power from the energy storage system
Q_L	Reactive power of load
Q_s	Reactive power from the upstream grid system
Q_w	The reactive power harnessed by wind turbine
r	Radius of the wind turbine
r_n, $r_n(t)$	Residue function
$\overrightarrow{R_S}$	Source resistance of Thevenin equivalent of the upstream grid system
t	Time

$t_0, t_1, t_2, \ldots, t_6$	At time $t = t_0, t_1, t_2, \ldots, t_6$
T_s	A period of time
U	The voltage across the SC
$U_{S,max}$	Nominal voltage of the SC
$U_{S,min}$	Minimum voltage of the SC
V	Weight matrix connecting the input and hidden layers
$v_1, v_2, \ldots, v_n$	Weighting variables in weight matrix connecting the input and hidden layers
v_{in}	The cut-in wind speed
$\overrightarrow{V_L}$	Load voltage
V_L	Magnitude of load voltage
V_m	Average wind speed
v_{out}	The cut-off wind speed
$v_{w,r}$	The rated wind speed
$v_w, v_{w1}, v_{w2}, v_{wx}$	Wind speed
W	Weight matrix connecting the hidden and output layers
$w_1, w_2, \ldots, w_n$	Weighting variables in weight matrix connecting the hidden and output layers
X	Input variable set of a three-layer BP network
$\overrightarrow{X_s}$	Source reactance of Thevenin equivalent of the upstream grid system
$x(t)$	Original data set in the time domain
$x_1, x_2, \ldots, x_n$	Input variables of a three-layer BP network
Y	Output variable set of a three-layer BP network
$y_1, y_2, \ldots, y_l$	Output variables of a three-layer BP network
$\overrightarrow{Z_s}$	Source impedance of Thevenin equivalent of the upstream grid system

β	Pitch angle
ε	A small positive tolerance
η_c	The efficiency of the PHS charging process
η_d	The efficiency of the PHS discharging process
θ	Phase angle of load voltage
λ	Tip speed ratio
λ_{opt}	Optimum value of tip speed ratio
ρ	Air density
ω	Rotor speed of synchronous generator
ω_r	Rotational speed of wind turbine rotor
ω_{r_opt}	Optimal rotational speed of wind turbine rotor
$\Delta E_B(t)$	Change in the stored energy level in the BESS
$\Delta E_{B,max}$	Maximum value of $\Delta E_B(t)$
$\Delta E_{B,min}$	Minimum value of $\Delta E_B(t)$
$\Delta E_P(t)$	The change in the stored energy level in the PHS
$\Delta E_{P,max}$	Maximum value of $\Delta E_P(t)$
$\Delta E_{P,min}$	Minimum value of $\Delta E_P(t)$
$\Delta E_S(t)$	Change in the stored energy level in the SC
$\Delta E_{S,max}$	Maximum value of $\Delta E_S(t)$
$\Delta E_{S,min}$	Minimum value of $\Delta E_S(t)$
$\Delta E_i(t)$	Change in the energy level contained in $c_i(t)$ and $r_n(t)$
Δf	Frequency deviation
γ_{max}	Maximum allowable wind power ramp rate
ΔT	The dispatch bid interval

CHAPTER 1. Introduction

1.1 Background and Motivation

In the mid-eighteenth century, the industrial revolution began. The revolution was further promoted by the electrification and relevant technologies in the nineteenth and twentieth century [1]. Human life was completely changed. All of this cannot be achieved without an abundant and economical supply of energy. The demand on energy supply will continue to increase with the growth of the population, enhanced lifestyle and the development of economy and technology [2]. The International Energy Agency (IEA) declared that the world's energy demand will rise from 12 billion tonne oil equivalents (t.o.e) in 2009 to about 17.5 billion t.o.e by 2035 [3].

About 80% of the energy in the world is derived from the fossil fuels, such as oil, coal and natural gas. However, the fossil fuels are exhaustible, so the human race will face the problem of their depletion after one or two generations at the current rate of extraction. Besides, the burning of the fossil fuel has a harmful influence on the environment [4]. The first environmental problem is global warming which is the result from the carbon-dioxide emissions [5]. It is estimated that the carbon-dioxide emissions will increase from 29 gigatonnes per year (Gt yr^{-1}) to 43 Gt yr^{-1} under the current policies on fossil-fuel usage or to 36 Gt yr^{-1} under new policies: The new policies consider the commitment by the countries to decrease the emission of the gas that contributes to the greenhouse effect and plan the allowance for the fossil energy [1]. Other environmental problems include air contamination, acid rain, ozone depletion, deforestation, and emission of radioactive materials [2]. Furthermore, the

production cost of the fossil fuels will rise since more advanced technologies are needed to exploit these resources.

The energy crises and the environmental degradation are the two main impetus which drive the human race to look for and to develop renewable energy (RE) resources such as wind, solar, hydroelectric, geothermal, ocean, and biomass [6]. These sources are clean, practical, sustainable and environmental-friendly alternative sources compared to conventional energy sources. The integration of electric power generation from RE brings about advantages such as decreased use of the fossil-fuels and CO_2 emissions [7]. Each kind of RE has its own particular strengths as well [8]. RE which has strong potential is regarded as a significant source in many countries all over the world [9-16]. As a result, there has been a significant rise in the share of RE in some countries for the past two decades [17]. For instance, approximately 11% of the main electric power generation in the US is from RE. In China, RE shares 26% of installed gross generation capacity. Similarly, in Germany, about 11% of the energy consumption comes from RE [18]. The UN's Intergovernmental Panel on Climate Change (IPCC) has projected that around 77% of electrical power all over the world can be provided by RE by 2050. Deployment of 100% RE system is also envisaged to be economically and technically feasible in the future [19].

Among all the renewable alternatives, wind power is one of the most promising replacement sources to the conventional fuels. Wind energy use has a history of over 3000 years. Wind began to be harnessed in electricity generation around 120 years ago [20]. When oil crisis occurred in 1973, oil price increased sharply and it provided an opportunity for the fast development of wind power. The American government started on research and development (R&D) of wind energy and it is one of the most significant milestones in wind history [21-24]. Unfortunately the momentum did not sustain in subsequent years [25]. It was only in the past decade that the world has witnessed rapid development in wind energy market and the evolution of the wind

turbine technology due to policies enacted by many countries. Countries including Germany, the US, Denmark, Spain and China devoted themselves to the wind energy development [25-27]. From the 21st century, the global capacity of the wind power has doubled about every 3.5 years. World-wide total installed wind power capacity has grown from 17 GW in 2000 to 238 GW in 2011 [28]. The World Wind Energy Association (WWEA) has declared that the capacity will soar to 1500 GW by 2020 [29].

Unfortunately, nearly all the RE generation is highly dependent on the weather and climate conditions. Electricity production from wind is random and intermittent. Its stochastic nature makes large-scale introduction of wind power generation into grid systems extremely challenging because wind power variability poses threats to the reliability and security of the electrical power systems. Specifically, the wind variability has a negative impact on the system voltage quality. This is an extremely significant aspect of power delivery because of its impact on economic benefit [30]. Also, it brings about negative influence on power balance problems. Due to the fluctuations of wind power, more reserves are necessary to compensate for the variability. Furthermore, the stochastic nature of the wind power makes the accurate forecast of it an extremely difficult task. This impedes the dispatch commitment of significant proportion of wind power generation into the grid system. The detailed discussions on the stochastic nature of wind speed and wind power, the impact of wind power variability on the power system and the wind power dispatch problem are given in Chapter 2.

One possible solution to enable the intermittent RE to be more competitive with the traditional fuels is to use energy storage system (ESS) [31-33]. ESS can be used to smooth out the wind power fluctuations [34, 35] and to improve on the dispatchability of the wind power [36, 37]. These are therefore the two main topics in this thesis. Other applications of the ESS in wind power include improving the low-voltage-ride-

through (LVRT) ability of the wind generators [38, 39], controlling the voltage and frequency of the grid system [40, 41], load following [42, 43]. In meeting these objectives, many types of ESS could be considered for use. When choosing an ESS for a specific application, some factors such as energy density, power density, cycle times, response time, power rating, capital cost must be taken into considerations. The introduction of some common ESS and the comparison of their main technical characteristics are also presented in Chapter 2.

As the total installed wind capacity increases, it is important to ensure that the wind generators should not negatively impact excessively on the power quality of the power systems. Also, it is desirable that the power output of the wind generators can be scheduled in a way similar to that of conventional generators. Hence, method(s) to achieve these objectives is most desirable. With these objectives in mind, a three-level ESS scheme is proposed in this thesis to realize the large-scale integration of wind power generation into grid system. Specifically, supercapacitors (SC) and battery energy storage system (BESS) are designed to remove high-frequency and mid-frequency wind power fluctuations. The pumped hydroelectric scheme is also designed to buffer the low-frequency components to achieve wind power dispatchability. The design is realized by firstly segregating the wind power into high-, mid- and low-frequency bands using high-pass, band-pass and low-pass filters. The cutoff frequencies of the filters are determined based on the developed minimum overlap energy concept and its application to the results of empirical mode decomposition (EMD) of the wind power.

1.2 Major Contributions

The main contributions of this study can be summarized as follows.

1. **Proposition of the wind power generation-three level ESS scheme for wind power smoothing and wind power dispatch planning.** A large-scale wind power scheme containing three types of ESS is proposed in Chapter 3. The SC, working in conjunction with the designed high-pass filter (HPF), is to remove the high-frequency perturbations of the wind power while the BESS and the band-pass filter (BPF) work to deal with the mid-frequency wind power oscillations. The pumped hydroelectric storage (PHS) and the low-pass filter (LPF) act to buffer the low-frequency components, for the purpose of realizing the dispatch planning of the wind power.

2. **Proposition of an EMD-based method to determine the cutoff frequencies of the HPF, BPF and LPF.** In order for the power smoothing and dispatch planning tasks to be carried out satisfactorily, the cutoff frequencies of the three filters must be appropriately set. The author of this thesis is unaware of any reported work on method to determine the filters' cutoff frequencies for achieving the said objectives. A method to determine the cutoff frequencies is described in Chapter 3 and it is based on the concept of minimum overlap energy applied to the results of EMD of wind power data.

3. **Design of battery-supercapacitor energy storage system for the purpose of eliminating wind power fluctuations.** In practice, it is not possible to utilize only one type of ESS to buffer both the high- and mid-frequency oscillations of wind power generated at a wind farm. Consequently, a hybrid ESS which consists of BESS and SC is utilized in Chapter 4 to remove the wind power perturbations. A real-time control scheme of the battery-supercapacitor hybrid energy storage system (BSHESS) for wind power smoothing is also presented. Furthermore, as capital investment of the ESS can be significant, the capacity of the ESS has to be carefully determined at the planning stage. A statistical method to determine the power and energy capacities of the minimum-cost BSHESS is therefore developed

to smooth the wind power fluctuation. The designed BSHESS is to achieve successful power smoothing at pre-specified probability level.

4. **Dispatch planning of wind power based on low-frequency components of the wind power and the utilization of PHS.** For generators participating in power market, including wind turbine generators (WTG), they are expected to submit their generation bids a day or so ahead so that grid operators can carry out short-term dispatch planning. Generally it is challenging to forecast wind power accurately. Hence wind farm operators find it extremely difficult to commit the generation schedule a day or so ahead. To overcome this difficulty, a method is proposed in Chapter 5 to enhance the dispatchability of the wind power. A strategy is developed to control the power flows of the PHS so as to buffer the low-frequency components of the wind power. The components are focused on for dispatch planning because these power components are expected to contribute the most significant proportion of the net export of energy to the grid system from the wind farms. Also, accurate forecast of the low-frequency wind power components is much readily achievable, compared to that of forecasting the complete wind power. Finally, the chapter also describes a method to determine the power and energy capacities of the PHS based on a statistical approach.

1.3 Organization of the Report

The focus of this thesis is on the design of the energy storage systems for the smoothing and dispatch planning of large-scale wind power generation. Hence, the organization of the thesis is designed to provide a logical flow of the work, as follows. Background materials and literature review pertaining to the subject matter are given in Chapters 1 and 2. Then the general energy storage scheme proposed in this thesis is described in Chapter 3. Chapters 4 and 5 respectively focus on the smoothing and

dispatch planning of wind power generation. Main findings and suggested future works are included in Chapter 6.

Hence specifically in this thesis:

Chapter 1 provides the background, motivation and the main contributions of this project.

A brief review on the variability nature of wind power and the current wind power forecasting methods is given in Chapter 2. A discussion on the impacts of wind power variations on power system and the difficulty of dispatch planning of wind power is included. The chapter also contains a description of some common ESS and the comparisons among these storage technologies.

An ESS wind power smoothing and wind power dispatch scheme is proposed in Chapter 3. The method to determine the cutoff frequencies of the HPF, BPF and LPF which segregate the wind power into high-, mid- and low-frequency components is included. Results of this chapter pave the way for the development of the smoothing and dispatch planning schemes described in subsequent chapters.

In Chapter 4, the design of battery-supercapacitor energy storage system for removing wind power perturbations is presented. The motivation for utilizing the BESS and SC to smooth the wind power is given. The study also includes the BSHESS control scheme. A statistical method to determine the optimum BSHESS storage capacity is described.

A new method to carry out dispatch planning of wind power is proposed in Chapter 5. The study also explains why the low-frequency wind power components are considered for dispatching and provides the reason for the choice of the PHS as the

storage media to buffer the low-frequency wind power components. Furthermore, the PHS power and energy capacities are determined.

Chapter 6 concludes the main findings of this thesis and provides some research directions for future works.

CHAPTER 2. Wind Power, its Impacts on Grid and the Role of Energy Storage Systems in Wind Power Smoothing and Dispatch Planning: A Literature Review

As has pointed out in the previous chapter, wind power generation has seen rapid growth in recent years. However, wind tends to be unsteady and as the proportion of wind generation increases in a grid, the perturbing wind power may degrade the grid system reliability and security to unacceptable level. The main practical problem is due to the difficulty to predict wind power accurately. This means that firm power dispatch commitments from wind farms remain a challenging task. While research attention continues on developing accurate wind power forecasting techniques, in recent years, the use of ESS has been extensively investigated as one possible solution to mitigate the impacts of the fluctuating wind power and to improve wind power dispatchability. In view of this, the purpose of this chapter is to provide a brief introduction on wind power variability in Section 2.1. The impacts of the variable wind power on power quality and dispatch are explained in Section 2.2 and Section 2.3 respectively. Finally, ESS commonly found in power systems shall be described in Sections 2.4.

2.1 Wind Power Generation

As a fluid, the motion of wind is governed by the Navier- Stokes (N-S) equation, which includes such parameters such as density, velocity, pressure, dynamic viscosity of the fluid and so on. However, wind velocity tends to be stochastic and difficult to predict accurately since wind is random and is dictated by the weather [44]. Wind speed changes all the time, with the result that the amount of wind power that can be

extracted by wind turbines also varies. The uncertain nature of the wind speed and thus wind power can be characterized as a random variable. In this section, the random wind speed and wind power shall be described in statistical terms.

2.1.1 Wind speed variability

2.1.1.1 Statistical characterization of wind speed

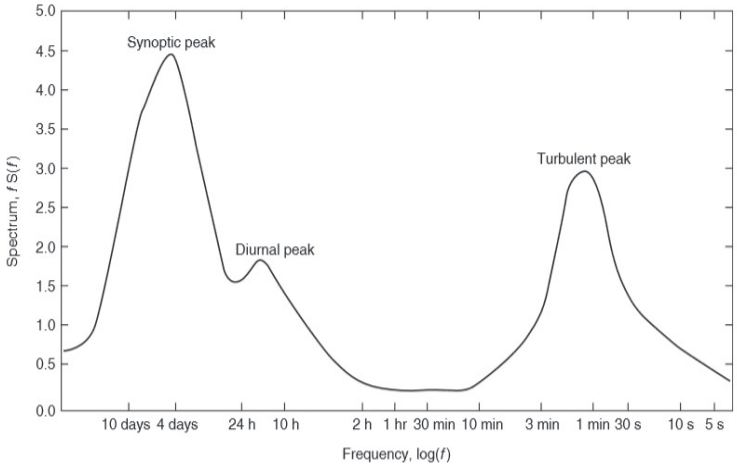

Figure 2.1. Wind frequency spectrum [45]

The variation of wind speed is a function of time and a convenient way to describe the variation is through the use of its frequency spectrum. Figure 2.1 shows the frequency spectrum of wind speed variations, from the time scales of a few seconds to over several days. It is a measure of the distribution of the variance of the wind speed over the various frequencies or periods. The unit of the y-axis is $(\text{speed})^2$. The figure shows the turbulent peak results from the wind gust in the range of tens of seconds to a minute or so. The daily wind speed variations determine the diurnal peak. The synoptic peak which includes daily to weekly or even seasonal cycles is dependent on the varying weather patterns. In the context of the impacts of wind power on grid systems, the turbulent peak would influence the grid power quality while the diurnal

and synoptic peaks would cause the power imbalance of grid system in the daily and longer term [7].

2.1.1.2 Weibull and Rayleigh distributions of wind speed

The random wind speed variations can be represented by standard statistical functions. In order to find out the most suitable function to describe the variations, various statistical functions had been applied and the results compared with the distribution of the actual wind data. The Weibull and Rayleigh functions were found to be able to represent the wind speed distribution with certain degree of accuracy [44, 46-49]. This method of quantification was firstly proposed in 1970s and has been widely used to-date when analyzing wind characteristics in a statistical manner [50].

In Weibull distribution, the wind speed can be described by the following functions:

- The probability density function (PDF)
- The cumulative distribution function (CDF)

The PDF $f(v_w)$ refers to the probability that the wind speed is equals to v_w and it is given by

$$f\left(v_w\right)=\left(\frac{k}{e}\right)\left(\frac{v_w}{e}\right)^{(k-1)}\exp\left[-\left(\frac{v_w}{e}\right)^{k}\right],\ 0<v_w<\infty \tag{2.1}$$

where e is scale factor (unit of wind speed), k is shape factor (dimensionless).

The CDF indicates the probability that the wind is equal to or less than v_w, so it is the integral of PDF, i.e.

$$F(v_w) = \int_0^{\alpha} f(v_w) dv_w = 1 - \exp\left[-\left(\frac{v_w}{e} \right)^k \right] \quad (2.2)$$

The probability density and CDF of wind speed which follows the Weibull distribution are shown in Figure 2.2 and Figure 2.3 respectively. In these figures, k = 2.8 and e = 6.9 m/s. From Figure 2.2 , it can be seen that the most frequent wind speed is about 6 m/s because its corresponding probability density is the largest.

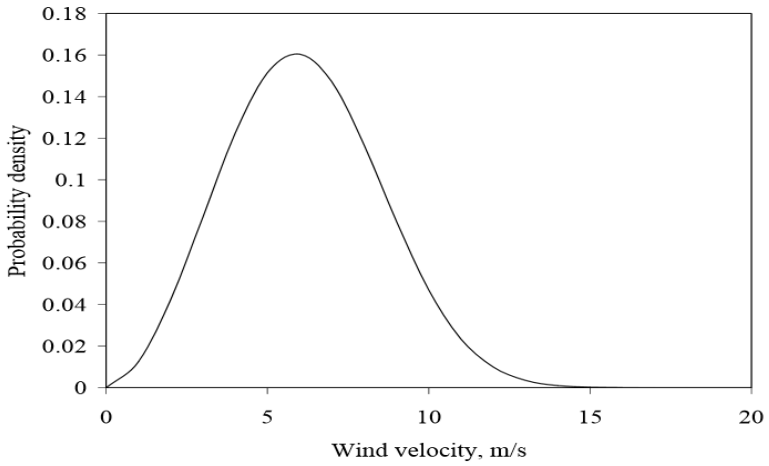

Figure 2.2. Weibull probability density function [47]

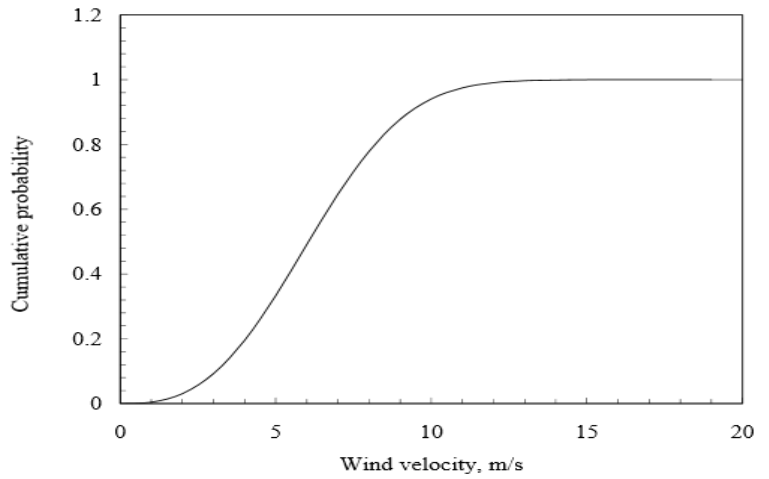

Figure 2.3. Weibull cumulative distribution function[47]

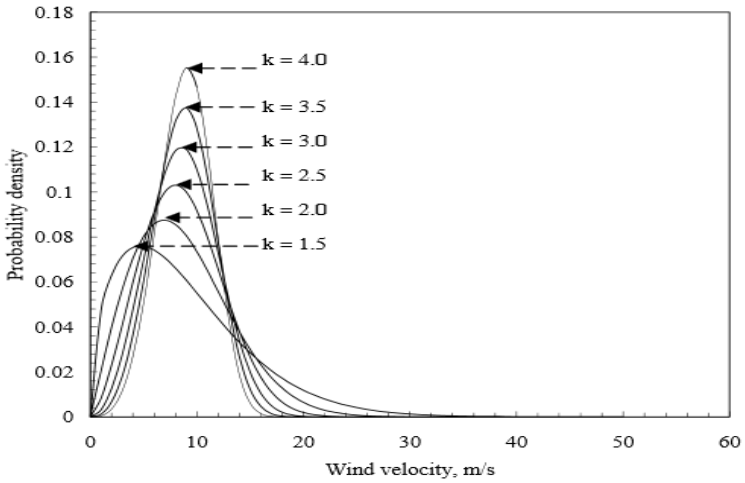

Figure 2.4. Weibull probability density function for different shape factors [47]

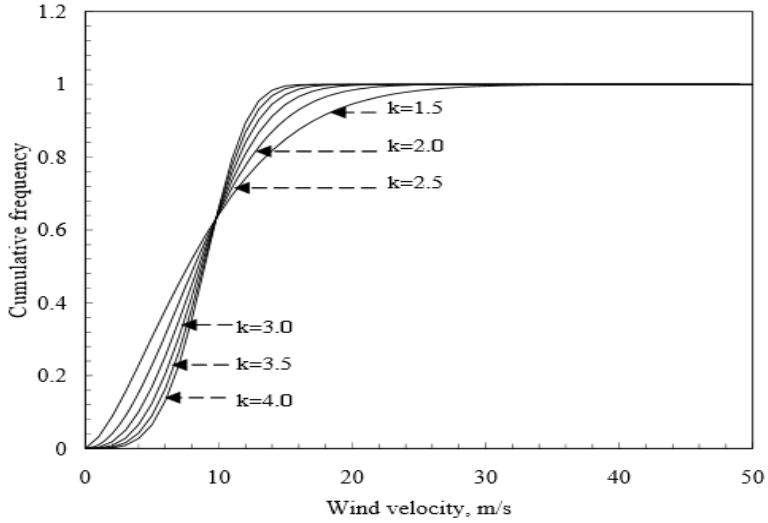

Figure 2.5. Weibull cumulative distribution function for different shape factors [47]

The parameter k determines the uniformity of the wind. This is why k is called the shape factor. Figure 2.4 and Figure 2.5 show the influence of the shape factor k on the Weibull probability density and Weibull cumulative distribution. The scale factor *e* is constant at 9.8 m/s. From the figure, one observes that with the increase of k, the uniformity of wind also increases.

The probability that the wind speed is within the range of v_{w1} to v_{w2} can be obtained from the CDF. It is the difference between the cumulative probability corresponding to v_{w1} and v_{w2}, i.e.,

$$P\{v_{w1} < v_w < v_{w2}\} = F(v_{w2}) - F(v_{w1}) = \exp\left[-\left(\frac{v_{w1}}{e}\right)^k\right] - \exp\left[-\left(\frac{v_{w2}}{e}\right)^k\right] \quad (2.3)$$

In (2.3), P{·} denotes the probability the condition {·} is met.

In order to satisfy the maximum probable loads, the probability that the wind velocity is higher than certain value v_{wx} is important and it is given by

$$P\{v_w > v_{wx}\} = 1 - \{1 - \exp\left[-\left(\frac{v_{wx}}{e}\right)^k\right]\} = \exp\left[-\left(\frac{v_{wx}}{e}\right)^k\right] \quad (2.4)$$

When sufficient wind data for a short time is not available, the wind data are assumed to be in a form of average wind speed V_m over a given period. Take k = 2 for Weibull distribution, Rayleigh distribution can be derived. It is a special and simplified case of Weibull distribution. The PDF of Rayleigh distribution is

$$f(v_w) = \frac{\pi}{2}\frac{v_w}{V_m^2}\exp\{-[\frac{\pi}{4}(v_w / V_m)^2]\} \quad (2.5)$$

And the CDF is

$$F(v_w) = 1 - \exp\{-[\frac{\pi}{4}(v_w / V_m)^2]\} \quad (2.6)$$

The probability that the wind speed is within the range of v_{w1} to v_{w2} is

$$P\{v_{w1} < v_w < v_{w2}\} = \exp\{-[\frac{\pi}{4}(v_{w1} / V_m)^2]\} - \exp\{-[\frac{\pi}{4}(v_{w2} / V_m)^2]\} \quad (2.7)$$

The probability that the wind velocity is higher than certain value v_{wx} is

$$P\{v_w > v_{wx}\} = 1 - (1 - \exp\{-[\frac{\pi}{4}(v_{wx} / V_m)^2]\}) = \exp\{-[\frac{\pi}{4}(v_{wx} / V_m)^2]\} \quad (2.8)$$

2.1.2 Wind Power Variability

The variability of wind speed has been described in statistical term in the previous section. Next, the relationship between the wind speed and the generated wind power will be shown and the wind power distribution can be derived based on the wind speed distribution. The derived expressions can be used to describe the stochastic nature of wind power.

2.1.2.1 Wind power generation

The active power harnessed by wind turbine can be estimated from the equation:

$$P_w = 0.5\rho\pi r^2 C_p v_w^3 \quad (2.9)$$

where ρ is the air density; r is the radius of the wind turbine; v_w is the wind speed. C_p is the turbine-rotor-power coefficient defined as a function of the pitch angle β and of the tip speed ratio $\lambda = \omega_r r / v_w$. ω_r is the rotational speed of turbine rotor [51]. The approximate expression of C_p is

$$C_p = 0.22(116z - 0.4\beta - 5)e^{-12.5z} \quad (2.10)$$

$$z = 1/(\lambda + 0.08\beta) - 0.035/(\beta^3 + 1)) \quad (2.11)$$

where z is just an intermediate variable.

Equation (2.9) indicates that the wind power generated by a wind turbine varies by the cube power of the wind speed. Consequently, the generated power varies with the wind speed in a highly non-linear manner.

Maximum power from the wind can be extracted by controlling the rotational speed of turbine rotor ω_r. The reason is as follows. From (2.9), it is clear that P_w depends on the selection of C_p. When C_p is controlled at the optimal value C_{p_opt}, maximum wind power can be reached. For a specific pitch angle β, there is an optimal λ_{opt} corresponding to C_{p_opt}. When the pitch angle β is zero, the corresponding value of C_{p_opt} is the maximum. This is because the moving fluid of wind can generate a torque to drive the shaft of wind turbine. When β is zero, the torque is at the maximum. Considering $\lambda = \omega_r r / v_w$, the rotor speed of turbine ω_r must change with the variation of wind speed v_w in order to maintain the optimal λ_{opt}. The optimal rotor speed is denoted as ω_{r_opt}. [52]. In practice, a control system is used to ensure the wind turbine to operate at ω_{r_opt} [53]. This is the so called "rotor speed control" (RSC). As a result, a variable rotor-speed wind turbine is capable of achieving maximum power point tracking (MPPT). The maximum wind power can be expressed as [51]

$$\begin{aligned} P_{w\_opt} &= 0.5\rho\pi r^2 C_{p\_opt} v_w^3 \\ &= 0.5\rho\pi r^5 C_{p\_opt} \omega_{r\_opt}^3 / \lambda_{opt}^3 \end{aligned} \tag{2.12}$$

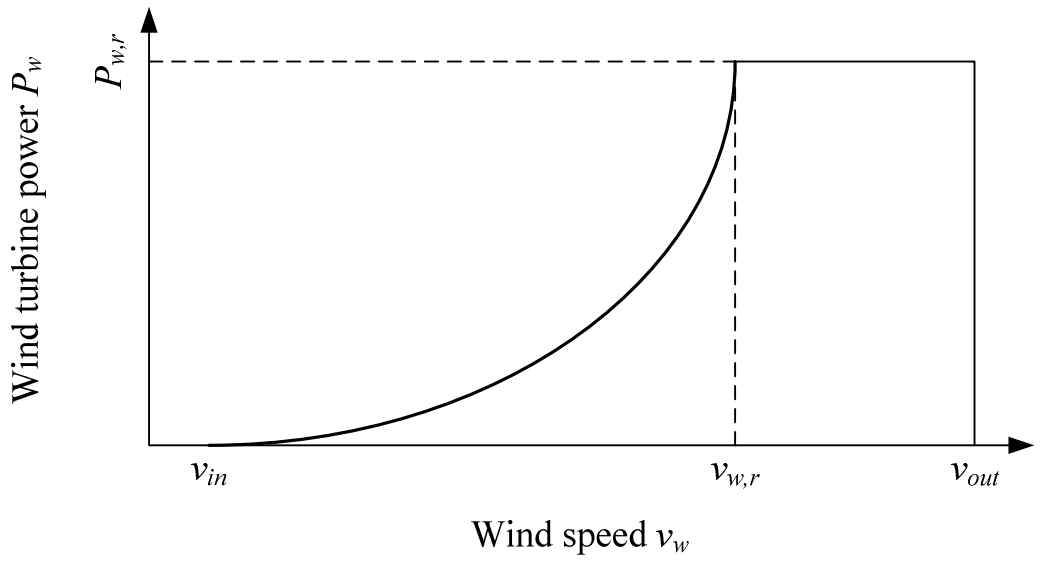

Figure 2.6. Turbine output power – wind speed curve of wind power generator.

The output power of a wind turbine reaches its rated value at rated wind speed. When the wind speed is higher than its rated value, pitch angle control would be used to increase the pitch angle of the blades in order to decrease C_p so that the generated wind power is maintained at the rated power. Furthermore, the turbine requires certain amount of power to overcome rotational losses. At lower than the cut-in wind speed, the generated power is insufficient to make up the losses. Hence when the wind speed is lower than the cut-in wind speed, the wind turbine would stop working. On the other hand, if the wind speed is higher than the cut-off wind speed, the turbine would also stop working so as to protect the turbine from mechanical damage.

In summary, the relationship between the wind turbine power (P_w) and wind speed (v_w) shown in Figure 2.6 can be stated as

$$P_w = \begin{cases} 0; & (v_w < v_{in} \ or \ v_w \geq v_{out}) \\ P_{w,r}; & (v_{w,r} \leq v_w < v_{out}) \\ 0.5\rho\pi r^2 C_p v_w^3; & (v_{in} \leq v_w < v_{w,r}) \end{cases} \tag{2.13}$$

where v_{in} is the cut-in wind speed, v_{out} is the cut-off wind speed, $v_{w,r}$ is the rated wind speed and $P_{w,r}$ is the turbine rated power.

2.1.2.2 Statistical characterization of wind power

As the wind speed distribution and the relationship between the wind power (P_w) and wind speed (v_w) are now known, the statistical distribution of the wind power can be derived.

Firstly, the PDF of wind power is discussed. PDF refers to the probability that the wind power is equals to P_w. From (2.13), P_w is a piecewise function, so the PDF of wind power would be considered for each of the intervals.

Suppose the wind speed follows Weibull distribution. Thus if $v_w < v_{in}$ or $v_w \geq v_{out}$, P_w is zero. According to (2.4), the PDF when this occurs is

$$\begin{aligned} & P\{P_w = 0\} \\ &= P\{v_w < v_{in}\} + P\{v_w \geq v_{out}\} \\ &= (1 - P\{v_w \geq v_{in}\}) + P\{v_w \geq v_{out}\} \\ &= 1 - \exp\left[-\left(\frac{v_{in}}{e}\right)^k\right] + \exp\left[-\left(\frac{v_{out}}{e}\right)^k\right] \end{aligned} \tag{2.14}$$

If $v_{w,r} \leq v_w < v_{out}$, $P_w = P_{w,r}$ and the PDF of this happening is

$$\begin{aligned} & P\{P_w = P_{w,r}\} \\ &= P\{v_{w,r} \leq v_w < v_{out}\} \\ &= \exp\left[-\left(\frac{v_{w,r}}{e}\right)^k\right] - \exp\left[-\left(\frac{v_{out}}{e}\right)^k\right] \end{aligned} \tag{2.15}$$

Lastly, if $v_{in} < v_w < v_{w,r}$, the PDF of P_w is

$$f(P_w) = \frac{khv_{in}}{P_{w,r}e}\left[v_{in}(1 + \frac{hP_w}{P_{w,r}}) / e\right]^{k-1} \times \exp\left\{-\left[v_{in}(1 + \frac{hP_w}{P_{w,r}}) / e\right]^k\right\} \tag{2.16}$$

where $h = (v_{w,r}/v_{in})$-1. (2.14), (2.15) and (2.16) are derived based on the theory of statistics of random variables [54, 55] and from the wind speed distribution.

The CDF of wind power is the probability the wind power is equal to or less than P_w and it is the integral of PDF. The derivation of CDF of wind power also has to consider the piecewise property of P_w. Thus when $v_{in} < v_w < v_{w,r}$, the integration of the PDF of wind power (i.e. (2.16)) is

$$\phi(P_w) = 1 - \exp\left\{-\left[v_{in}(1 + \frac{hP_w}{P_{w,r}}) / e\right]^k\right\} \tag{2.17}$$

Moreover,

$$P\{P_w > P_{w,r}\} = 0 \tag{2.18}$$

Based on (2.14), (2.15), (2.17) and (2.18) and according to the probability theory [54], the CDF of P_w is

$$F(P_w) = \begin{cases} 0; & (P_w < 0) \\ 1 - \exp\left\{-\left[v_{in}(1 + \frac{hP_w}{P_{w,r}})/e\right]^k\right\} + \exp\left[-\left(\frac{v_{out}}{e}\right)^k\right]; & (0 \le P_w < P_{w,r}) \\ 1; & (P_w \ge P_{w,r}) \end{cases} \tag{2.19}$$

Examples of PDF and CDF of wind power with different values of the shape factor k are shown in Figure 2.7 and Figure 2.8 respectively.

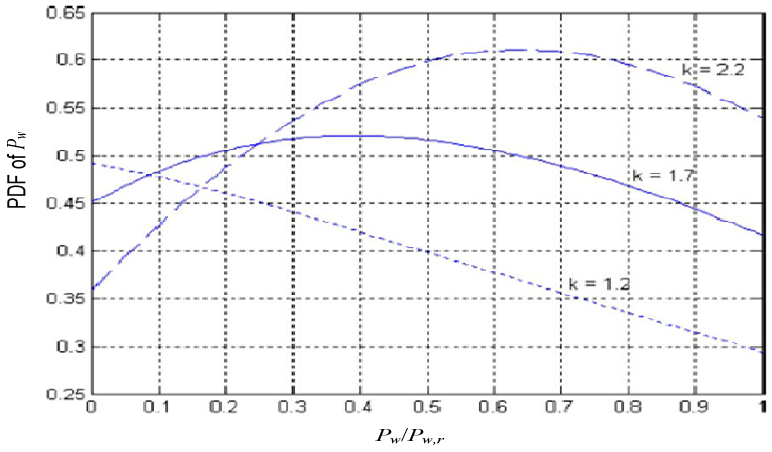

Figure 2.7. Examples of PDF of wind power [56]

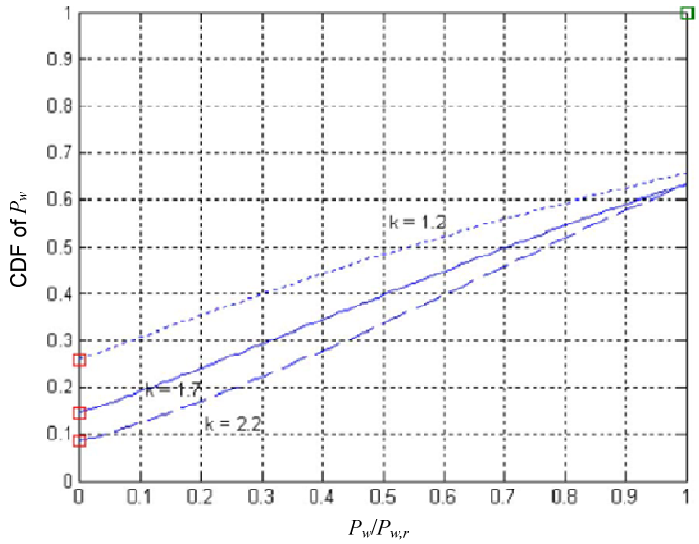

Figure 2.8. Examples of CDF of wind power [56]

Figure 2.7 shows that the shape of the PDF of wind power depends on the value of k. Figure 2.8 shows that the CDF of the wind power is not that sensitive to k. With the increase of P_w, the CDF also increases.

Suppose the wind speed obeys Rayleigh distribution. Thus if $v_w < v_{in}$ or $v_w \geq v_{out}$, P_w is zero. According to (2.8), the PDF when this occurs is

$$\begin{aligned} & P\{P_w = 0\} \\ &= P\{v_w < v_{in}\} + P\{v_w \geq v_{out}\} \\ &= (1 - P\{v_w \geq v_{in}\}) + P\{v_w \geq v_{out}\} \\ &= 1 - \exp\{-[\frac{\pi}{4}(v_{in}/V_m)^2]\} + \exp\{-[\frac{\pi}{4}(v_{out}/V_m)^2]\} \end{aligned} \tag{2.20}$$

If $v_{w,r} \leq v_w < v_{out}$, $P_w = P_{w,r}$ and the corresponding PDF is

$$\begin{aligned} & P\{P_w = P_{w,r}\} \\ &= P\{v_{w,r} \leq v_w < v_{out}\} \\ &= \exp\{-[\frac{\pi}{4}(v_{w,r}/V_m)^2]\} - \exp\{-[\frac{\pi}{4}(v_{out}/V_m)^2]\} \end{aligned} \tag{2.21}$$

Lastly, if $v_{in} < v_w < v_{w,r}$, the PDF of P_w is

$$f(P_w) = \frac{\pi v_{w,r}}{2V_m^2}(\frac{P_w}{P_{w,r}})^{\frac{1}{3}} \times \exp\left\{-\left[\frac{\pi v_{w,r}^2}{4V_m^2}(\frac{P_w}{P_{w,r}})^{\frac{2}{3}}\right]\right\} \tag{2.22}$$

The derivation of CDF of wind power also has to consider the piecewise nature of P_w. Thus when $v_{in} < v_w < v_{w,r}$, the integration of the PDF of the wind power (i.e. (2.22)) is

$$\phi(P_w) = \frac{3\pi^2 v_{w,r}^3}{16V_m^4 P_{w,r}}[1 - \exp(P_w^{\frac{2}{3}})] \tag{2.23}$$

Moreover,

$$P\{P_w > P_{w,r}\} = 0 \tag{2.24}$$

In summary, the CDF of P_w is

$$F(P_w) = \begin{cases} 0; & (P_w < 0) \\ \dfrac{3\pi^2 v_{w,r}^3}{16V_m^4 P_{w,r}}[1 - \exp(P_w^{\frac{2}{3}})]; & (0 \le P_w < P_{w,r}) \\ 1; & (P_w \ge P_{w,r}) \end{cases} \tag{2.25}$$

2.2 Impacts of Wind Power on the Quality of Supply

The fact that the wind power fluctuates all the time has negative influences on the power system. There are two main problems: The impacts on voltage quality and on power balance. They will be explained in detail as follows.

2.2.1 Impacts on voltage quality

Voltage quality is an extremely important issue because it has great economic impact on industrial loads, electric utility and consumers [57]. Unfortunately in a power

system with high penetration of wind power, the variability nature of wind brings about the voltage quality problem [58-60].

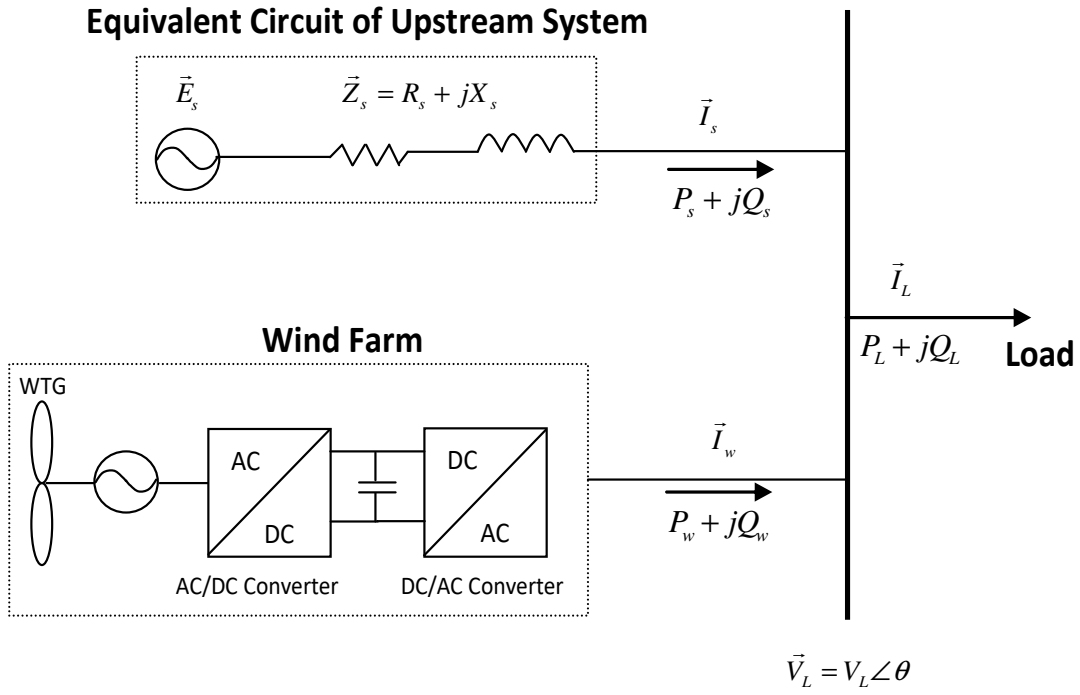

Figure 2.9. Schematic of grid-connected wind farm

As an initial attempt to gain an understanding of the impacts of wind power on voltage quality, the rather generic power system shown on Figure 2.9 is examined. It can be used to represent a network in which power is supplied to a remote area which has its own local renewable generation. Thus, in terms of power flows, the wind farm is intended to meet part of the local load demand, and the supply is supplemented by the upstream grid system. The wind farm operates as a local power supplier when wind blows and the farm is likely to consist of a number of WTG. Hence the single WTG-converter unit shown in the figure would represent the aggregate of a number of WTG and their associated power converters, to yield the total complex output power P_w+jQ_w. While there are many other versions of power converters used in conjunction

with WTG, the form shown in Figure 2.9 has been adopted as it is one of the most common and well-established types used in present-day wind farms.

As the upstream grid system generally tends to be complex, it is proposed to represent the grid by its Thevenin equivalent: $\overrightarrow{E_S}$ and $\overrightarrow{Z_S}$ are the source voltage and source impedance, respectively. The phase angle of the source voltage is set as the reference angle in this study. $\overrightarrow{V_L}$ is the load voltage. This representation is acceptable as in this study and the focus is on the impacts of the wind farm on the load area voltage quality. Hence the grid system can be represented in this simpler way.

The WTG capture the wind power from the wind and the power is transmitted through the AC/DC rectifier and the DC/AC inverter. The rectifier is controlled to extract the maximum power from the wind and to optimize the WTG operation. Since there is limited energy storage capacity in the converter system, thus at any given instance, P_w would be equal to the wind power harnessed from the wind. Thus the inverter is usually controlled to manipulate the output reactive power Q_w. This is done, for example, to exercise certain amount of load bus voltage control.

In Figure 2.9, $\overrightarrow{I_W}$ represents the injected current from the wind farm into the load area. By applying KCL to Figure 2.9 and based on power balance in the equivalent circuit, the steady-state equations can be obtained:

$$\left.\begin{aligned} V_L^{\,2} - E_s V_L \cos\theta - R_s P_w - X_s Q_w + R_s P_L + X_s Q_L = 0 \\ E_s V_L \sin\theta - X_s P_w + R_s Q_w + X_s P_L - R_s Q_L = 0 \end{aligned}\right\} \tag{2.26}$$

A brief derivation of (2.26) is given below. By applying KCL and KVL to Figure 2.9,

$$\vec{I}_L = \vec{I}_w + \vec{I}_s \tag{2.27}$$

$$\vec{V}_L = \vec{E}_s - \vec{Z}_s \vec{I}_s \tag{2.28}$$

Complex power of the load and the WTG injected power are given as

$$\vec{V}_L \times \vec{I}_L^* = P_L + jQ_L \tag{2.29}$$

$$\vec{V}_L \times \vec{I}_w^* = P_w + jQ_w \tag{2.30}$$

From (2.28), (2.29) and (2.30), $\vec{I}_s$, $\vec{I}_L$ and $\vec{I}_w$ can be expressed as

$$\vec{I}_s = \frac{\vec{E}_s - \vec{V}_L}{\vec{Z}_s} \tag{2.31}$$

$$\vec{I}_L = \frac{P_L - jQ_L}{\vec{V}_L^*} \tag{2.32}$$

$$\vec{I}_w = \frac{P_w - jQ_w}{\vec{V}_L^*} \tag{2.33}$$

By substituting (2.31), (2.32) and (2.33) into (2.27), and after some manipulations and the separation of the real and imaginary parts, it can be readily shown that (2.26) will be obtained.

Equation (2.26) governs the steady-state behavior of the system. For a fixed upstream grid system, E_s, R_s and X_s are constant and known. As wind speed varies continuously, so P_w would fluctuate in manner which is often difficult to predict precisely. Furthermore, the load P_L+jQ_L also tends to vary with time. Hence, the values of P_w, P_L and Q_L are continually varying. Hence the magnitude of the load voltage cannot remain constant. This has explained how the voltage of the load area near wind farms is impacted by the wind power fluctuations.

2.2.2 Impacts on power balance

Another influence of wind power variation on the power system is on the power balance [61-64]. This is also explained by using Figure 2.9. In Figure 2.9, the power balance equation is

$$P_s + P_w = P_L \tag{2.34}$$

Equation (2.34) holds on any condition and at any time. The generation and demand are required to match with each other at any moment. Whatever generated is consumed at the same time. Apart from P_w, the load P_L also tends to vary with time. Any change of P_w and P_L has to be offset by P_s at the same time. In conventional generators, P_s is more readily "controllable" compared to the wind and demand, so one can readily adjust the amount of fuel to produce the needed power for power balance.

P_s is generally produced by synchronous generators in traditional power stations. The rotor of the synchronous generator is driven by turbine (hydro or steam). The power from the synchronous generator P_s is the sum of the power from the hydro/steam turbine P_T and the power stored in the rotating mass P_R. If P_s and P_T remain unchanged, the kinetic energy stored in the rotating mass and the rotor speed ω are constant. If there is a sudden change in P_s, it results in variation in P_R as the balance of power is broken. Then it causes the rotating speed of the rotor ω to change. Whence

$$\frac{d\Delta\omega}{dt} = \frac{1}{2H}(\Delta P_T - \Delta P_s) \tag{2.35}$$

where H is the inertia constant and ω is the rotor speed of synchronous generator. After taking Laplace transform for (2.35),

$$\Delta\Omega(s) = \frac{1}{2Hs}(\Delta P_T(s) - \Delta P_s(s)) \tag{2.36}$$

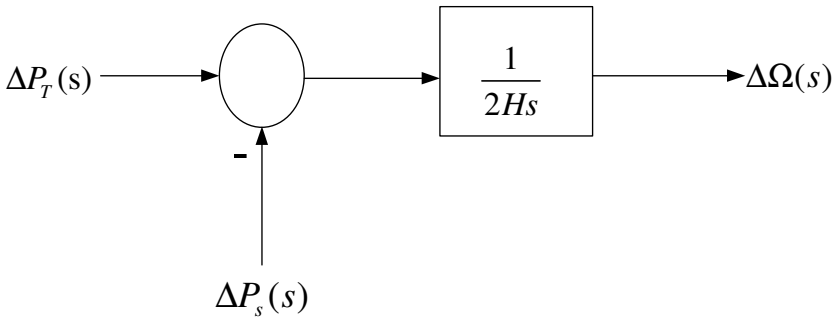

Figure 2.10. Generator block diagram [65]

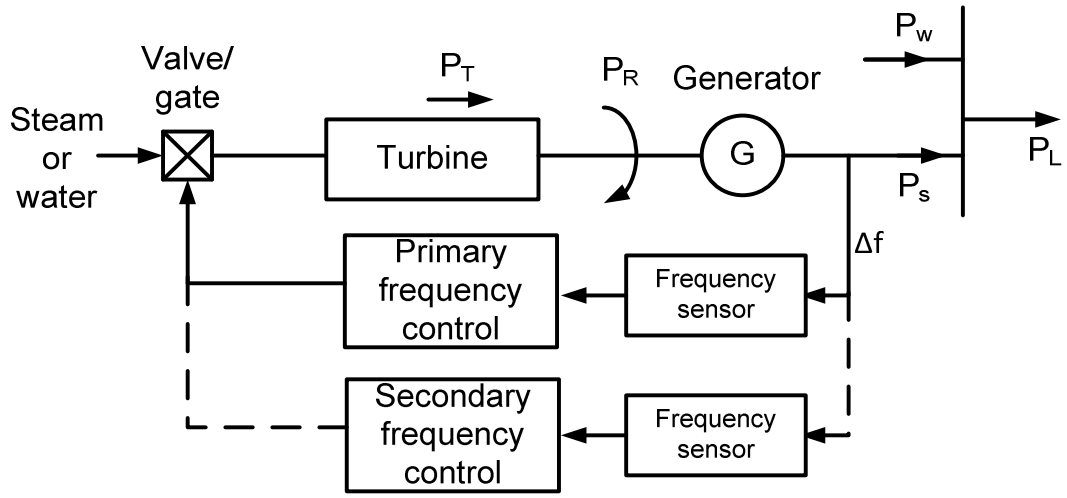

Figure 2.11. Schematic diagram showing the frequency control mechanism of a synchronous generator

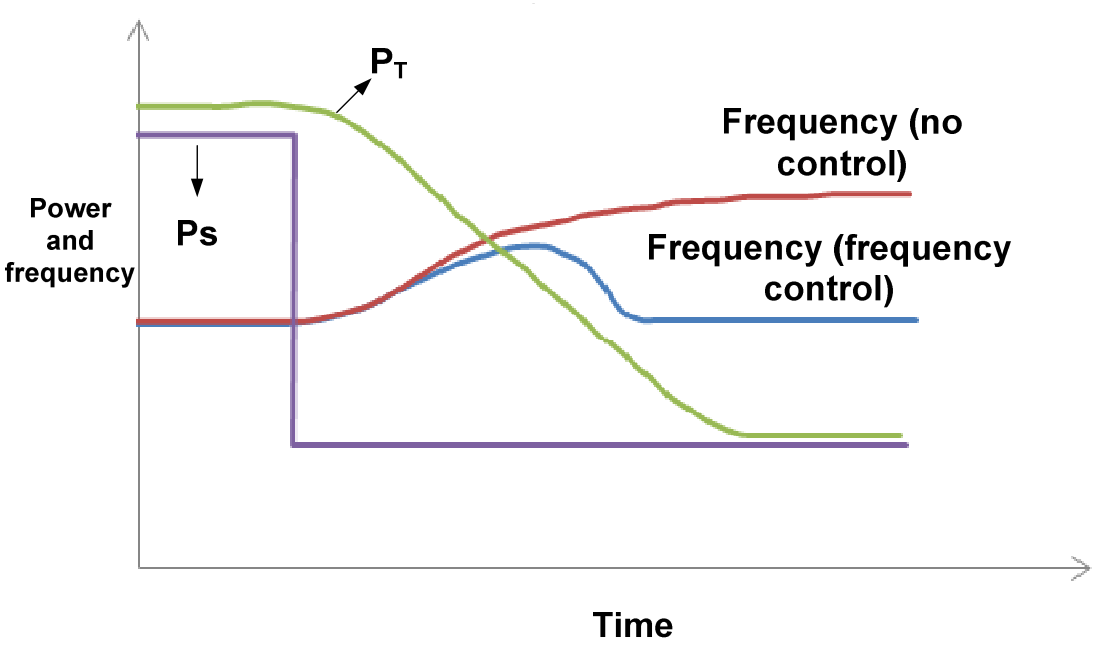

Figure 2.12. The network frequencies with and without frequency control after a sudden decrease in P_s

As the rotor speeds of many synchronous generators in the power system synchronize with each other to produce the common frequency of the power system, the change of rotor speed would lead to the deviation of network frequency. Thus, the variations of the wind power and demand which have to be offset by P_s would bring about the change in the network frequency. The frequency deviation means the mismatch between power generation and consumption in the power system.

In order to restore the frequency back to the nominal frequency or to within acceptable range, frequency control [64, 66-69] is necessary. The schematic diagram of frequency control mechanism of a synchronous generator is shown in Figure 2.11. Firstly, primary control system would sense the frequency deviation (Δf). The turbine input valve would be adjusted to regulate the power output P_T from the turbine within 30 seconds to 1 minute since the occurrence of the frequency change. P_T would be

increased when the frequency drops. Conversely it would be reduced if frequency increases. Secondary control, i.e. automatic generation control (AGC), would be in operation in 10-30 minutes to replace the primary control if the electrical frequency still deviates from the nominal frequency or beyond the allowed limits. The secondary control capacity (also known as secondary reserve) would replace the primary control capacity (also called primary reserve). With the frequency control, the generation and demand mismatch will be reduced and the frequency deviation would be alleviated. Figure 2.12 illustrates the advantage of the frequency control. The process begins with the sudden decrease of the generated power P_S due to an external grid disturbance for example. So P_S is suddenly less than P_T. Under the no-control scenario, this power difference causes the generator to speed up, eventually to another steady-state value. However, with speed-governor control action, the control system would sense the speed increase. The turbine input valve would then be adjusted to decrease the power output P_T until the frequency is brought back to the pre-set value.

If wind power generation is connected to the power system as shown in Figure 2.9, compared with a power system with only varying load, the fluctuating P_w would increase the variability factor. This will increase the difficulty in the balancing of the generation and consumption. The primary and secondary control must balance more mismatch. More primary and secondary control capacities (therefore, higher costs) are required to maintain the frequency within reasonable limits. As the wind power penetration increases, the influence of wind power fluctuation on the primary and secondary control capacity also increases. For example, reference [70], which focuses on the hourly variations of wind power, shows that for a power system with 10% wind power penetration, the operating reserve needs to increase by 1.5%-4% of the total wind capacity in order to ensure adequate level of system security and reliability. So in order to participate in modern power market in which up-to-a-day ahead short-term power dispatch commitments need to be made, the wind generators would have to rely on wind power forecast. Unfortunately wind power forecast cannot be 100% accurate, with the result that the forecast error has to be dealt with by the provision of

the secondary reserve. A report in 2006 drew the conclusion that the cost of reserves associated with the wind power variability and day-ahead forecast errors would increase the wind power generation cost by $2.11 per MWh for 15% wind power integration level to $4.41 per MWh for 25% wind power integration level [71]. On-line conventional generators that can provide the reserves for wind power generation are fast responding balancing generators, such as gas turbines, small fossil fuels and hydroelectric plants [72, 73]. They are able to quickly ramp up and down. However, they must be part-loaded, thus resulting lower operating efficiency [74]. The efficiency decreases by 10%-20%. The efficiency reduction for new gas plant is even higher. In addition, with the higher penetration of wind power generation which brings about more fluctuations, it is quite hard to forecast the back-up generation that is needed.

2.2.3 A literature review on the application of ESS for power quality enhancement

As shown in the previous sections, variations in wind power can bring about the voltage and frequency deviations of power systems. In the context of Figure 2.9, therefore, it is highly desirable to smoothen the output power P_w to mitigate the degradation the quality of supply. Wind power fluctuations can be smoothed out by controlling the kinetic energy of the WTG inertia, or by pitch angle control of the WTG turbine blades, or by controlling the dc link voltage of the dc link capacitor contained in the power conditioning units often found in modern WTG [75].

As an alternative to the above techniques, the use of ESS has been extensively examined in recent years as a possible solution to mitigate the negative impacts of the perturbing wind power on grid systems [31-33, 75-78]. A review on various types of ESS and their comparison in the next section shall indicate that SC, flywheels, superconducting magnetic energy storage system (SMES) and conventional batteries

have fast response, high power ramp rate and high cycling ability. These ESS are suitable candidates for such power quality enhancement application [31, 32]. In this section, a literature review of the applications of SC, batteries and the combination of supercapacitor-battery ESS for wind power smoothing shall be presented.

The applications of SC for mitigating wind power oscillations have been extensively reported in the literatures. In [79], the supercapacitor is connected to the dc bus of a doubly fed induction generator (DFIG) WTG via a bidirectional dc/dc converter. During normal state, the supercapacitor is used to remove short-term fluctuations in wind power. During transients, it is applied to improve the LVRT ability of the wind farm and the sizing of supercapacitor is based on the LVRT requirement. The dc/dc converter controls the real power of the supercapacitor. In [80], a supercapacitor associated with the dc/dc converter is connected across the dc link of the back-to-back converters of the permanent magnet synchronous generator (PMSG) wind turbine system. The reference power signal for the supercapacitor is obtained by passing the wind power signal through a HPF, although the method to determine the filter cutoff frequency is not presented. The control block for controlling the supercapacitor to track the reference power is proposed. In [81], a supercapacitor bank's ability to diminish the wind power fluctuations in the seconds time range (thus reducing the frequency fluctuations) is demonstrated in a scaled-down power system model consisting of diverse type of generators (wind, hydro, thermal and nuclear generators). The supercapacitor is controlled by an adaptive ANN. For the continuous variations of wind power, the controller proposed in the paper has excellent dynamic response ability. In [82-84], a supercapacitor bank is connected at the terminal of the wind turbine generator/wind farm through a bi-directional converter. For a wind farm consisting of a number of wind turbines, it is a rather complex scheme and would be costly if the supercapacitor is installed at the dc link of every one of the WTG and is controlled individually. In terms of the inverter, a current-source inverter, a sinusoidal pulse width modulation (PWM) voltage source converter (VSC) and a current-controlled voltage-source inverter are used respectively in the three literatures. The

authors of [82] have examined the use of current-source supercapacitor energy storage system and its associated control system. They have demonstrated the effectiveness of the proposed design in mitigating the wind power fluctuations. In [83], the supercapacitor bank is to suppress fluctuations in the minute time-range of the output power from a wind farm composed of fixed-speed wind generators. The method of exponential moving average is presented to obtain the reference signal for the total wind farm output power. By controlling the charging and discharging power of the supercapacitor, the reference power for the wind farm can be tracked. In [84], a fuzzy-logic-aided reference adjuster is incorporated in the control of the dc/dc converter of the supercapacitor. The adjuster monitors the energy stored in the supercapacitor. If the energy is less than 40% or higher than 90%, the adjuster would decrease the operations of the supercapacitor. Hence, the number of incidents of over-charging and over-discharging of the SC can be decreased and the service life of supercapacitor is prolonged. Regardless of whether the supercapacitor is connected to the dc link of the back-to-back converters or to the terminal of wind turbine generator, interfacing converters have to be used. Higher cost and losses are associated with the converters. Therefore, the authors of [85] have proposed a dual inverter topology for the direct integration of the supercapacitor to the wind power system in order to smooth out the short-term wind power fluctuations. The interfacing converters are not needed.

Like SC, there are usually two ways to connect BESS to the wind turbine generator/wind farm. One way is to connect it across the dc-link of the back-to-back converters of WTG, such as that considered in [86]. The most common way is to connect the BESS to the terminals of the WTG/wind farm through an inverter, and interposing transformers such as that shown in [87] and [88]. Besides the connection method of BESS, the main focus of reported works is on the design of power flows control strategy for the BESS. As BESS is expensive, an efficient and effective control strategy is indispensable to ensure the optimal design of the BESS in terms of cost, and its utilization. For example, [34] utilizes a first order LPF to calculate the total expected power from the wind farm and BESS. The BESS is used to smooth out

the high-frequency wind power. A particle swarm optimization (PSO) algorithm is used to update the cutoff frequency of the filter for the purpose of minimizing the BESS capacity, while satisfying the power smoothing requirement. The study then applies the state switching constraint based on residual energy to decrease the number of switching between charging and discharging operations, which is beneficial for the lifetime of BESS. To be specific, the switching from charging to discharging state is only allowed when the residue energy is higher than certain specified value and vice versa. In [89], a BESS state of charge (SOC) controller is developed to firstly work as a LPF to remove the high-frequency components. Then the controller is used to adjust the SOC of BESS in order to prevent the SOC from deviating from the secure range and to keep ramp up/down rate of BESS power lower than a specified rate so as to prolong the lifetime of BESS. A fuzzy adaptive Kalman filter rather than a LPF is proposed in [90]. To be specific, the fluctuating wind power is firstly filtered by the basic Kalman filter (BKF). Then the fuzzy logic control is introduced to modify the filter's output so as to maintain the SOC of BESS within the specified range and to keep the BESS charging and discharging power within power capacity of BESS. In [91], a controller is designed based on model predictive control technique. A wind power forecasting model is proposed to optimize the SOC of BESS while meeting requirement for the maximum change rate of wind power output.

Recently, active research attention has been directed toward the design of BSHESS suitable for undertaking the wind power smoothing task. Justifications in selecting battery-supercapacitor energy storage system for wind power smoothing are given in Section 4.1. In an attempt to suppress the short- and long-term perturbations using BSHESS, the authors of [92] have proposed using wavelet signal decomposition technique to segregate wind power into different frequency domains. Unfortunately, wavelet analysis is non-adaptive and the interpretation of the wavelet can be counter-intuitive. In contrast, this thesis shall utilize the EMD method. EMD technique is an efficient way to analyze nonlinear and non-stationary data set [93]. A short introduction of EMD shall be given in Chapter 3. In [94], a BSHESS is used to limit

the wind power ramp rates. The ESS consists of zinc bromide flow battery and lithium-ion capacitors. However, it is not at all clear how the reference signals used to control the battery and capacitors are to be determined. The authors of [95] consider the design of the BSHESS to help maintain a high quality supply to loads in a microgrid supplied by renewable sources. They propose to use a LPF to generate the reference signal for a control scheme to mitigate the impacts of low-frequency perturbations caused by the unsteady renewable generation. However, the method to determine the filter cut-off frequency appears to be based on a trial-and-error process. The impact of the design of the filter on the performance of the power smoothing task is also not studied. The authors of [96] have also used filters in a flow battery-SC hybrid energy storage scheme for wind power smoothing. Unfortunately, the selection of the cutoff frequencies of the filters is again not based on rigorous analysis. In investigating the use of BSHESS for wind power smoothing, the authors of [97] have concluded that the choice of the time constant of the LPF used in their scheme is a matter of trade-offs between the battery life-time, SC capacity, among other considerations. However, the inter-relationship between the filter design and the trade-offs has yet to be quantitatively studied. In [98], a method is described in the design of least-cost BSHESS for which a coordinated power flows control strategy for the battery and supercapacitor is proposed. The BESS power ramp rate is constrained to prolong the life span of BESS. The focus there is to realize the dispatchability of the wind power, rather than for power smoothing.

Chapter 4 of this thesis also considers the design of the battery-supercapacitor energy storage system for power smoothing at a wind farm. Unlike [95-97], however, a BPF and a HPF are used to divert the mid-frequency and the high-frequency components of the wind power to the BESS and to the SC respectively. The method to determine the cutoff frequencies of the filters is described. It is based on the developed concept of minimum overlap energy, and its application to the results of EMD of the wind power.

2.3 Dispatch Planning of Wind Power

In spite of the advantages of wind energy, the perturbing wind power can impact negatively on power system performance, as explained in Section 2.2. Also, wind power unsteadiness and variability make the dispatchability of wind power generation a challenging task.

2.3.1 Issues pertaining to wind power dispatch

In order to stimulate wind power generation, varieties of policies have been set up and implemented in many counties, especially in America, Canada, Denmark, Germany, Turkey, Australia, China, Japan and South Korea [99, 100]. Different countries have developed policies in accordance to their national conditions and goals. The most effective policies include feed-in-tariff (FIT), renewable portfolio standard (RPS), production incentives, pricing law and quota system [101]. Among these policies, FIT and RPS are more popular. FIT requires transmission or distribution companies to pay for electricity generated from renewable energy sources at a fixed price set by the government [69, 102]. RPS, also called renewable electricity standard (RES), requires increased generation of electricity from renewable sources [101]. Pricing law fixes the price of electricity from the wind. Quota system sets a certain quota for electricity generation from renewable sources.

However, due to the uncertainty in the harnessable wind power, wind power generation is often regarded as not dispatchable and it has often been excluded in the dispatch planning of the grids. For example, wind power has not been included in [103] in which the independent system operator uses security-constrained unit commitment program to do the dispatch planning for the day-ahead electricity market. Typically short-term dispatch planning is conducted by the electricity grid operators a day ahead. The grid operators carry out generators' schedule according to the

generation plans of all the generators, which are committed a day ahead of power delivery [104]. For example, in Singapore, the power system operator (PSO) of Energy Market Authority (EMA) requires all the generation companies in Singapore to indicate the time of operation and the quantity of electricity they can supply in advance. Then the market clearing engine will do the dispatch schedule. In order to achieve economic dispatch, one has to find the optimal allocation of power output from different power generators so that minimum cost of electricity generation is realized. Prior to the large-scale integration of RE, the grid operator only has to consider the conventional power generators. For the conventional coal-fired or natural gas-fired power plants, accurate forecast of power supply can be achieved. If the operator were to include the contributions from the renewable generators such as wind and solar, it will be challenging to predict accurately the harnessable output power from these renewable sources due to the stochastic characteristic of wind and solar irradiation. This is despite varieties of power forecast methods have been developed in recent years. Expensive generation reserves have to be provided for grid system to ensure adequate level of security and reliability [7]. Thus penalties (i.e. imbalance charge) will be charged for the difference between the committed generation schedule and actual power supply [105].

One possible way to improve on the dispatchability of the wind power is to utilize ESS such that the net output power of the combined wind power-ESS can be more readily committed to realize economic advantage [106]. Accordingly, a literature review on the application of ESS in dispatch planning of wind power is given in the next section.

2.3.2 Literature review on the application of ESS in dispatch planning of wind power

A variety of dispatch strategies for a wind farm incorporated with an ESS have been proposed in the literature. In [72, 107], the ESS is used to balance the difference between the committed and the actual available wind generations such that the combined power from wind generators and ESS matches pre-committed power. The references have shown that the ESS enables the wind farm to deliver firm hourly power output to the grid, thus enhancing the dispatchability of wind power generation. In [108], stochastic optimization is utilized to determine the day-ahead and week-ahead reference power for pumped hydro energy storage which aims to offset the wind power forecast error. The benefit from using stochastic optimization is the reduction of the overall system production cost when compared to a conventional approach. In [109], a dispatch scheme is developed to achieve power dispatchability of a wind farm by using a BESS. The required energy capacity of the BESS is determined by optimizing the life span worth of the BESS. In the scheme, the BESS is allowed to operate cyclically between fully discharged and fully charged modes, so that it can make full use of the energy capacity and can prolong the lifetime of BESS. The confidence level of the wind farm with BESS to meet the committed power schedule is investigated based on the confidence level of wind power forecast accuracy. In [110, 111], the fluctuating wind power goes to a stand-by BESS and an in-service BESS delivers constant power to the grid. When the in-service BESS reaches the maximum the depth of discharge (DoD), the two BESS interchange their roles. The scheduled power from the wind farm with dual BESS committed ahead is decided according to the predicted wind power and the SOC of the two BESS. Besides, the method to determine power capacity of the BESS has been proposed. In [112], an operational dispatch scheme for a wind farm incorporated with a BESS is proposed based on wind power forecasts. The scheme attempts to mitigate negative impacts of wind power forecast errors on the dispatch planning, as well as to prolong

the lifetime of the BESS. It only utilizes one BESS to imitate the dual BESS system shown in [110, 111]. To be specific, the interchange of the two BESS is replaced by switching the combined wind farm-BESS power between the optimistic and pessimistic forecasted wind power obtained by interval prediction. The advantages of the single BESS system are the lowered capital cost and the easier operation. Furthermore, another improvement is that both the power and energy capacities of BESS have been decided. In [113], two ESS are also utilized to help the power dispatch for a wind farm. One ESS functions to optimize the schedule of total power output from the wind farm and ESS; while another ESS offsets the forecast errors in real-time operation.

Other research works consider the economic value of the wind farm incorporated with an ESS when developing the dispatch strategy. In [114, 115], the strategy is for the ESS to store wind energy during period of low tariff while the stored energy shall be released over periods of high tariff to increase the economic gain. In [116], the optimal bidding and operation of a wind generation company and a hydro-generation company is obtained by maximizing the total revenue of the two companies and minimizing the penalties because of the difference between the committed and the actual available wind generations. The authors of [86] determine the constant power dispatched from the wind farm equipped with BESS and the power and energy capacities of BESS by maximizing the net profit obtained by the wind farm.

All the above works propose the various dispatch schemes for a wind farm incorporated with ESS. The dispatch strategies are based on wind power forecasts and the ESS are used to mitigate the negative impacts due to the errors in the forecast. The dispatch bids would consist of the wind farms' output power specified at regular interval of ΔT, with ΔT in the order of 15 – 60 minutes. Therefore, only the low-frequency oscillating wind power components in which their periods are comparable or larger than ΔT will be expected to contribute significantly to the net export of energy to the grid system within each bit. Furthermore, it is much easier to obtain

accurate forecast of the low-frequency wind power in comparison to the approach shown in the above works in which the complete wind power is forecasted, since the variations of the low-frequency wind power components would be slower compared to those in the higher frequency components. Hence, only the low-frequency components should be considered for the short-term dispatch planning. This is the approach used in Chapter 5 of this thesis, and it is a distinct advantage over that proposed by the other researchers. These low-frequency components are extracted using a LPF. On the design of filter, [117] indicates that the setting of filter's cutoff frequency depends on the power market rules. Using discrete Fourier transform and the filters, the wind power is decomposed into four components: intraweek, intraday, intrahour and real time. Each component is addressed by a suitable ESS. The energy capacity of each ESS can be determined to deal with the corresponding fluctuating component. The authors in [118] explain the selection of the cutoff frequency should consider the cost of the ESS and that the response time of the ESS would impose an upper limit on the cutoff frequency setting. However, there is no analysis in [117, 118] on how the cutoff frequency can be determined. Although [109] also develops the power dispatch strategy based on the forecasted low-frequency components of wind power, the method to determine the cutoff frequency of the LPF has not considered the frequency range that the BESS has the ability to deal with. Unlike [109, 117, 118], this thesis proposes a new method to design the LPF based on a rigorous analysis of wind power using EMD technique and the developed concept of minimum overlap energy. Chapter 3 will provide greater details of the proposed method.

2.4 Energy Storage Systems (ESS)

As elaborated in Section 2.2, the random and uncontrollable nature of wind power could degrade grid security and reliability. This issue makes large-scale introduction of wind power generation into grid systems an extremely challenging task. One possible solution is to include a power buffering mechanism, through the introduction

of ESS. Indeed, the application of ESS into wind power generation system has attracted great attention in recent years [119-121].

2.4.1 Some common ESS

An introduction of selected ESS which could be utilized in conjunction with wind power generation is presented as follows.

The development of supercapacitor started from 1960s [122]. This type of capacitor is an electrochemical double layer capacitor (EDLC) in essence. No electronic transfer and chemical reaction occur in this energy storage medium. Long cycle-life, high power density, small volume, fast response and high efficiency are the strong points of supercapacitor. It is suitable for short-term applications. However, it is relatively costly and its energy density is low compared to the conventional batteries [32, 76, 123].

Flywheels and SMES have similar characteristics with SC [33]. For flywheels, the energy is stored up in the form of kinetic energy, with the high-speed wheel as the carrier. With regard to SMES, a superconducting electromagnetic coil stores the energy in magnetic field [124]. Compared with SC and flywheels, SMES has negative impacts on the environment because the strong magnetic field is bad for health [125]. Also, SMES is a less mature technology when compared to the other two ESS [126].

Electro-chemical batteries have high energy density and cycling ability. They can respond to load fluctuations at their terminals very quickly and have relatively high round trip efficiency [122]. Batteries are modular, so they can be readily installed nearly anywhere in grid systems, and the construction period is short. Battery modules connected in shunt and series can produce a BESS with high voltage and power capacity. Indeed, BESS has seen ready applications for power quality enhancement,

load leveling, area regulation and protection, voltage and frequency control, spinning reserve duty and VAR support [124, 127]. However, BESS has some disadvantages as well. One is that the battery's lifetime is influenced by the temperature change during the charging and discharging processes. This is due to the chemical reactions occurring within the battery cells. Therefore it is necessary to control the temperature change in order to prolong battery life. Another problem is the effects of the DoD and rate of discharge on life-cycle of the battery. The life-cycle will be lowered if the DoD is large. In addition, high discharge rate is also harmful to the battery because of the heat produced. Furthermore, the disposal of used battery can be a major concern due to certain harmful or toxic materials contained in the batteries [122, 127].

Flow battery energy storage system's major advantages over conventional batteries are its small self-discharge and that the power capacity is independent from the energy capacity [31, 76, 123]. Its cycle life is not affected by over-discharge. The efficiency ranges from 70% to 85%. Drawbacks are relatively high cost and more complicated structure [128]. It is a relatively new system compared with the conventional batteries, so there are not many flow battery energy storage systems applied commercially [129].

PHS for practical large-scale utility application dated back to some 75 years ago. Off-peak AC power is used to pump water from a low level to a high level and then the water is released to drive turbine so as to meet the demand at peak load periods [31]. The round trip efficiency is normally about 70%-85% [123, 130]. It has long storage period. The power ratings is up to several thousand MW [78]. The weakness of PHS is that a vast wide area with suitable geographical features is required. While such landscape can meet the requirement, one has to consider the environmental impacts of the storage scheme. The applications of PHS involve energy management, frequency control and supply of reserve. An example of large PHS is the Bath county with capacity of 2710 MW in U.S [131].

Besides PHS, compressed air energy storage system (CAES) is also a large-scale ESS suitable for long-term application. The power rating is in the range of 5-300 MW. CAES is a system where the air is compressed either in underground cavern or over ground tanks. When needed, the air under high pressure is released for electric power generation. Its major disadvantage is also the problem in obtaining sites for use. The 290 MW CAES plant in Germany and the 110 MW CAES plant in US are typical CAES plants [78]. Currently, the advanced adiabatic CAES (AA-CAES) is under development [132, 133]. Examples of CAES used in RE applications can be found in [134-136].

2.4.2 Characteristics of various ESS: a comparison

Table 2.1 Comparison of characteristics of various ESS [78]

Systems	Power rating and discharge time		Storage duration		Capital cost		
	Power rating	Discharge time	Self discharge per day	Suitable storage duration	$/kW	$/kWh	¢/kWh-Per cycle
PHS	100–5000 MW	1–24 h+	Very small	Hours–months	600–2000	5–100	0.1–1.4
CAES	5–300 MW	1–24 h+	Small	Hours–months	400–800	2–50	2–4
Lead-acid	0–20 MW	Seconds–hours	0.1–0.3%	Minutes–days	300–600	200–400	20–100
NiCd	0–40 MW	Seconds–hours	0.2–0.6%	Minutes–days	500–1500	800–1500	20–100
NaS	50 kW–8 MW	Seconds–hours	~20%	Seconds–hours	1000–3000	300–500	8–20
ZEBRA	0–300 kW	Seconds–hours	~15%	Seconds–hours	150–300	100–200	5–10
Li-ion	0–100 kW	Minutes–hours	0.1–0.3%	Minutes–days	1200–4000	600–2500	15–100
Fuel cells	0–50 MW	Seconds–24 h+	Almost zero	Hours–months	10,000+		6000–20,000
Metal-Air	0–10 kW	Seconds–24 h+	Very small	Hours–months	100–250	10–60	
VRB	30 kW–3 MW	Seconds–10 h	Small	Hours–months	600–1500	150–1000	5–80
ZnBr	50 kW–2 MW	Seconds–10 h	Small	Hours–months	700–2500	150–1000	5–80
PSB	1–15 MW	Seconds–10 h	Small	Hours–months	700–2500	150–1000	5–80
Solar fuel	0–10 MW	1–24 h+	Almost zero	Hours–months	–	–	–
SMES	100 kW–10 MW	Milliseconds–8 s	10–15%	Minutes–hours	200–300	1000–10,000	
Flywheel	0–250 kW	Milliseconds–15 min	100%	Seconds–minutes	250–350	1000–5000	3–25
Capacitor	0–50 kW	Milliseconds – 60 min	40%	Seconds–hours	200–400	500–1000	
Super-capacitor	0–300 kW	Milliseconds – 60 min	20–40%	Seconds–hours	100–300	300–2000	2–20
AL-TES	0–5 MW	1–8 h	0.5%	Minutes–days		20–50	
CES	100 kW–300 MW	1–8 h	0.5–1.0%	Minutes–days	200–300	3–30	2–4
HT-TES	0–60 MW	1–24 h+	0.05–1.0%	Minutes–months		30–60	

Table 2.2 Comparison of characteristics of various ESS [78]

Systems	Energy density (Wh/L)	Power density (W/L)	Specific energy (Wh/kg)	Specific power (W/kg)	Life time(years)	Cycle times(cycles)	Influence on environment
PHS	0.5-1.5	0.5-1.5	0.5-1.5	-	40-60	10,000-30,000	Negative
CAES	3-6	0.5-2	30-60	-	20-40	8000-12,000	Negative
Lead-acid	50-80	10-400	30-50	75-300	5-15	500-1000	Negative
NiCd	60-150	80-600	50-75	150-300	10-20	2000-2500	Negative
NaS	150-250	~140-180	150-240	150-230	10-15	2500	Negative
Li-ion	200-500	1500-10,000	75-200	150-315	5-15	100-10,000	Negative
Fuel cell	500-3000	500+	800-10,000	500+	5-15	1000+	Negative
VRB	16-33	~<2	10-30	166	5-10	12,000+	Negative
ZnBr	30-60	~<25	30-50	100	5-10	2000+	Negative
PSB	~20-30	~<2	~15-30	-	10-15	-	Negative
Solar fuel	500-10,000	-	800-10,000	-	-	-	Benign
SMES	0.2-2.5	1000-4000	0.5-5	500-2000	20+	100,000+	Negative
Flywheel	20-80	1000-2000	10-30	400-1500	~15	20,000+	Almost none
Capacitor	2-10	100,000+	0.05-5	~100,000	~5	50,000+	Small
Super-capacitor	10-30	100,000+	2.5-15	500-5000	10-30	100,000+	Small
TES	80-500	-	80-200	10-30	10-20	-	Small

Table 2.3 Comparison of characteristics of various ESS [76]

Systems	Discharge efficiency (%)	Cycle efficiency(%)	Response time	Operating and maintenance cost	Maturity
PHS	~87	70-85	Minutes	0.004$/kWh, ~3$/kW/year	Mature
CAES	~70-79	54	Minutes	0.003$/kWh, 19-25$/kW/year	CAES commercialized, AA-CAES developing
Lead-acid	85	70-80	Milliseconds,<1/4 cycle	~50$/kW/year	mature
NiCd	85	~60-70	Milliseconds,<1/4 cycle	~20$/kW/year	Commercialized
NaS	85	~75-90	-	~80$/kW/year	Commercialized
Li-ion	85	~90-97	Milliseconds,<1/4 cycle	-	Demonstration
Fuel cell	59	~20-50	seconds,<1/4 cycle	0.0019-0.0153$/kW	Developing/demo.
VRB	~75-82	75-85	<1/4 cycle	~70$/kW/year	Demo/early commercialized
ZnBr	~60-70	~65-75	<1/4 cycle	-	Demonstration
PSB	-	~60-75	20 ms	-	Developing
Solar fuel	-	~20-30	-	-	Developing
SMES	95	~95-97	Milliseconds,<1/4 cycle	0.001$/kWh, 18.5$/kW/year	Demo/early commercialized
Flywheel	90-93	~90-95	Seconds,<1 cycle	~0.004$/kWh, ~20$/kW/year	early commercialized
Capacitor	~75-90	~60-70	Milliseconds,<1/4 cycle	<0.05$/kWh, 13$/kW/year	Commercialized
Super-capacitor	95-98	~90-97	Milliseconds,<1/4 cycle	0.005$/kWh, ~6$/kW/year	Developing/demo.
TES	-	~30-60	Not for rapid response	-	Demo/early commercialized

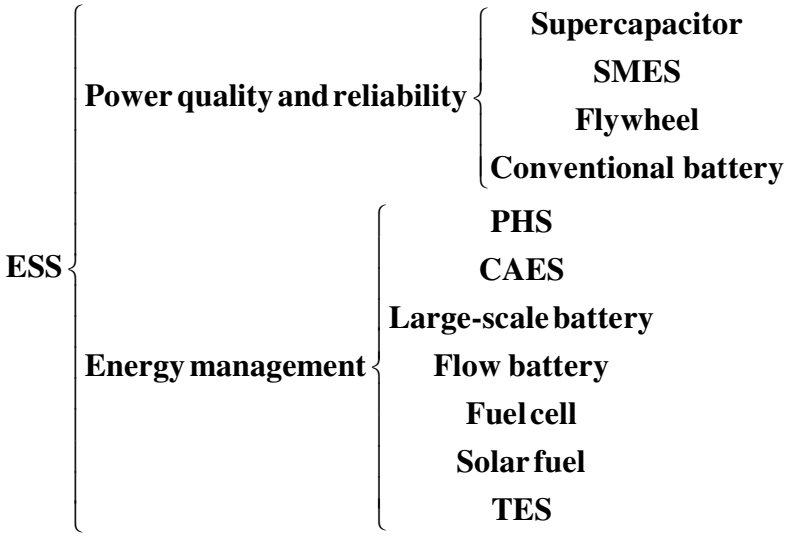

Figure 2.13. ESS classification [78]

The main technical characteristics of the common energy storage mediums are compared in Table 2.1, Table 2.2 and Table 2.3. These parameters have significant reference value when choosing ESS for a specific application. Generally, the choice of suitable storage medium should be in accordance to the purpose of application.

According to the comparisons of the power rating and discharge time of different ESS listed in Table 2.1, ESS can be classified into two categories. The first category includes SC, flywheels, SMES and conventional batteries. They have high power capacity but relatively low energy capacity due to relatively short discharge time. They are usually used in power quality or uninterruptible power supply (UPS). The other category is mainly applied for energy management. The ESS under this category include PHS, CAES, thermal energy storage system (TES), large-scale batteries, flow batteries, fuel cells and solar fuel. They have higher energy capacity and longer discharge time. The ESS classification is summarized in Figure 2.13.

Furthermore, from the tables, the following conclusions can also be drawn.

Since SC, SMES and flywheel have large self-discharge per day, so they are suitable for short-term applications. PHS, CAES, flow batteries, fuel cell and solar fuel have almost zero or very small self-discharge. They can be used for long-term storage durations. Most conventional batteries are applied for the medium-term storage durations.

In terms of the cost of ESS, the cost per kWh per cycle and the energy capital cost of PHS and CAES are the lowest. Lead-acid battery, NaS and VRB's operating and maintenance cost is relatively high. SC, SMES and flywheel's cost/kW is low but cost/kWh-cycle is high, so they are suitable for the high power short-term (up to several hours) applications.

PHS and CAES have low power and energy densities and they usually occupy vast wide geographical area. SC, SMES and flywheel have high power density and specific power but low energy density and specific energy. The density of conventional batteries is higher than that of flow batteries.

The cycle life of SC, SMES and flywheel are among the highest of all the ESS (>20,000). The mechanical ESS such as PHS, CAES and flywheels also have high cycle times (>10,000). In addition, because of chemical deterioration, the conventional batteries, flow batteries and fuel cell have relatively lower cycle times.

On the impact on the environment, the solar fuel has positive impacts while PHS, CAES, batteries, flow batteries, fuel cells and SMES all have negative influences on the environment.

SC, SMES and flywheel have very high cycle efficiency (>90%); while CAES, TES, solar fuels and fuel cells have low cycle efficiency (<60%).

PHS and lead-acid battery are the two most mature ESS technologies (>100 years). AA-CAES, PSB and solar fuel are still in the developing stage while the remaining ESS are either in demonstration stage or are being commercialized.

From the above discussion and considering the impacts of the unsteady wind power on the quality of power supply and the dispatch planning, the subsequent chapters of this thesis propose to utilize the supercapacitor and BESS in the smoothing of the high-frequency and mid-frequency components of the wind power and to buffer the low-frequency wind power by PHS for the dispatch planning of wind power.

2.5 Conclusions

This chapter provides a literature review on wind power, its impacts on grid and the roles ESS could play in wind power smoothing and dispatch planning. First, wind power variability is discussed. Then a detailed explanation of how the wind power fluctuations could impact power systems in terms of degrading voltage quality and introducing network frequency deviations. A brief literature of existing reported works on the applications of ESS in smoothing wind power is then presented. Challenges to wind power dispatch planning are discussed and the relevant research related to using ESS to improve on the dispatchability of the wind power is given. As ESS can play a vital role in the wind power application, an introduction on the various types of ESS and a brief comparison of their technical characteristics is also included.

CHAPTER 3. Segregation of Wind Power for Power Quality Enhancement or Dispatch Planning Purposes Using Minimum Overlap Energy Concept

As explained in Section 2.2, unsteady wind power could degrade power quality as well as making the dispatch planning of wind generation a challenging task. For this reason, maximum allowable ramp rates in the output power of wind farms have been stipulated in grid interconnection documents such as [137]. The stipulation is required because traditional method to mitigate the negative impact of the perturbing power is through the application of the regulating actions of other on-line conventional generators. However, the practice is expensive. Unless other viable techniques to smoothen the fluctuations are found, this issue can be one major impediment to the successful large-scale integration of wind power generation into grid systems. The focus of the thesis is to develop methods, with the view to alleviate these difficulties through the application of ESS. In the attempt to achieve the objectives, it shall be seen shortly that a signal processing technique known as EMD shall be utilized. Furthermore, the outcome of EMD analysis on wind power shall be applied to the design of a hierarchical energy storage scheme. The scheme involves the use of filters in the control of power flows of the energy storage elements. The method to design the filters is developed in this chapter. It is based on the developed concept of minimum overlap energy, and its application to the results of EMD of the wind power. In this way, the design of the filters is founded on a more credible theoretical basis than that given in [95-97, 109, 117, 118].

This chapter is therefore organized in the following way. The technique of EMD is briefly introduced in Section 3.1. The three-level ESS and its associated control loop

shall be explained in Section 3.2. The main contribution, on the method to design the filters is described in Section 3.3. Numerical examples are included in Section 3.4 to illustrate the proposed filter design approach while the main findings are presented in Section 3.5.

3.1 Empirical Mode Decomposition: An Introduction

Fourier spectral analysis is a general method for data analysis. Although it has the advantages of prowess and simplicity, it is only valid for analysis data obtained from linear and stationary process. For the processing of non-stationary data-set, methods include the spectrogram, the wavelet analysis, the Wigner-Ville distribution, evolutionary spectrum, the empirical orthogonal function (EOF) expansion and others. Most of them are still based on Fourier analysis, so they can only deal with linear systems.

A new and a powerful method suitable for analyzing non-stationary and nonlinear data is based on the EMD. EMD is adaptive, intuitive, direct and highly efficient. With EMD, any complex data set can be decomposed into several intrinsic mode functions and a residue function. The residue is a trend and a monotonic function. The resulted intrinsic mode function (IMF) can be linear or nonlinear and can be non-stationary. The reason why EMD is applicable for nonlinear and non-stationary process is that it is based on the local characteristic time scale of the signal. All the events have to be identified by the time of occurrences. The decomposition is a process which straightforwardly extracts the energy with different intrinsic time scales that characterize the oscillation of the data set. For only by adapting to the local variations of the data can the decomposition fully account for the underlying physics of the processes and not just to fulfill the mathematical requirements for fitting the data. Also, the decomposition method is complete and practically orthogonal. Completeness guarantees the precise extent. The instantaneous frequencies of the IMF

can be obtained by the Hilbert transform. The resulted energy-frequency-time distribution is called the Hilbert spectrum.

Although EMD is versatile and robust for nonlinear and non-stationary signal processing, there are several points for further improvements. EMD is a series of sifting processes. In each sifting process, the upper and lower envelops are formed by spline fitting from the local maxima and minima. Hence, firstly the spline fitting should be improved. Second, the spline fitting resulted in problems at two ends of the fit due to wide swing. Third, weak signals may embed in stronger ones. When weak signals embed in strong signals, it may be difficult to pick up the extrema. In this case, the strong and weak signals can be separated before the sifting process, when necessary. Finally, the individual IMF does not ensure a clear physical meaning. Research effort is continuing to overcome these problems.

Interested readers may refer to [93] for more details on EMD.

3.1.1 Intrinsic mode function

The IMFs are obtained in the first step of EMD analysis. A better understanding of the process can be gained by referring to Figure 3.2.

An IMF refers to a function that satisfies the following conditions:

1) Over the complete period, the total number of extrema must be equal to the total number of zero crossing points; or they must be different by no more than one;
2) For each point, the mean of the upper and lower envelopes must be zero.

The condition 1) is evident and a stationary Gaussian process has a similar requirement: the conventional narrow-band requirements. While condition 2) is innovative since it has requirement on the local rather than the global.

Figure 3.1 shows a typical IMF. IMF stands for the vibration mode in the non-stationary and nonlinear signal. Each cycle contains only one mode of oscillation. Therefore, IMF is not a narrow-band signal but it is both amplitude and frequency modulated. IMF can be regarded as a generalized Fourier expansion. So the IMFs are of variable frequency and amplitude, with respect to time.

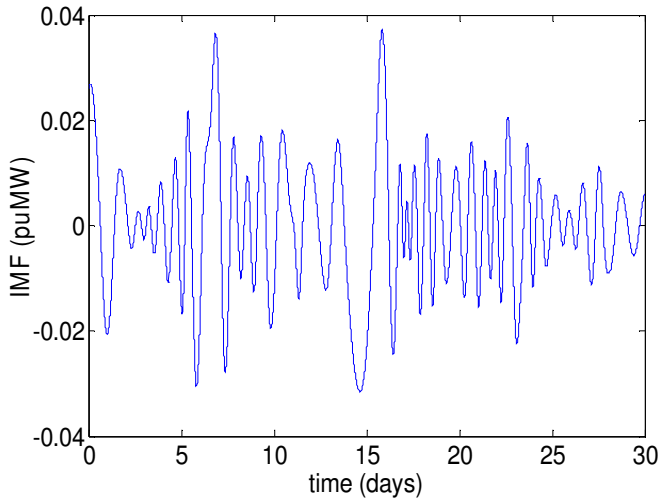

Figure 3.1. A typical intrinsic mode function

3.1.2 The empirical mode decomposition method

In the original non-stationary data set, one oscillation is riding on top of another. Every oscillation is of one characteristic time scale. The decomposition is actually a sifting process and it is a systematic way to extract the IMFs which have different intrinsic time scales. The different scales can be identified by the time lapse either between two consecutive zero crossings or between successive maxima and minima.

In this thesis, the decomposition adopts the time lapse between consecutive extrema as the time scale for one IMF. This will result in a higher resolution and it is also applicable to non-zero mean data set, such as the non-stationary wind power.

The procedure of EMD is as follows. Assume $x(t)$ is the original data set.

1) First recognize all the extrema include the maxima and minima in the signals. Connect all the local maxima of the original data by a cubic spline line to produce the upper envelop. The lower envelop is obtained using the same method from all the local minima.

2) Obtain the mean of the upper and lower envelops and denoted as m_1.

3) Obtain the difference between the original data and the mean which is designated as h_1.

$$h_1 = x(t) - m_1 \tag{3.1}$$

The above three steps can be illustrated by Figure 3.2.

4) Based on condition (1) and (2) above, determine whether h_1 is an IMF. If it is not an IMF, h_1 is treated as the data set. Calculate h_{11} using (3.2) where m_{11} is the mean of the upper and lower envelops in the second sifting process

$$h_{11} = h_1 - m_{11} \tag{3.2}$$

Repeat the above procedure until h_{1k} is determined to be an IMF.

$$h_{1k} = h_{1(k-1)} - m_{1k} \tag{3.3}$$

h_{1k} is the first IMF of the original data and denoted as c_1.

5) Treat the difference between $x(t)$ and c_1 as the new data and repeat the above sifting process.

$$x(t)-c_1=r_1 \tag{3.4}$$

$$r_1-c_2=r_2 \tag{3.5}$$

…

$$r_{n-1}-c_n=r_n \tag{3.6}$$

6) Stop the sifting procedure if c_n or r_n is less than certain pre-set value of substantial consequence or r_n is monotonic.

7) The original data is thus decomposed into n IMFs and one residue.

$$x(t)=\sum_{i=1}^{n} c_i + r_n \tag{3.7}$$

The n IMF components are locally non-overlapping time scale components. Although adjacent IMFs may include the same scale vibrations, they would occur at different locations.

From the decomposition process, it can be seen that the EMD has effectively utilized the data-set because all the data are needed to form the longest period component. Furthermore, the zero or mean references are not necessary since the trend is excluded automatically. The above two points are the distinct advantages of EMD.

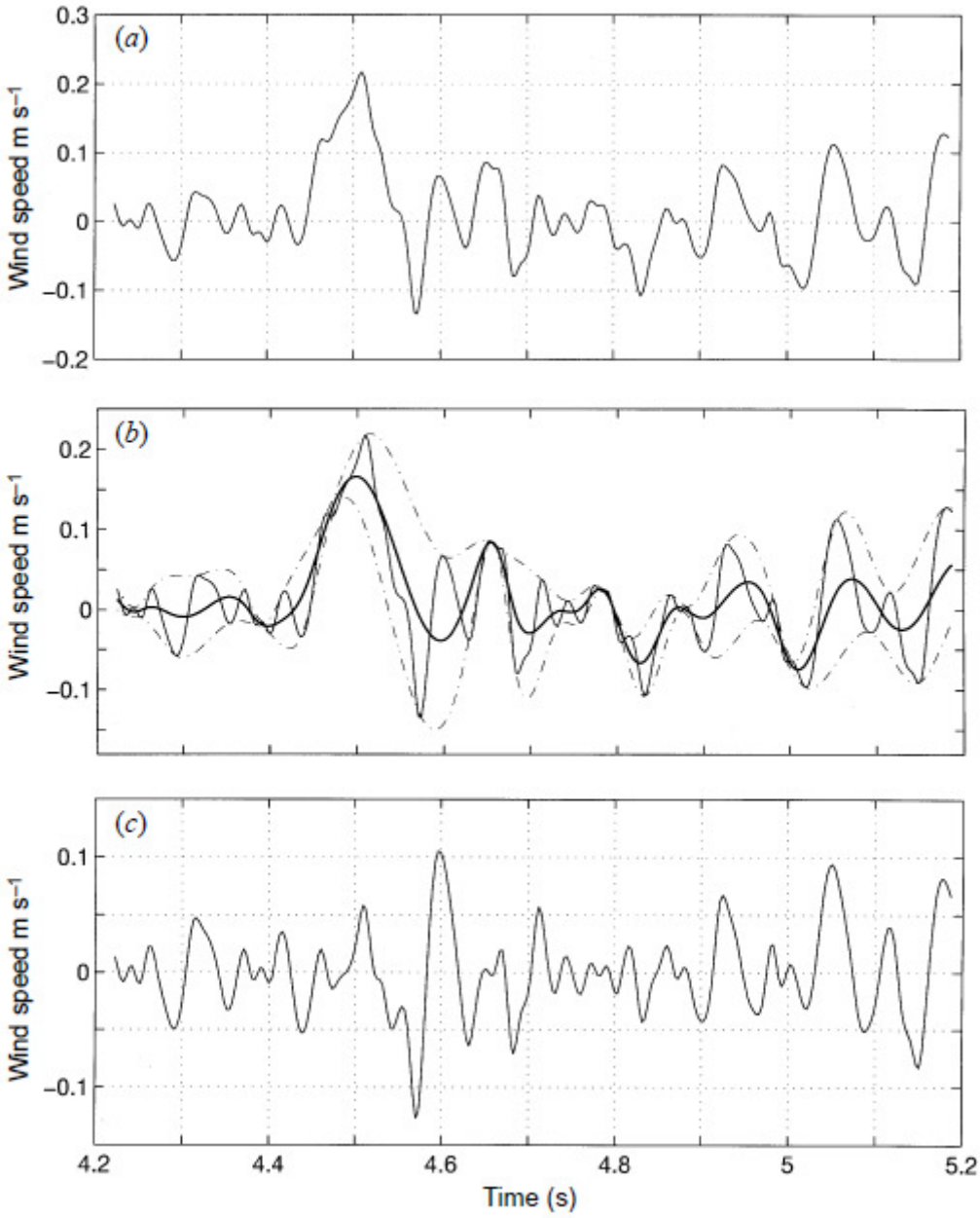

Figure 3.2. Illustration of the sifting processes: (a) The original wind speed; (b) The original wind speed in thin solid line, the upper and lower envelops in dot-dashed lines and the mean of the two envelops in thick solid line; (c) The difference between the original wind speed and the mean. [93]

3.2 A Conceptual Hierarchical ESS Scheme for Wind Power Smoothing and Dispatch Planning

As stated in the previous section, the objective of the thesis is to develop ESS scheme. The purpose is to alleviate the degradation of power quality due to the perturbing wind power and to overcome the issue of the non-dispatchability of the wind power. To set the scene for such a study, consider a large geographical area containing n groups of WTG. Each group of the WTG is assumed to have the typical capacity of up to 100 MW. The groups are interconnected to a large transmission-distribution (T&D) system, as shown in Figure 3.3. Within the area, it is also assumed there is ample water resource to support a large-scale PHS.

The n groups of the WTG are dispersed within the area, with the result that the harnessed wind powers $P_{w,i}(t)$, i = 1, …n will not be perfectly correlated. Notwithstanding the fact that the so-called spatial smoothing effect [138] applies and the stochastic nature in the aggregated wind power $\sum P_{w,i}(t)$ will be reduced, the direct injection of $P_{w,i}(t)$ into the grid system would induce variations in the network voltage and frequency, in the manner as described in Section 2.2. The extent of the voltage and frequency variations would depend on the level of injections and the short-circuit level at the point of injection, among other factors. Hence, in the proposed hierarchical ESS scheme, Figure 3.3 shows the inclusion of a BSHESS. The choice of the BSHESS as the medium of energy buffer is based on the assumed power capacity of the WTG group of up to 100 MW, and on the characteristics of the various currently-available ESS shown on Table 2.1, Table 2.2 and Table 2.3. While more detail of the design of the BSHESS shall be explained in the next chapter, it is sufficient to state herewith that the BSHESS is installed at the group level of the WTG such that the net output wind power $P_{L,i}(t)$ of group i is much smoother than that seen in $P_{w,i}(t)$. Next, it is reasonable to expect the total power contribution from the n groups of the WTG would be much larger than 100 MW and $P_L(t)$ would still be

perturbing, the smoothing action by the BSHESS notwithstanding. Hence, the inclusion of the high-energy capacity PHS is to provide another level of smoothing. The design of the PHS would be described in greater detail in Chapter 5.

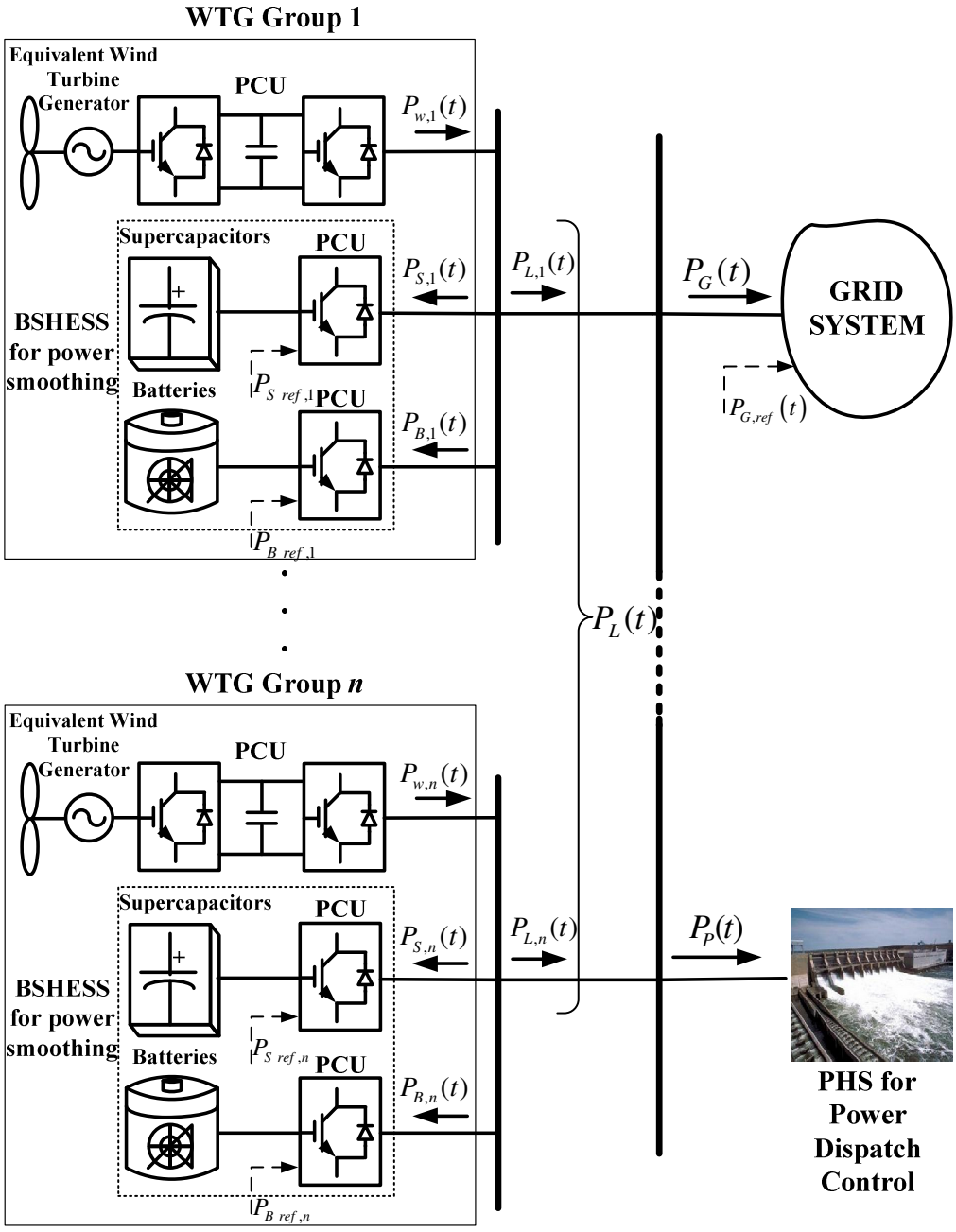

(a)

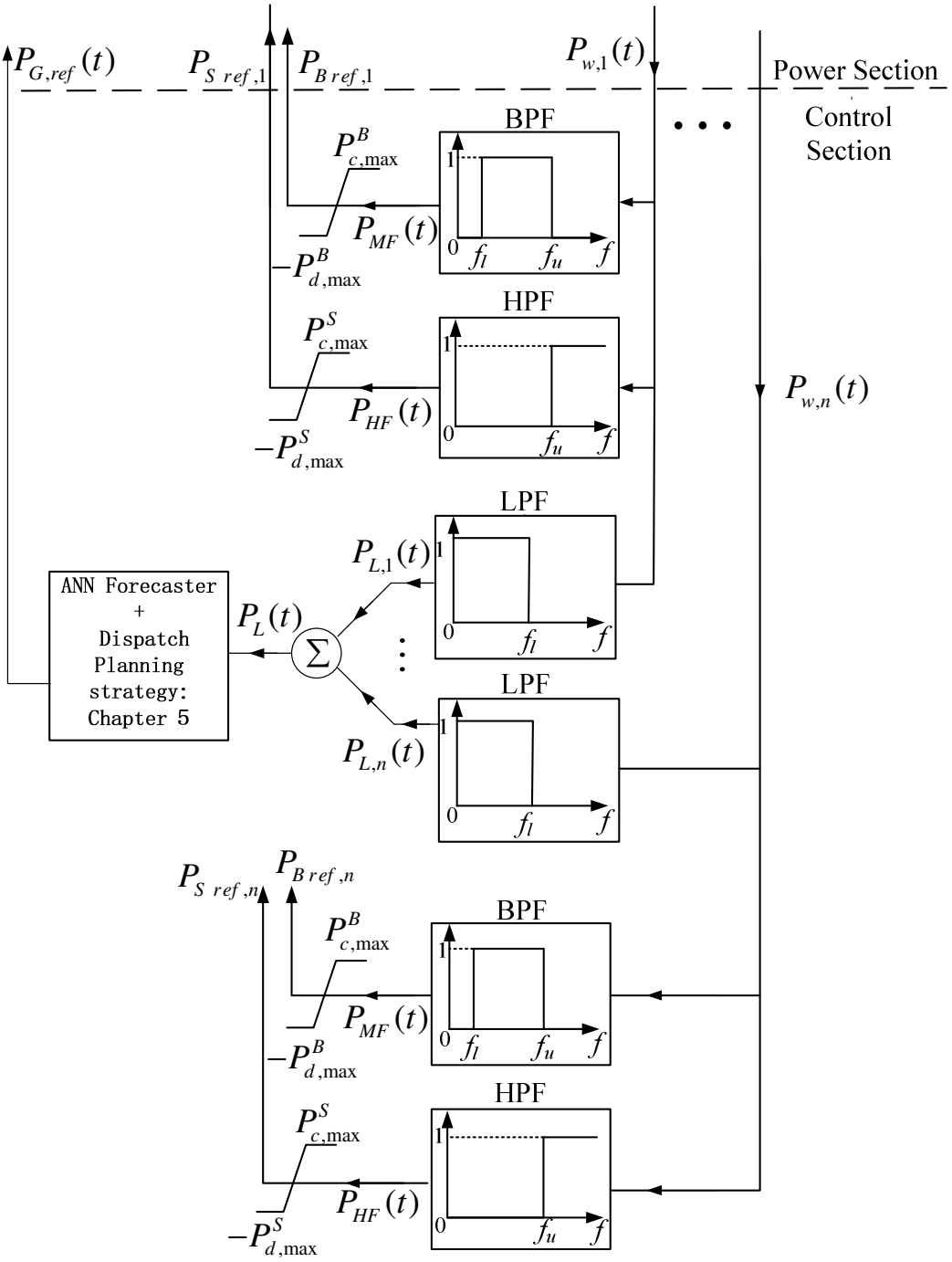

(b)

Figure 3.3. A conceptual large-scale wind power generation scheme incorporated with BSHESS for power smoothing and the PHS for power dispatch: (a) power section; (b) control section.

Next consider the power flows shown in Figure 3.3. Within the WTG group i, $P_{w,i}(t)$ denotes the aggregated output power from all the WTG within the group. Also shown is an equivalent power conditioning unit (PCU) consisting of a generator-side converter, dc-link capacitor and a grid-side inverter. The function of the generator-side converter is to achieve MPPT through controlling the speed of the generator while the grid-side inverter controls the dc-link voltage. The precise manner how this is done is well-described in [139] and shall not be elaborated here. As explained earlier, there are grid connection rules such as [137] which govern the maximum allowable ramp rate in the delivered power to the grid. Comprising of BESS and SC, the BSHESS is therefore to smooth the net power flows $P_{L,i}(t)$ so that $P_L(t)$ complies with the connection rules. As shall be detailed in Chapter 4, the BESS acts to buffer the mid-frequency variations of the wind power while the SC perform to remove the high-frequency wind power perturbations. $P_{S,i}(t)$ and $P_{B,i}(t)$ are the output powers of the SC and BESS respectively.

After the high- and mid-frequency components of the wind power have been smoothed out by the BSHESS, only the low-frequency wind power $P_{L,i}(t)$ flows to the T&D system and the PHS. The PHS is included here to buffer the aggregated low-frequency wind power $P_L(t)$ through a power flows control strategy. Details of the strategy will be described in Chapter 5, with the aim that short-term dispatch planning of the wind power can be realized. $P_P(t)$ denotes the power flows to the PHS while $P_G(t)$ is the net dispatched power from the n groups of the WTG-ESS which is to track the reference signal $P_{G,ref}(t)$.The arrows of the figure indicate the assumed positive direction of the power flows. Accordingly,

$$P_{w,i}(t) = P_{S,i}(t) + P_{B,i}(t) + P_{L,i}(t) \tag{3.8}$$

$$P_L(t) = \sum_{i=1}^{n} P_{L,i}(t) \tag{3.9}$$

Figure 3.3(b) shows the corresponding power flows control loop of the scheme. It shows that the signal corresponding to the wind power is filtered to yield the high-, mid- and low-frequency components. This is achieved by the HPF, BPF and LPF respectively. The HPF contains the passband $f \geq f_u$ where f_u is the filter cutoff frequency. The HPF only allows components in $P_{w,i}(t)$ which have frequencies higher than f_u to pass through. Concurrently, the BPF has the lower and upper cutoff frequencies f_l and f_u respectively: The BPF only allows components in $P_{w,i}(t)$ having frequencies between f_l and f_u to pass through. Finally, the LPF contains the passband $0 \leq f \leq f_l$ where f_l is the filter cutoff frequency: The LPF only allows components in $P_{w,i}(t)$ which have frequencies lower than f_l to pass through. The functions of the HPF, BPF and LPF are complementary. In practice, SC and BESS have finite charging and discharging power capabilities. $P_{HF}(t)$ is constrained to the range $[-P^S_{d,max}, P^S_{c,max}]$ to produce the signal $P_{S\ ref,\ i}(t)$, where $P^S_{c,max}$ and $P^S_{d,max}$ denote the maximum charging and discharging power limits of the SC. Similarly, $P_{MF}(t)$ must be constrained to within the power range $[-P^B_{d,max}, P^B_{c,max}]$ to yield the signal $P_{B\ ref,\ i}(t)$, where $P^B_{c,max}$ and $P^B_{d,max}$ are the charging and discharging power capabilities of the BESS. The output signals $P_{S\ ref,\ i}(t)$ and $P_{B\ ref,\ i}(t)$ constitute the reference signals for the PCU of the SC and BESS in the BSHESS of the i^{th} WTG group so that the output powers of the SC and BESS are to track $P_{S\ ref,\ i}(t)$ and $P_{B\ ref,\ i}(t)$. Thus the SC and BESS act as buffers to the high- and mid-frequency components of $P_{w,i}(t)$. Similarly, the low-frequency wind power components of the group $P_{L,i}(t)$ are obtained at the output of the LPF. As shown in the figure, the summated signal $\sum P_{L,i}(t)$ then forms the control input to the PHS power flows control strategy. Detail of the strategy shall be described in Chapter 5 when the dispatch planning of the large-scale wind generation will be discussed.

The above paragraphs have outlined the concept behind the design of the hierarchical ESS scheme. However, an important aspect of the design remains unanswered and this is pertaining to the precise manner on how the values of f_u and f_l are to be determined. Indeed, the authors are unaware of any reported rigorous analysis

pertaining to the determination of the filters' cutoff frequencies to achieve wind power smoothing and power dispatch. The remaining part of this chapter is devoted exclusively to this topic.

3.3 Determination of Filters' Cutoff Frequencies

In the following procedure to design the filters, it is assumed long-term historical data on $P_w(t)$ is available over a period T_s. The subscript i to denote the i^{th} WTG group has been omitted as the following analysis is equally applicable for all groups.

3.3.1 Segregation of wind power intrinsic mode functions for power quality enhancement or dispatch planning purposes

The proposed approach to determine the filters' cutoff frequencies requires the application of the EMD technique. From the introduction to EMD given in Section 3.1, it is clear that any data set can be decomposed into a number of IMFs $c_i(t)$), i = 1, 2, …, n and a mean trend or residue $r_n(t)$. Thus for the problem in hand, $P_w(t)$ can be expressed in terms of $c_i(t)$ and $r_n(t)$ as

$$P_w(t) = \sum c_i(t) + r_n(t) \tag{3.10}$$

The IMFs represent the oscillation modes embedded in the data set while the residue indicates the trend. EMD would be a suitable tool to analyze $P_w(t)$ produced by the non-stationary wind resource. For example, Figure 3.4(b) shows the results obtained following the decomposition of a sample of the wind power data $P_w(t)$ measured at an existing wind farm. All the quantities are expressed in per unit MW (puMW) in the figure. $c_i(t)$, i = 1, g, k, m, are four IMFs where $1<g<k<m$. The wave-profile of each of the IMFs is a deformation from the simple sinusoidal form: The IMFs are both amplitude- and frequency-modulated, and are non-stationary. As the order i of the

IMF increases, the fluctuations in $c_i(t)$ become slower. Even within each $c_i(t)$, its frequency varies with time.

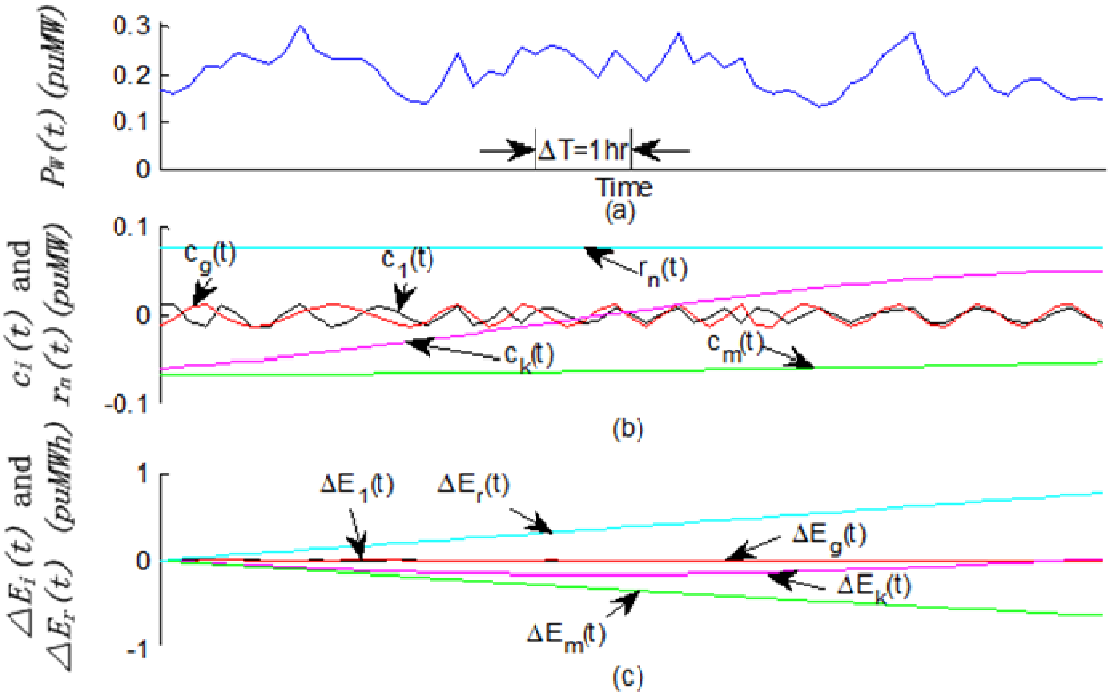

Figure 3.4. (a) A sample of wind power $P_w(t)$; (b) A sample of IMFs $c_i(t)$ and residue $r_n(t)$ obtained from the decomposition of $P_w(t)$ using EMD; (c) The changes of energy level $\Delta E_i(t)$ in $c_i(t)$ and $r_n(t)$.

An interesting analysis is to calculate the corresponding changes in the energy level $\Delta E_i(t)$ in $c_i(t)$ and $r_n(t)$ obtained by integrating these functions with respect to time. $\Delta E_i(t)$, expressed in per unit MWh, are shown in Figure 3.4(c). The fluctuating $\Delta E_i(t)$ indicates energy level contained in $c_i(t)$ is oscillating. $\Delta E_1(t)$ and $\Delta E_g(t)$ are excellent examples of those $\Delta E_i(t)$ which show insignificant amounts of the fluctuating energy contained in the wind power components $c_1(t)$ and $c_g(t)$ over the dispatch bid interval ΔT referred to in Section 2.3.2, provided ΔT is large compared to the periods of oscillations in $c_1(t)$ and $c_g(t)$. Thus $c_1(t)$ and $c_g(t)$ do not need to be considered in the dispatch planning as they would not contribute to any significant amount the net

change of energy over the interval ΔT. Instead, these fluctuating $c_i(t)$ have to be smoothed out in order to maintain acceptable power supply quality. Conversely, of the remaining $c_i(t)$ in which their $\Delta E_i(t)$ can be significant over ΔT, these lower-frequency components of $P_w(t)$ would need to be taken into consideration in the dispatch planning. In Figure 3.4(b), $c_k(t)$ and $c_m(t)$ are examples of these components. Another interesting point is the behavior of the residue function $r_n(t)$ in which the change in its energy level $\Delta E_r(t)$ is shown to increase with time: This is hardly surprising as $r_n(t)$ is a monotonic function. Hence, the low-frequency $c_i(t)$ and $r_n(t)$ are relevant in the dispatch planning.

In summary, the EMD allows $P_w(t)$ to be segregated into those $c_i(t)$ which would need to be dealt with for power quality consideration, whereas the remaining lower-frequency $c_i(t)$ and residue $r_n(t)$ functions will have to be considered for dispatch planning.

3.3.2 Ideal cutoff frequencies of the filters

Section 3.3.1 explains that the IMF of $P_w(t)$ can be grouped for either power quality improvement or dispatch planning purposes. In this section, the method to determine the ideal cutoff frequencies of the HPF, BPF and LPF which segregate $P_w(t)$ into the high-, mid- and low-frequency bands shall be described.

The segregation process starts from the examination of the frequency-time characteristics of the IMF. Through the application of Hilbert transform, the so-called instantaneous frequencies of the IMFs can be obtained [93]. However, it is difficult to relate the concept of instantaneous frequency with the conventional concept of filters' cutoff frequencies. Rather, in conventional concept, frequency is obtained by taking the reciprocal of the period between two consecutive zero-crossings of stationary waveforms. Thus, one could define the cycle frequency f_{ac} by inferring to the

reciprocal of the periods for all the cycles in each $c_i(t)$. Since $c_i(t)$ is frequency-modulated, while f_{ac} is time-varying, and to reflect this characteristic, f_{ac} is more appropriately re-written as $f_{ac,i}(t)$. A sample of $f_{ac,i}(t)$ obtained for $c_i(t)$, i = 1, g and m is shown in Figure 3.5. In this instance, again $1<g<m$. The curves are layered distributed: i.e., $f_{ac,i}(t)$ of lower order c_i has higher frequency and is shown in the upper layer. As the order i increases, its corresponding cycle frequency $f_{ac,i}(t)$ will reside in the lower layers. This is because from $c_1(t)$ to $c_m(t)$, the IMFs vary from fast to slower oscillations, as explained earlier.

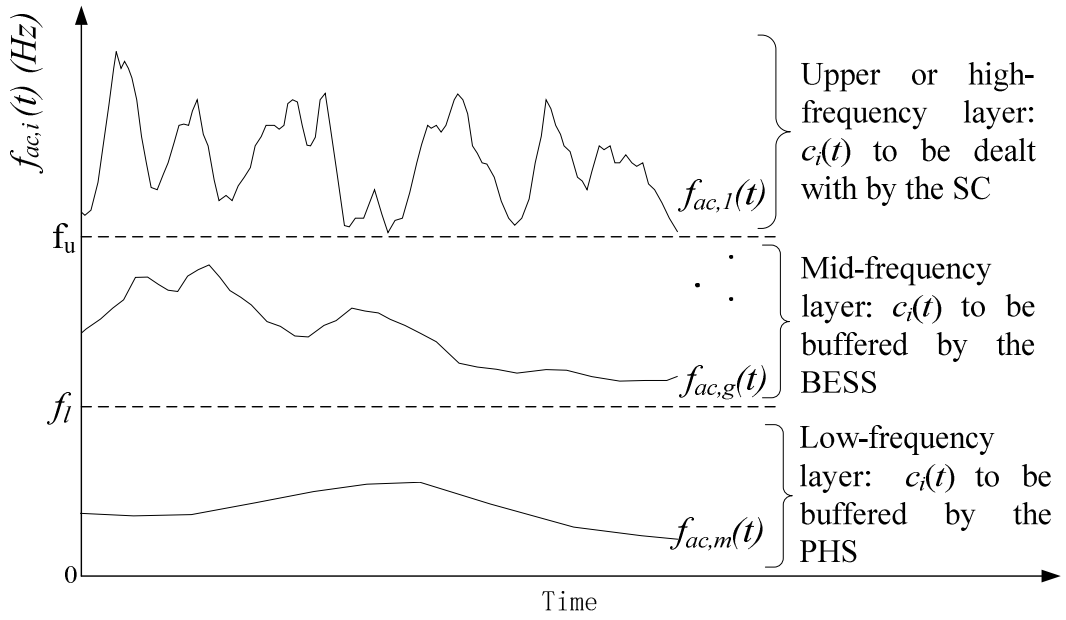

Figure 3.5. Typical plots of the cycle frequency $f_{ac,i}(t)$ of IMFs, their segregation into the upper or high-frequency, mid-frequency and low-frequency groups by the specification of the upper and lower cutoff frequencies of BPF.

Recall that working in conjunction with the HPF, the SC are to act as an energy buffer to smooth out the high-frequency wind power fluctuations while the BESS and the BPF are to reduce wind power perturbations of the mid-frequency band. The low-frequency wind power components and residue, which contain most of the energy in

the wind, are to be used for dispatch planning purpose by means of the LPF and the PHS. In view of this, it is next proposed to segregate the cycle frequencies $f_{ac,i}(t)$, i = 1,…, n into three domains. This is achieved by the specification of the upper and lower cutoff frequencies f_u and f_l, as reflected by the inclusion of the two cutoff frequencies in the $f_{ac,i}(t)$ plots in Figure 3.5. The key point in the specification of f_u is to ensure that ideally, there shall be a first group of $f_{ac,i}(t)$ curves which will reside entirely above f_u; the selection of f_l will lead to a second group of $f_{ac,i}(t)$ curves which shall lie exclusively below f_u but above f_l; a third group of $f_{ac,i}(t)$ curves which shall lie exclusively below f_l. While the exact method by which f_u and f_l can be so selected shall only be discussed later, nevertheless, the consequence would be that the IMFs $c_i(t)$ would also be segregated into three groups: There shall be one group of $c_i(t)$ corresponding to the first group of $f_{ac,i}(t)$ in which their cycle frequencies would be above f_u at all time, a second group of $c_i(t)$ corresponding to the second group of $f_{ac,i}(t)$ whereby for this group, $f_l < f_{ac,i}(t) < f_u$ for all t. Finally, the third group of the $c_i(t)$ would have their $f_{ac,i}(t) < f_l$. Since as the order i of $c_i(t)$ increases, $f_{ac,i}(t)$ decreases, the segregation has resulted in the IMFs being divided into the high-frequency IMFs, the mid-frequency IMFs and the low-frequency IMFs. As SC are amenable to buffer high-frequency power perturbations, the high-frequency IMFs with $f_{ac,i}(t) > f_u$ shall be dealt with by the charging-discharging actions of the SC. Conversely, as BESS would be more suited to buffer the mid-frequency power perturbations, thus the mid-frequency IMFs shall be handled by the BESS. In addition, the low-frequency IMFs with $f_{ac,i}(t) < f_l$ and the residue function buffered by the PHS will be used for the planning of the power dispatch. This desirable outcome is reflected in Figure 3.5, where it is shown that the high-frequency and the mid-frequency bands of the IMFs are to be dealt with by the SC and BESS respectively while the low-frequency IMFs are to be buffered by the PHS.

It would be most desirable if the above ideal situation can be reached because it would mean the buffering actions of the SC, BESS and the slower-responding PHS are completely decoupled from each other. The design of one ESS can then be carried out

without the need to consider the actions of the other two ESS. This is especially attractive as the BSHESS installations are dispersed within the area in the form of distributed storage. Each BSHESS can be designed in conjunction with its respective group of the WTG, whereas the PHS is a large-capacity centralized storage facility designed to cater for the whole area. Also, to ensure the BSHESS and the PHS can have a reasonable lifetime, bounds should be placed on the charge-discharge frequencies of the SC, BESS and PHS. For instance, typical duration to fully charge and discharge SC is less than 60 minutes. This would result in a cycle life of over 100,000 cycles [78] and a charge-discharge cycle frequency of some 2.7×10^{-4} Hz. Thus the SC could be tasked to buffer power fluctuations with cycle frequency higher than 2.7×10^{-4} Hz: a suitable choice of the lower bound on f_u, denoted as $f_{u,min}$, can be 2.7×10^{-4} Hz. Based on the ranges of life time and cycle life of various BESS shown in [78], it is estimated that the typical duration to fully charge and discharge BESS is less than 3 days, corresponding to a charge-discharge cycle frequency of some 3.9×10^{-6} Hz. The BESS should only be tasked to buffer power fluctuations with cycle frequency higher than 3.9×10^{-6} Hz and so a suitable choice of the lower bound on f_l, denoted as $f_{l,min}$, can be 3.9×10^{-6} Hz. Conversely, the typical charge-discharge cycle time for PHS is usually more than 6 hours [32], corresponding to a cycle frequency of about 4.63×10^{-5} Hz: thus the upper bound on f_l, denoted as $f_{l,max}$, can be set at 4.63×10^{-5} Hz. With life cycle of 2×10^{4}-5×10^{4} cycles, the lifetime of the PHS is expected to be 30 - 50 years [32]. Thus from these practical considerations, suitable bounds for the upper and lower cutoff frequencies of the BPF can be derived.

3.3.3 Determination of cutoff frequencies based on the minimum overlap energy concept

While the concept of ideal cutoff frequencies in the previous section appears attractive, unfortunately in practice, it is generally not possible to determine the ideal set of values for f_u and f_l such that the three groups of IMFs can be completely decoupled

over the whole study period T_S. This less-than ideal situation can be readily demonstrated by examining Figure 3.6. Figure 3.6(a) shows the cycle frequencies corresponding to the two consecutive IMFs $c_j(t)$ and $c_{j+1}(t)$ shown in Figure 3.6(b) and Figure 3.6(c). It is seen that by positioning f_u as shown in Figure 3.6(a), the sectors *ab* and *cd* of $f_{ac,j}(t)$ are below f_u whereas the sectors *ef* and *gh* of $f_{ac,j+1}(t)$ are above f_u. Hence, the choice of such a value for f_u would be less than ideal as over the instances *ab* and *cd,* the SC would not be providing the buffering action as the HPF would not allow those parts of $c_j(t)$ corresponding to these instances to pass through. The BESS shall be called upon to perform the buffering function instead. Hence, one cannot ignore the actions of the BESS over these overlapping instances *ab* and *cd*. Conversely, over the instances *ef* and *gh*, there would be buffering actions from the SC instead of from the BESS. Such overlapping incidents over *ab*, *cd*, *ef* and *gh* would complicate the design of the BSHESS because one cannot assume the complete decoupling between the buffering actions of the SC and the BESS at all time in T_S.

While the ideal set of f_l and f_u does not exist in general, one could nevertheless attempt to find the set of f_l and f_u which would lead to the so-called minimum overlap energy condition between the SC and BESS and between the BESS and PHS. The meaning of minimum overlap energy is now explained, again using Figure 3.6. In the figure, suppose the choice of f_u is such that the perturbations represented by the IMF c_j(t) are to be smoothened by the SC while those in c_{j+1}(t) are to be buffered by the BESS. Firstly, examine the intervals *ab* and *cd* in which $f_{ac,j}(t)$ of c_j(t) is lower than f_u. Therefore, the energy contained in c_j(t) over these instances would correspond to the shaded areas $E_1,\ldots,E_4$ under that segments of c_j(t) labeled as $a_1a_2a_3$ and a_4a_5. The energies will now be compensated by the charging or discharging actions of the BESS instead of, as intended, by the SC. By the same reasoning, one can also conclude that the energies corresponding to the areas $E_5,\ldots,E_8$ are now being dealt with by the charging or discharging of the SC instead of by the BESS. One can evaluate the total amount of the overlap energy E_o contained in all the shaded areas over T_S, by summing the absolute values of all E_i, i.e.

$$E_0 = \sum |E_i| \tag{3.11}$$

E_o is the total amount of energy pertaining to the un-intended, and un-desirable, cross-coupling charging and discharging actions of the SC and BESS. The degree of the cross-coupling increases with E_o. Clearly one could adjust the cutoff frequency f_u so that the corresponding E_o is minimum. This shall be the minimum overlap energy condition when there is the least amount of cross-coupling between the SC and the BESS over T_S.

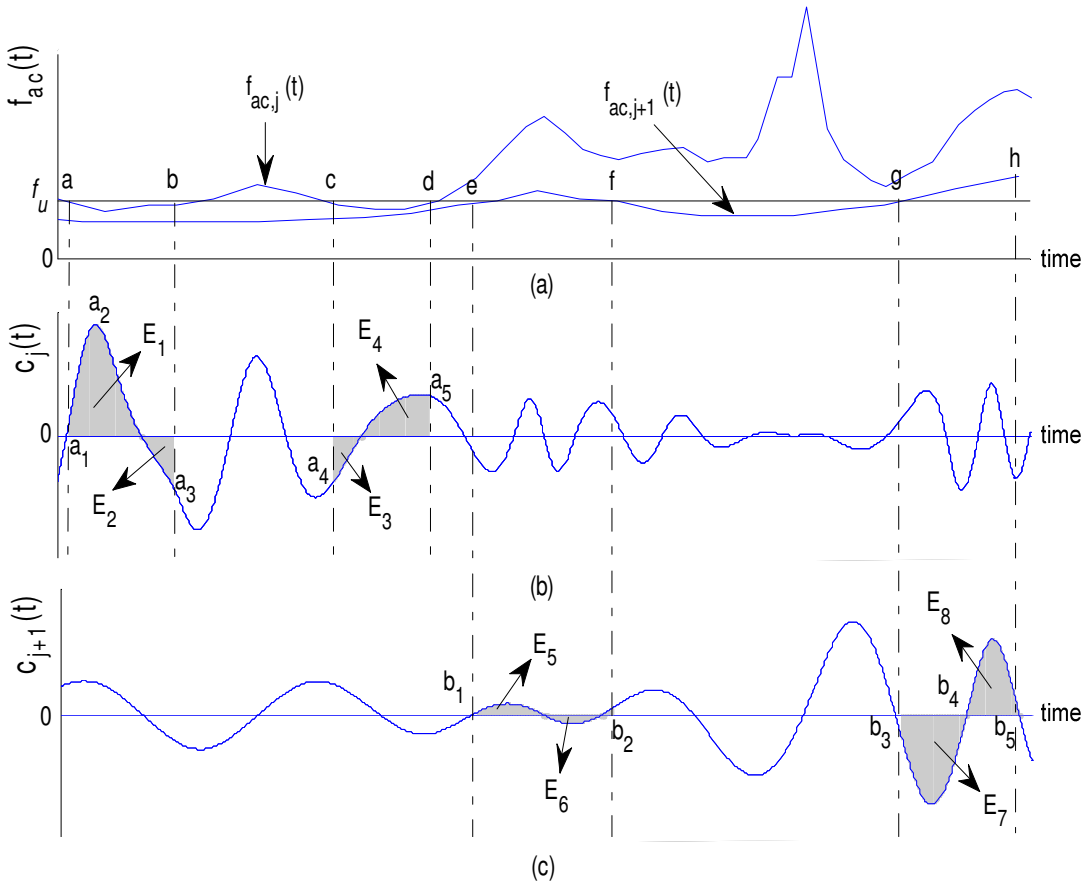

Figure 3.6. Determination of f_u using the minimum overlap energy method: (a) $f_{ac,j}(t)$ and $f_{ac,j+1}(t)$, (b) $c_j(t)$, and (c) $c_{j+1}(t)$.

Thus far, the search for the minimum overlap energy condition has only considered the overlap areas between the two consecutive IMFs $c_j(t)$ and $c_{j+1}(t)$, as dictated by the placement of f_u. However, it is also possible for segments of the cycle frequencies of $c_1(t),\ldots, c_{j-1}(t)$ to be below f_u, and for segments of the cycle frequencies of $c_{j+2}(t),\ldots, c_m(t)$ to be above f_u. Therefore, it is also necessary to track the respective values of these possible overlap energies between $f_{ac,i}(t)$ and f_u, $i= 1,\ldots, m$ and include these overlap energies into the calculation of E_o. The order m is selected in such a way that $f_{ac,i}(t)$, $i = m+1, \ldots, n$ are all below the lower bound of the lower cutoff frequency f_l, i.e. below $f_{l,\,min}$. This condition is expressed as

$$f_{ac,i}(t) < f_{l,\min}, for i = m+1,...,n \tag{3.12}$$

As explained earlier, the BESS is unsuitable as a buffer for IMFs which have cycle frequencies lower than $f_{l,\,min}$, and therefore $c_{m+1}(t),\ldots,c_n(t)$ need not be considered when determining f_u of the BPF. Instead, $c_{m+1}(t),\ldots,c_n(t)$ are low-frequency fluctuations to be dealt with by the PHS.

Based on the above observation, clearly f_u could be adjusted until the minimum overlap energy condition is reached. The search for the minimum E_o is facilitated by the fact that there is a lower bound $f_{u,\,min}$ below which the SC are not suitable as an energy buffer. Hence the search for f_u would start from $f_{u,\,min}$ and then over a range of higher frequencies. Over this frequency range, the minimum E_o condition can be found. f_u corresponding to this minimum E_o is the most appropriate f_u setting for the BPF for the set $c_j(t)$ and $c_{j+1}(t)$.

Next, the above search procedure to determine the most suitable f_u must be carried out for $j = 1,\ldots, m$-1 such that for each set of $c_j(t)$ and $c_{j+1}(t)$, one would obtain the corresponding f_u for which E_o is minimum. Denote the values of f_u and E_o so obtained as $f_{u,Eo\,min,\,j}$ and $E_{o\,min,\,j}$ respectively. There shall be m-1 sets of $f_{u,Eo\,min,\,j}$ and $E_{o\,min,\,j}$, with each $f_{u,Eo\,min,\,j}$ being a possible setting value for f_u. However, as the desired design

objective is to achieve the minimum cross-coupling between the SC and BESS, thus one has only to select among the m-1 sets of $f_{u,Eo\ min,j}$ and $E_{o\ min,\ j}$, the set which has the lowest $E_{o\ min,\ j}$. Denote the condition when this occurs as $j = J$. The upper cut-off frequency for the BPF and the cut-off frequency for the HPF shall be set equal to $f_{u,Eo\ min,\ J}$.

$$f_u = f_{u,Eo\ min,\ J} \tag{3.13}$$

With this setting, the total amount of energy involved in the cross-coupling actions between the SC and BESS would have been reduced to the lowest level. The design procedure is summarized in the flowchart of Figure 3.7.

Using the same approach as described above, the setting of f_l corresponding to the least cross-coupling energy condition between the BESS and PHS can also be found. Again from Section 3.3.2, it is noted that f_l should be higher than $f_{l,\ min}$ and lower than $f_{l,\ max}$ when considering the effective operating range of the BESS and the PHS. So the search is to start from f_l equals to $f_{l,\ min}$ and up to the maximum value of $f_{u,Eo\ min,\ J}$, for each set of $c_i(t)$ and $c_{i+1}(t)$, for $i = k$+1, …,m-1. k should be selected such that $f_{ac,i}(t)$, i = 1,…, k are all above $f_{l,\ min}$, i.e.

$$f_{ac,i}(t) > f_{l,\min},\ for\ i = 1,...,k \tag{3.14}$$

However, from (3.12), $f_{ac,i}(t) < f_{l,\ min}$, $i = m$+1,…, n. Hence, the minimum overlap energy condition for determining f_l shall be searched among $f_{ac,i}(t)$ of $c_{k+1}(t)$ to $c_m(t)$. Following the same procedure as for determining $f_{u,Eo\ min,\ J}$, for each set of $c_i(t)$ and $c_{i+1}(t)$, determine the value of f_l for which E_o is minimum. Denote the values of f_l and E_o so obtained as $f_{l,Eo\ min,\ i}$ and $E_{o\ min,\ i}$ respectively. Select among the sets of $f_{l,Eo\ min,\ i}$ and $E_{o\ min,\ i}$ the set with the lowest $E_{o\ min,\ i}$. Denote the condition when this occurs as $i = I$. Set the lower cut-off frequency of the BPF as $f_{l,Eo\ min,\ I}$,

$$f_l = f_{u,Eo\ min,\ I} \tag{3.15}$$

In summary, the above design procedure has resulted in the BPF having the upper cutoff frequency setting of $f_{u,Eo\ min,\ J}$ and the lower cutoff frequency of $f_{l,Eo\ \min,\ I}$. The cut-off frequency of the HPF is $f_{u,Eo\ min,\ J}$ and that of the LPF is $f_{l,Eo\ \min,\ I}$. Under this minimum overlap energy condition, the energies contained in the cross-coupling actions between the SC and BESS, and that between the BESS and the PHS is at the minimum.

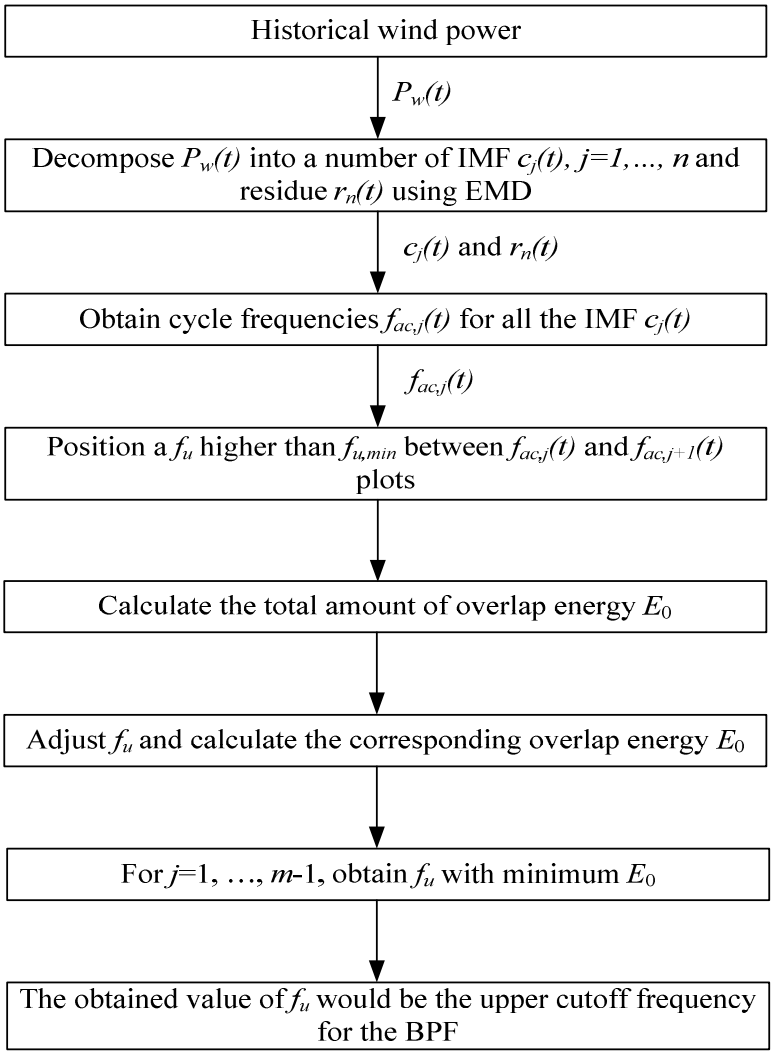

Figure 3.7. Design procedure to determine the upper cutoff frequency for the BPF.

The method introduced in this chapter requires long-term historical data on $P_w(t)$ is available. By following procedure introduced in Section 3.3, one can determine the cutoff frequencies of the filters. The implicit assumption is that future $P_w(t)$ will have the minimum overlap energy at the same cutoff frequencies as determined at the design stage. Based on this assumption, then in the real time application of the proposed scheme, the designed filters with the determined cutoff frequencies can still be used to decompose $P_w(t)$ into the high-, mid- and low-frequency bands so as to achieve minimum overlap energy.

3.4 Case study

The proposed approach is to be applied to the design of the HPF, BPF and LPF at an existing wind-farm in Jiangsu Province, China. Wind power data $P_w(t)$ shown in Figure 3.8, recorded between Jan to July 2007 and pertaining to the aggregated output power from 8×1.5 MW WTGs in the farm, is used in the design.

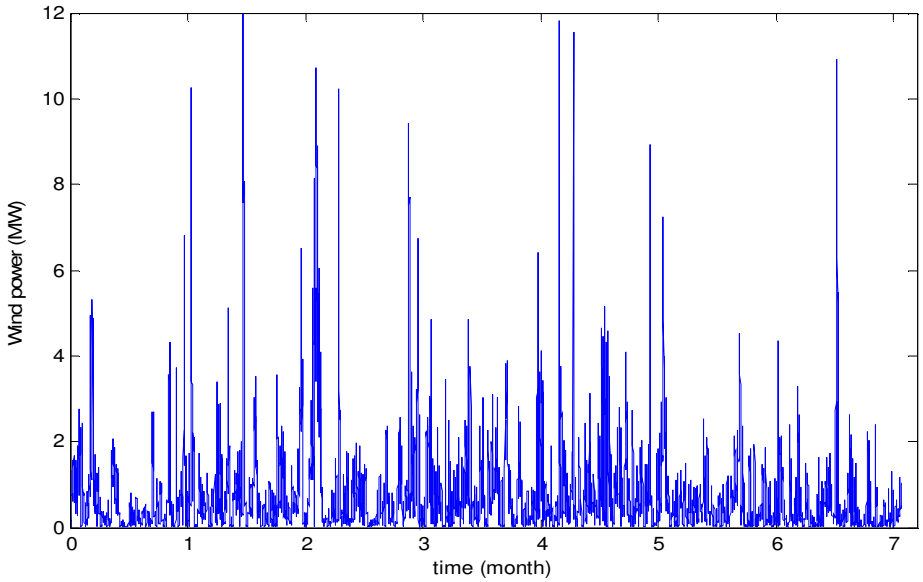

Figure 3.8. $P_w(t)$ over Jan-July 2007

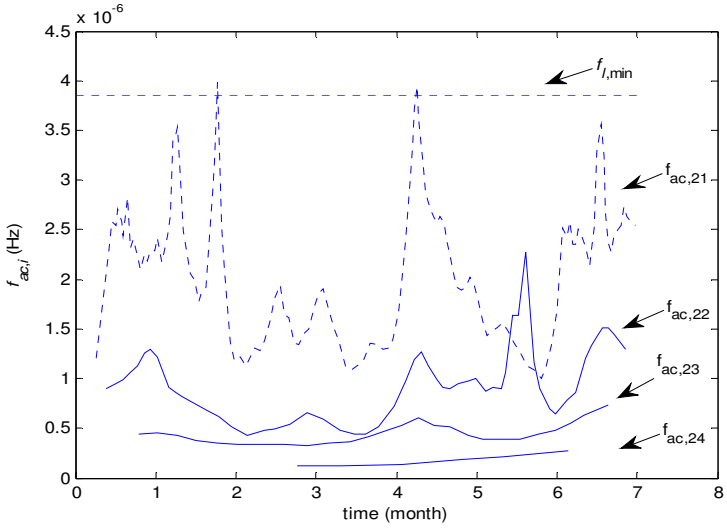

Figure 3.9. $f_{ac,i}(t)$ of $c_{21}(t)$ to $c_{24}(t)$

Firstly, the possible range for the upper cutoff frequency f_u of the BPF is to be determined. Using EMD, $P_w(t)$ was accordingly decomposed to yield 24 IMFs $c_i(t)$ ($c_1(t)$, …, $c_{24}(t)$) and the residue function $r_{24}(t)$ and a sample of which is as shown in Figure 3.4(b). The cycle frequencies $f_{ac,i}(t)$ for all $c_i(t)$ were calculated. Recall from Section 3.3.2 that the lower bound for f_l is in the vicinity of 3.9×10^{-6} Hz. As Figure 3.9 shows that $f_{ac,i}(t)$ for i = 22, 23 and 24 were all below this minimum value of f_l, hence, $c_{22}(t)$, $c_{23}(t)$ and $c_{24}(t)$ had not be taken into consideration when determining f_u.

The search procedure described in Section 3.3.3 was then performed to determine the minimum overlap energy (E_0) condition. Figure 3.10 summarizes the result of the search. It shows how E_0 varies with f_u and in this instance, the minimum E_0 condition (Point A) is reached when $f_{u,Eo\ min,\ j} = 4.38\times 10^{-4}$ Hz. This is in fact the minimum E_0 condition for j = 1, … , 22. The value of the minimum E_0 is 8.7 per unit MWh (puMWh) over the Jan-July 2007 period, on 12 MW base. Also, $f_{u,Eo\ min,\ J}$ of 4.38×10^{-4} Hz is above the lower bound on f_u of 2.7×10^{-4} Hz, a value alluded to in Section 3.3.2. Whence f_u of the BPF is set as 4.38×10^{-4} Hz.

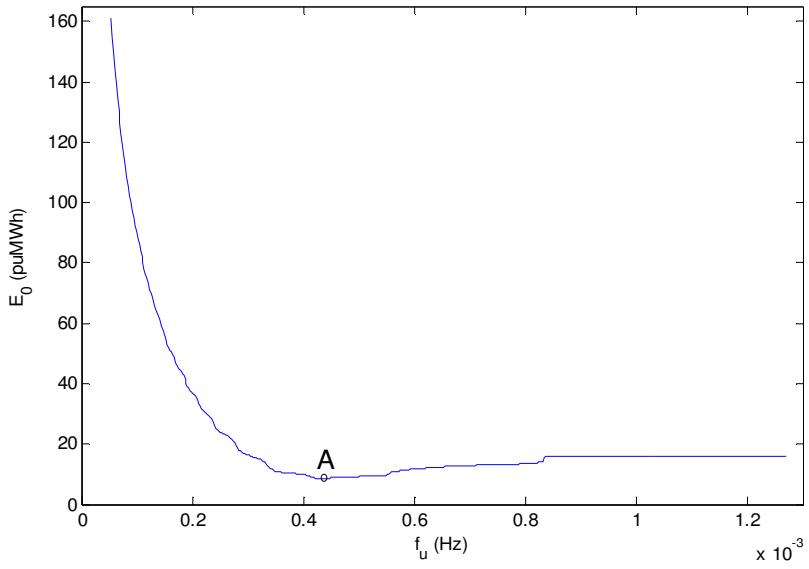

Figure 3.10. Outcome of the search for minimum E_0 condition: E_0 vs f_u for J=1.

It is interesting to note that in the filter designed by the authors of [97], f_u is selected to be 2.8×10^{-4} Hz. This cut-off frequency setting is relatively close to that determined using the present method. With $f_u = 2.8\times 10^{-4}$ Hz, however, Figure 3.10 indicates that E_0 is approximately 18.6 puMWh. It thus shows a higher level of coupling between the SC and the BESS.

Next, the lower cutoff frequency f_l is to be determined. Indeed, the search yielded the minimum E_o condition when f_l was set at 6.74×10^{-6} Hz. This setting is also above the lower bound $f_{l,\,min}$ and below the higher bound $f_{l,\,max}$ and is thus acceptable.

Thus by following the procedure described in Section 3.3.3, it has resulted in f_u and f_l of the BPF being determined to be 4.38×10^{-4} Hz and 6.74×10^{-6} Hz respectively. Although the cutoff frequencies selection will not completely decoupled the buffering actions of the SC, BESS and PHS, the selection will nevertheless result in minimal overlap energy between the ESS. Each of the ESS shall be able to maximize the amount of the energy it needs to deal with. Wind power fluctuations with frequencies

higher than 4.38×10^{-4} Hz are smoothed out by the SC. Those fluctuations between 6.74×10^{-6} Hz and 4.38×10^{-4} Hz are to be dealt with by the BESS. And the low-frequency wind power components with frequencies lower than 6.74×10^{-6} Hz are to be buffered by the PHS for dispatch planning purpose.

For a wind farm at a different location, due to different weather and atmosphere pattern, historical data on $P_w(t)$ over a sufficiently-long period T_s at that wind farm can be analyzed using the proposed EMD technique. The minimum overlap energy concept is applied to determine the cutoff frequencies of the filters for that wind farm. Furthermore, updated long-term historical data on $P_w(t)$ can be utilized to re-determinate the cutoff frequencies of the filter for the particular wind farm using the same method.

3.5 Conclusions

A conceptual large-scale wind power scheme consisting of BSHESS for power smoothing and the PHS for power dispatch has been described. The BESS, in conjunction with the BPF, acts to buffer the mid-frequency variations of the wind power while the SC and the HPF perform to remove the high-frequency wind power perturbations. Dispatch planning of the wind power is realized through buffering the low-frequency power fluctuations by a pumped hydroelectric system. By utilizing the EMD technique and the developed concept of minimum overlap energy, a new method to determine the cutoff frequencies of the high-pass, band-pass and low-pass filters has been described. In this way, the high-frequency, mid-frequency and low-frequency bands of the wind power fluctuations have been segregated to the extent that the SC, BESS and PHS can maximize the amount of energy they can deal with, with the least amount of cross-coupling between the three ESS. The proposed approach has been applied to the design of the HPF, BPF and LPF at an existing wind-farm.

CHAPTER 4. A Statistical Approach to the Determination of the BSHESS Storage Capacity to Achieve Wind Power Smoothing

In Chapter 3, the wind power is decomposed into high-, mid- and low-frequency bands based on the developed concept of minimum overlap energy applied to the IMF obtained from EMD analysis. To achieve the smoothing of the wind power, the high- and mid-frequency components of the wind power are then routed to SC and BESS respectively. The focus of this chapter is on the determination of the SC and BESS storage capacity required to undertake the wind power smoothing task for a group of WTG, such as at a wind farm. The dispatch planning for *n* groups of WTG in a large-scale wind power scheme will be discussed in the next chapter. Based on the designed filters, a statistical approach to determine the BSHESS capacity is developed in this chapter. The approach takes into consideration the cost of the BSHESS while the wind power smoothing objective is to be achieved at pre-specified probability level. Thus another new contribution of this thesis is that the proposed approach to determine the BSHESS capacity is unlike those contained in [92, 96]. In these two references, the BSHESS capacity has been obtained using deterministic methods. Effectiveness of the proposed design technique is demonstrated using data obtained from an existing wind farm.

This chapter is organized in the following manner. Section 4.1 presents the justifications in selecting the BSHESS for wind power smoothing. Section 4.2 proposes the control scheme of the BSHESS. A statistical method to determine the power and energy capacities of the BSHESS is then described in Section 4.3. Numerical examples are included in Section 4.4 to illustrate the proposed approach to

the design of the BSHESS. Main findings of this chapter are summarized in Section 4.5.

4.1 Justifications in Selecting Battery-Supercapacitor Energy Storage System for Wind Power Smoothing

Although Chapters 2 and 3 have considered the use of SC and BESS to mitigate high- and mid-frequency wind power fluctuations, this section shall explain why the combination of the SC and BESS is suitable for such an application. With due considerations to the attributes of the various ESS as described in Section 2.4, wind power variation components with periods of up to several hours are treated herewith as mid-frequency type whereas those having the cycle times of up to several minutes are regarded as high-frequency. Also, the nature of the wind power fluctuations is such that the mid-frequency wind power components tend to contain more energy than that in the high-frequency components [117]. Depending on the level of the wind power penetration, however, the high- and mid-frequency perturbations could degrade supply security to such an extent that grid code such as [137] is violated. Hence, to prevent the perturbing power components from being injected directly into the external grid system, power smoothing has to be carried out at the terminals of wind farms. This can be achieved by ESS of suitable specific energy and power densities and of adequate dynamic response ability. Notwithstanding the significant progress made in recent years on energy storage technology, hitherto, it is impractical to rely on one particular type of ESS to buffer both the high- and mid-frequency perturbations emanating from a wind farm which may have the capacity of up to 100-MW [140, 141]. Indeed, among the various types of ESS, SC have relatively high power density but its energy density is comparatively low. In contrast, BESS has higher energy density but lower power density [142]. Judicious use of the combination of the SC and the BESS would result in a hybrid ESS suitable for undertaking the wind power smoothing task. If only the BESS were to be used to

buffer the fluctuating wind power, the batteries will undergo more frequent charge/discharge sub-cycles when dealing with the high-frequency wind power components. The BESS useful life can be adversely reduced. On the other hand, if the SC were to be the only storage medium, its energy storage capacity would be such that the SC ESS is unlikely to be viable.

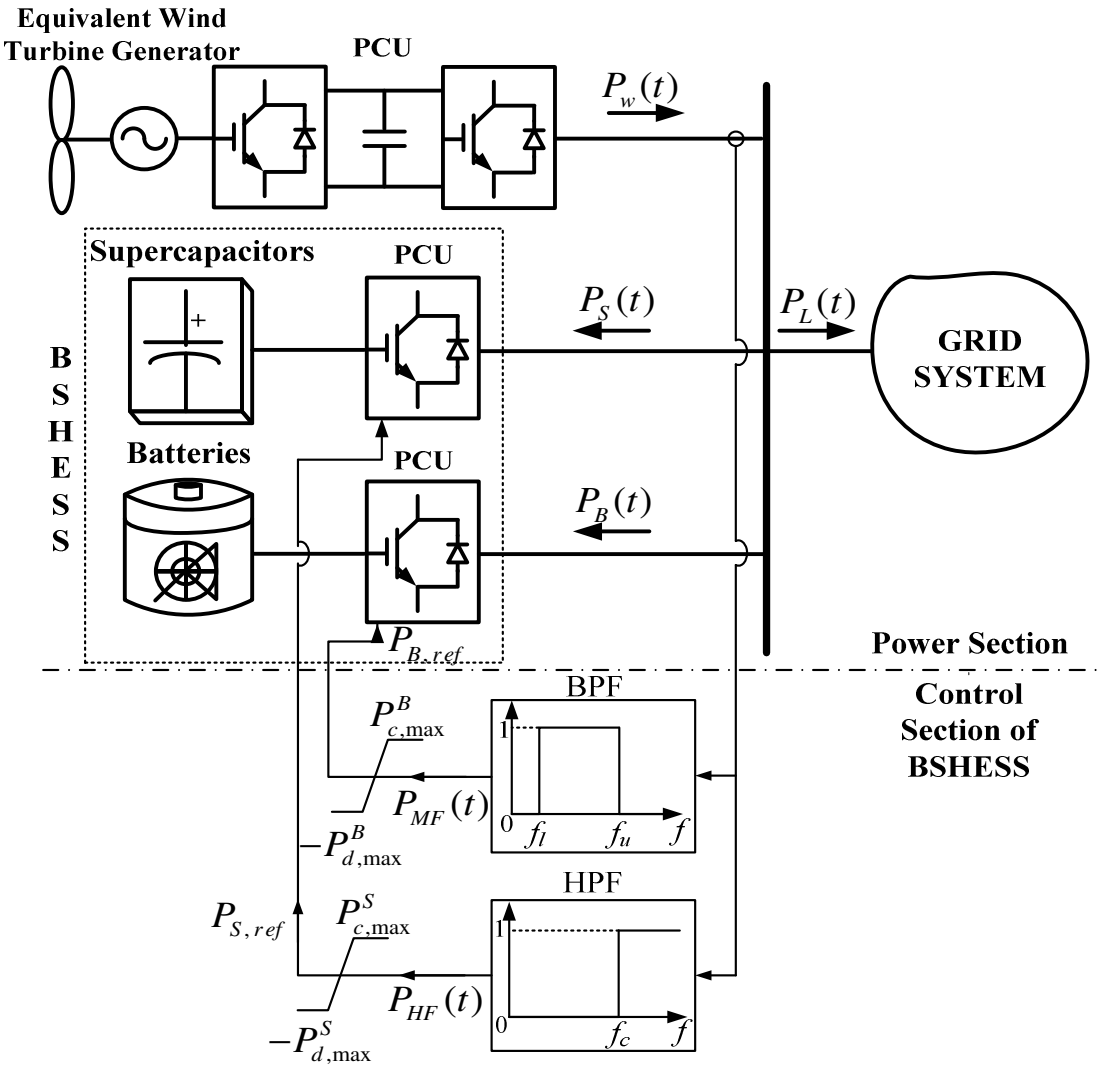

Figure 4.1. A grid-connected wind farm with BSHESS and the associated BSHESS control scheme for wind power smoothing.

In view of the above, a BSHESS is deemed suitable for undertaking the wind power smoothing task. Figure 4.1 shows a grid-connected wind farm incorporated with the BSHESS and its associated power flows control scheme.

4.2 BSHESS Control Scheme

The BSHESS control scheme for wind power smoothing is shown in the BSHESS "Control Section" in Figure 4.1. Recall that a BPF is to route components of $P_w(t)$ which have frequencies within certain band to the BESS and at the same time, the HPF is to be utilized to divert the relatively rapid fluctuating components in $P_w(t)$ to the SC. Thus as shown in Figure 4.1, the signal corresponding to $P_w(t)$ is filtered to yield the mid-frequency component $P_{MF}(t)$ of $P_w(t)$ at the output of the BPF. The upper and lower cutoff frequencies f_u and f_l of the BPF have already been determined based on the minimum overlap energy criteria using the search procedure described in Section 3.3.3. $P_{MF}(t)$ is to be used as the control signal to regulate the output power of the BESS.

In practice, however, BESS has finite charging and discharging power capabilities and they are denoted herewith as $P^B_{c,max}$ and $P^B_{d,max}$ respectively. While Section 4.3 shall explain how $P^B_{c,max}$ and $P^B_{d,max}$ are to be treated as design parameters, $P_{MF}(t)$ must therefore be constrained to within the power range $[-P^B_{d,max}, P^B_{c,max}]$ and yields the reference signal $P_{B,ref}(t)$. The BESS power flows $P_B(t)$ are to be regulated to track $P_{B,ref}(t)$. Similarly, the HPF produces the high-frequency component signal $P_{HF}(t)$ from the input $P_w(t)$. The cutoff frequency of the HPF is equal to the upper cutoff frequency of the BPF. Denote the maximum charging and discharging power limits of the SC as $P^S_{c,max}$ and $P^S_{d,max}$ respectively. The method to determine the values of the SC power limits shall also be explained in Section 4.3. Thus, $P_{HF}(t)$ is constrained to the range $[-P^S_{d,max}, P^S_{c,max}]$ to produce the reference signal $P_{S,ref}(t)$ which the output power $P_S(t)$ of the SC is to track. The generated reference signals $P_{B,ref}(t)$ and $P_{S,ref}(t)$

are directed to the respective PCU of the battery and supercapacitor banks to effect the power flows $P_B(t)$ and $P_S(t)$ respectively. Again the mechanism for controlling the power flows using the PCU can be found in [143] and shall not be repeated here.

4.3 Determination of BSHESS Storage Capacities

The next task in the design is to determine the SC and BESS power and energy capacities. The method to do so is as follows.

4.3.1 Impact of BESS and SC capacities on power smoothing

Since the BSHESS is subject to $P_w(t)$ varying in a random or stochastic manner, it is now proposed that a statistical approach be used to investigate the impact of the power and energy capacities of the BESS and SC on the power smoothing function. Firstly, one can readily obtain the mid-frequency component $P_{MF}(t)$ over the study interval T_S using $P_w(t)$ as the input to the designed BPF filter by following the design procedure described in Section 3.3.3. One can then construct the cumulative density function (CDF) of the $P_{MF}(t)$. Figure 4.2 shows an example of the CDF which shows that $P_{MF}(t)$ ranges from some -3.5 MW (discharging) to 9.5 MW (charging). One could therefore specify the BESS power capacity as 3.5 MW discharging and 9.5 MW charging, and in accordance to Figure 4.1, set the limits of the BPF to corresponds to $P^B_{d,max}$= 3.5 MW and $P^B_{c,max}$= 9.5 MW. Except for those overlapping instances between the SC and BESS and between the BESS and PHS for which the overlap energy has been reduced to the minimum, one can conclude that with these $P^B_{d,max}$ and $P^B_{c,max}$ capacities, the BESS can be expected to smooth out completely the perturbations $P_{MF}(t)$ by itself, provided the energy capacity of the BESS is also sufficiently large. Unfortunately $P^B_{d,max}$ and $P^B_{c,max}$ so determined may be so large that the BESS is uneconomical because such large capacity would only be fully utilized for extremely rare events.

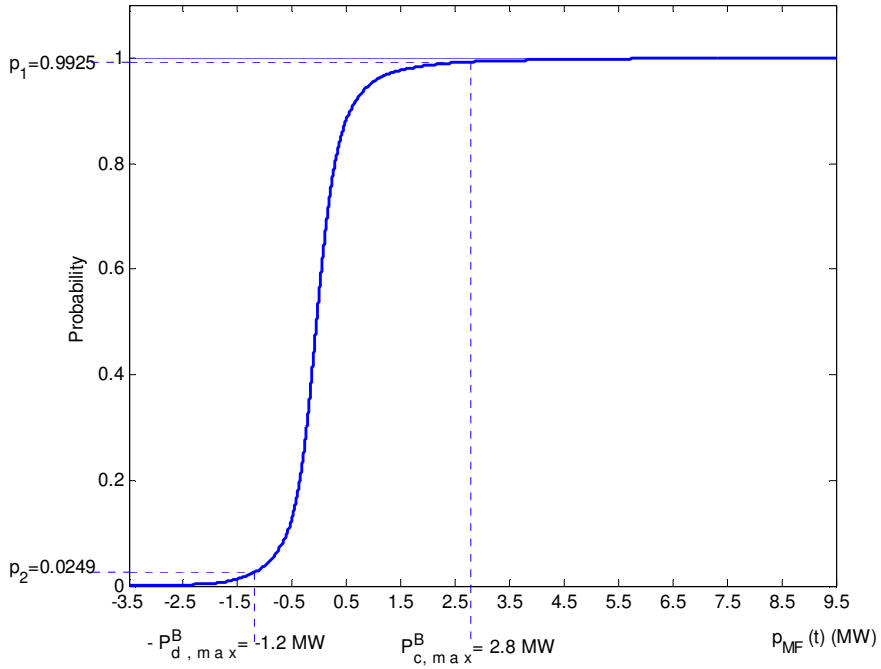

Figure 4.2. An example of CDF of $P_{MF}(t)$.

Instead, one should take into consideration the likelihood of the need. It is with this in mind that the proposed statistical approach is more suitable. It seeks to determine lower BESS charging/discharging power capacities such that the probability $P_{MF}(t)$ is within the BESS power capacities is at a pre-specified level of p_B. Mathematically, to achieve the power smoothing of the mid-frequency band using the BESS, this design task is expressed as the determination of $P^B_{d,max}$ and $P^B_{c,max}$ such that

$$P\left\{-P^B_{d,max} \le P_{MF}(t) \le P^B_{c,max}\right\} = p_B \tag{4.1}$$

In (4.1), $P\{\cdot\}$ denotes the probability the condition $\{\cdot\}$ is met. From the CDF, if

$$\left.\begin{aligned} P\{P_{MF}(t) \le P^B_{c,max}\} &= p_1 \\ P\{P_{MF}(t) \le -P^B_{d,max}\} &= p_2 \end{aligned}\right\} \tag{4.2}$$

From (4.1), therefore

$$p_B = P\left\{-P^B_{d,max} \le P_{MF}(t) \le P^B_{c,max}\right\} = p_1 - p_2 \tag{4.3}$$

With the discharging/charging power capacities $P^B_{d,max}$ and $P^B_{c,max}$, the reference signal $P_{B,ref}(t)$ for the BESS output power shall be forced to meet the following constraint equations

$$P_{B,ref}(t) = \begin{cases} P^B_{c,\max} & if\ P_{MF}(t) > P^B_{c,max} \\ P_{MF}(t) & if\ -P^B_{d,max} \le P_{MF}(t) \le P^B_{c,max} \\ -P^B_{d,max} & if\ P_{MF}(t) < -P^B_{d,max} \end{cases} \tag{4.4}$$

As an illustration of the above concept, suppose p_B is set to be 0.968. Again from Figure 4.2, then one possible set of charging/discharging power capacities of the BESS is $P^B_{c,max}$ = 2.8 MW and $P^B_{d,max}$= 1.2 MW. This is because from Figure 4.2, p_2 = 0.0249 when $P^B_{d,max}$= 1.2 MW, while p_1 = 0.9925 when $P^B_{c,max}$ = 2.8 MW. Thus, p_B = 0.9925 – 0.0249 or 0.968. Whence, $P_{MF}(t)$ is expected to be outside the range [-1.2 MW, 2.8 MW] with the probability of 0.032. When $P_{MF}(t)$ is outside the BESS power limits, the balance un-buffered power shall flow to the grid and the PHS in the form of out-of-range disturbances. With a judicious choice of p_B, however, one could arrive at an acceptable probability level for such out-of-range perturbations while still maintaining a viable BESS design.

Of course there are numerous combinations of $P^B_{d,max}$ and $P^B_{c,max}$ for a given p_B, and the method described in the next section shall be used to obtain the unique combination of $P^B_{d,max}$ and $P^B_{c,max}$.

The determination of the SC power capacities can also follow the same procedure: Obtain $P_{HF}(t)$ using $P_w(t)$ as the input to the designed HPF filter. The CDF of $P_{HF}(t)$ is calculated, and the SC charging/discharging power capacities ($P^S_{c,max}$, $P^S_{d,max}$) are selected in such a way that the probability $P_{HF}(t)$ is within the selected SC power capacities is p_S, i.e.,

$$P\left\{-P^{S}_{d,max} \le P_{HF}(t) \le P^{S}_{c,max}\right\} = p_S \tag{4.5}$$

Again the advantage of using this approach is to obtain a SC design which is viable, even though there would be the probability of 1- p_S when $P_{HF}(t)$ cannot be successfully buffered. Also the method described in the next section shall be used to obtain the unique combination of $P^{S}_{d,max}$ and $P^{S}_{c,max}$, from the numerous combinations of $P^{S}_{d,max}$ and $P^{S}_{c,max}$, to meet the pre-specified probability of p_S.

Taking as a whole the task of smoothing the mid-frequency and high-frequency components of $P_w(t)$, the probability the BSHESS shall have the sufficient power capacities to successfully smooth out the mid- and high-frequency fluctuations of $P_w(t)$ is $p_B \times p_S$. The charging/discharging power capacities of the BESS are ($P^{B}_{c,max}$, $P^{B}_{d,max}$) while that of the SC are ($P^{S}_{c,max}$, $P^{S}_{d,max}$).

Although the unique sets of the charging/discharging power capacities of the BESS and SC are yet to be determined in the next section, nevertheless, once the capacities are known, the energy capacity of the BSHESS is calculated using the method similar to that described in [98], as follows. The BESS output power $P_B(t)$ is to track the reference $P_{B,ref}(t)$ which is the constrained output of the BPF. With known $P_B(t)$, the change in the stored energy level in the BESS ($\Delta E_B(t)$) is obtained by integrating $P_B(t)$ with respect to time, i.e.

$$\Delta E_B(t) = \int_0^t P_B(\tau) \cdot d\tau \tag{4.6}$$

The maximum and minimum values of $\Delta E_B(t)$, denoted as $\Delta E_{B,\max}$ and $\Delta E_{B,\min}$ respectively, can then be obtained over T_S. As the BESS must not operate below its maximum DoD $d_{B,\max}$ [98], thus the rated energy capacity of the BESS is

$$E_{B,r} = \frac{\Delta E_{B,\max} - \Delta E_{B,\min}}{d_{B,\max}} \tag{4.7}$$

Similarly the change in the energy level in the SC ($\Delta E_S(t)$) is calculated from the known $P_S(t)$, i.e.

$$\Delta E_S(t) = \int_0^t P_S(\tau) \cdot d\tau \tag{4.8}$$

Denote the maximum and minimum values of $\Delta E_S(t)$ as $\Delta E_{S,\max}$ and $\Delta E_{S,\min}$ respectively. If the maximum DoD of the SC is $d_{S,\max}$, then the rated energy capacity of the SC is [98]

$$E_{S,r} = \frac{\Delta E_{S,\max} - \Delta E_{S,\min}}{d_{S,\max}} \tag{4.9}$$

The maximum DoD of the SC $d_{S,\max}$ can be calculated as follows. The stored energy in SC is given by

$$E = \frac{1}{2} C U^2 \tag{4.10}$$

In (4.10), C and U are the capacitance and the voltage across the SC respectively. The nominal and minimum voltages of the SC are denoted as $U_{S,\max}$ and $U_{S,\min}$ respectively. The allowable $d_{S,\max}$ of the SC is given by

$$d_{S,\max} = 1 - \frac{U_{S,\min}^2}{U_{S,\max}^2} \tag{4.11}$$

4.3.2 Optimum BSHESS capacities

In the previous section, the impact of SC and BESS power capacities on power smoothing function has been expressed in probabilistic term. The method to determine the unique solution set of the power capacities is described next.

The capital cost of the BESS includes that of the battery banks and the associated PCU and is given by

$$c_B = aP_{B,r} + bE_{B,r} \tag{4.12}$$

In (4.12), a and b are the respective cost/MW and cost/MWh of the BESS and their parametric values are usually available from the manufacturers or from the literature [78]. In this investigation, the larger of the values of $P^B_{c,max}$ and $P^B_{d,max}$ shall be selected as $P_{B,r}$ because the power capacity of the BESS is governed by the power capacity of the PCU rather than that of the battery [144]. Hence the power capacity cost of the BESS is based on the power capacity of the PCU which would be the larger of the values of $P^B_{c,max}$ and $P^B_{d,max}$. $E_{B,r}$ is obtained using (4.7).

Similarly, the capital cost of the SC is expressed as

$$c_S = cP_{S,r} + dE_{S,r} \tag{4.13}$$

In (4.13), c and d are the respective cost/MW and cost/MWh of the SC. As the SC is also interfaced with the PCU, $P_{S,r}$ is chosen to be the larger of the values of $P^S_{c,max}$ and $P^S_{d,max}$ to reflect the power capacity cost of the PCU.

The optimum power and energy capacities of the BESS are determined through the minimization of the capital cost c_B of the BESS. An iterative search method is used to achieve this design objective by following the design procedure shown in the

flowchart of Figure 4.3. With the known historical wind power $P_w(t)$ and using it as input to the designed BPF to obtain $P_{MF}(t)$ and its CDF. Suppose it is desired the probability of successful buffering of the mid-frequency perturbations must be no less than a pre-specified level $p_{B,\min}$. So from the CDF of $P_{MF}(t)$, select a set ($P^B_{c,max}$, $P^B_{d,max}$). Using (4.3), check the probability that $P_{MF}(t)$ is within the range of [$-P^B_{d,max}$, $P^B_{c,max}$] is at least equal to or higher than $p_{B,\min}$, i.e., $p_B = P\{-P^B_{d,max} \le P_{MF}(t) \le P^B_{c,max}\} \ge p_{B,\min}$. If this condition is met, the BESS power capacity $P_{B,r}$ is chosen to be the larger value of $P^B_{c,max}$ and $P^B_{d,max}$. Next, determine $P_B(t)$ and the energy capacity $E_{B,r}$ using (4.7). Whence, calculate the BESS cost c_B using (4.12). The above procedure is repeated for all conceivable sets of ($P^B_{c,max}$, $P^B_{d,max}$) for which $p_B \ge p_{B,\min}$. The set, denoted as ($P_{B,r}$ and $E_{B,r}$), corresponding to the case of the minimum c_B would be the power and energy capacities of the most economical BESS. The probability of successful buffering of the mid-frequency perturbations is at least $p_{B,\min}$.

Similarly, the power and energy capacities ($P_{S,r}$, $E_{S,r}$) of the SC shall be that which minimize the capital cost c_S of the SC under the probabilistic condition that $P\{-P^S_{d,max} \le P_{HF}(t) \le P^S_{c,max}\}$ is at least equal to pre-specified level $p_{S,\min}$. The above iterative search procedure for the BESS is also applicable in determining $P_{S,r}$, $E_{S,r}$ which correspond to the minimum c_S. The probability of successful buffering $P_{HF}(t)$ is at least $p_{S,\min}$.

The optimum power and energy capacities of the BSHESS would correspond to the condition that the total capital cost of the BESS and SC is at the minimum. The least-cost BSHESS is expected to be able to smooth out the high- and mid-frequency fluctuations of the wind power with a probability of no less than $p_{B,min} \times p_{S,min}$. Thus, the determination of the optimum BSHESS capacities become one of specifying the acceptable minimum probabilities $p_{B,\min}$ and $p_{S,\min}$ the BSHESS is expected to successfully smoothen the wind power.

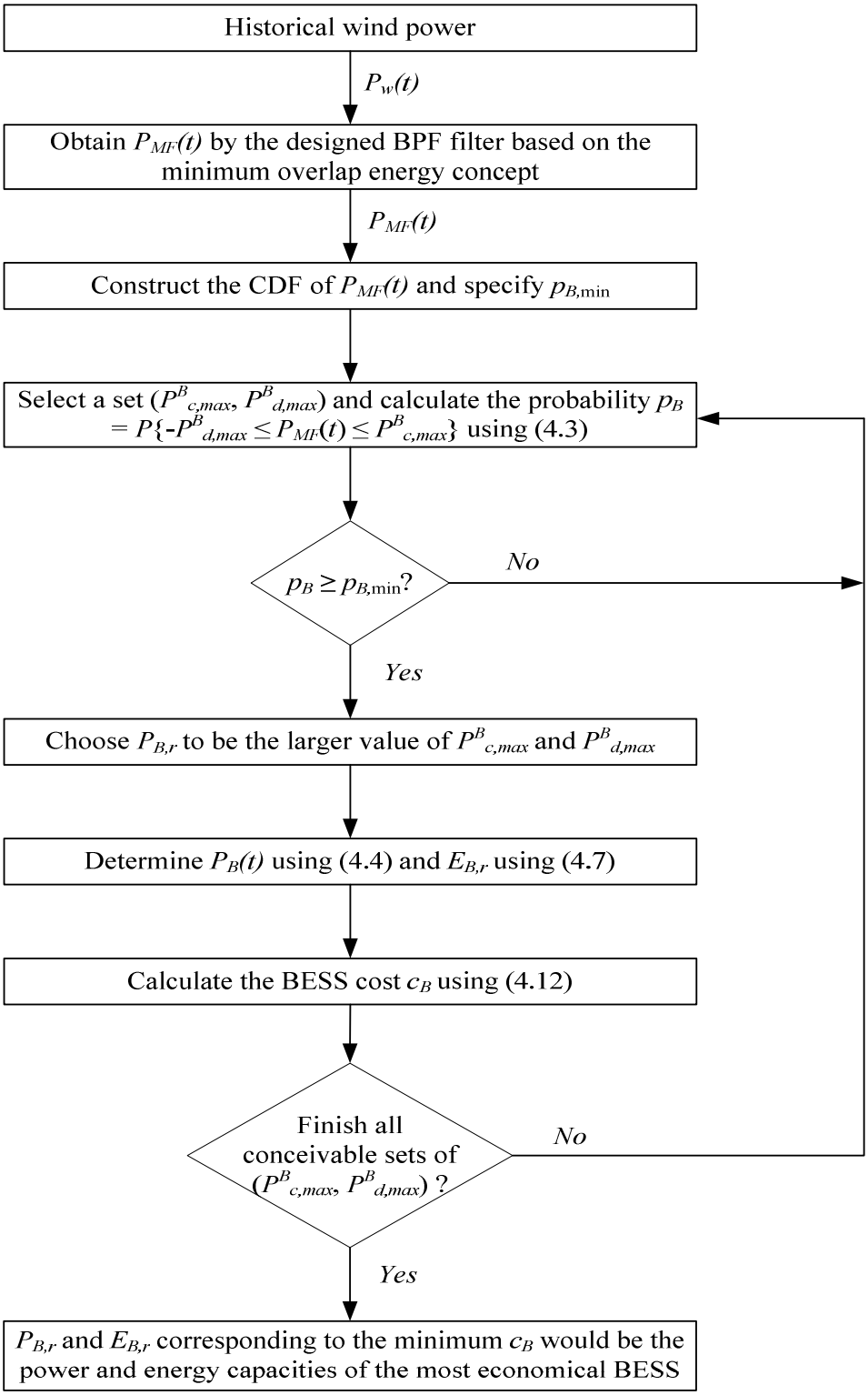

Figure 4.3. Iterative search method to determine the optimum power and energy capacities of the BESS.

The proposed approach described in Sections 3.3 and 4.3 thus complete the design of the BSHESS. It leads to the determination of the least-cost BSHESS and the successful high- and mid-frequency power smoothing with probability equal to or exceeding the pre-specified level.

Within the power smoothing scheme shown in Figure 4.1, the PCU for the BSHESS can be constructed based on the well-established power conditioning practices described in [143]. Similarly, the HPF and BPF can be readily realized using any one of the methods shown in [145]. Thus real-time power smoothing can be achieved using the proposed design.

4.4 Illustrative Example

The proposed approach is to be applied to the design of the BSHESS at the existing wind-farm in Jiangsu Province, China. The wind farm is interconnected to the State Grid system of East China. Reference [137] stipulates the maximum ramp rates permissible in the output power emanating from any State Grid-connected wind farm. Hence, the role of the BSHESS is to smoothen the perturbing wind power harnessed at the farm so as to comply with the grid requirement. Accordingly, the wind power data $P_w(t)$ shown in Figure 3.8, recorded between Jan to July 2007 and pertaining to the aggregated output power from 8×1.5 MW WTGs in the farm, is used in the design.

4.4.1 Design of the BPF and HPF

In Section 3.4, based on the minimum overlap energy criteria and by following the search procedure described in Section 3.3, it has resulted in f_u and f_l of the BPF being determined to be 4.38×10^{-4} Hz and 6.74×10^{-6} Hz respectively. As a result, wind power fluctuations with frequencies higher than 4.38×10^{-4} Hz are smoothed out by the SC and those fluctuations between 6.74×10^{-6} Hz and 4.38×10^{-4} Hz are to be dealt

with by the BESS. Although the buffering actions of the SC and BESS will not be completely decoupled, it will nevertheless result in minimal overlap energy between the ESS. Each of the ESS shall be able to maximize the amount of the energy it needs to deal with. Note that those components in $P_w(t)$ with frequencies lower than 6.74×10^{-6} Hz have the typical periods of a day or longer. These components are outside the scope of this chapter as they are pertaining to the longer-term power-energy management of $P_w(t)$. They need to be dealt with by the PHS which has higher energy capacity but of slower response, as compared to the BESS. This will be discussed in Chapter 5.

4.4.2 Optimum power and energy capacities of BSHESS

Having determined the cutoff frequencies of the HPF and BPF, the high-frequency components $P_{HF}(t)$ and mid-frequency components $P_{MF}(t)$ of $P_w(t)$ are obtained next. $P_{MF}(t)$ is shown Figure 4.4 and its corresponding CDF is that shown in Figure 4.2. Suppose the desired probability of successful smoothing of $P_{MF}(t)$ by the BESS must be at least 0.95, while the successful smoothing of $P_{HF}(t)$ by the SC must meet the minimum probability of 0.995, i.e. $p_{B,\min}$=0.95 and $p_{S,\min}$=0.995. Table I summarizes the parametric values of *a, b, c* and *d* extracted from [98] and used herewith to evaluate c_B and c_S. The search procedure described in Section 4.3.2 was used and it yielded the optimum BESS charging and discharging power capacities of $P^B_{c,max}$ = 2.8 MW and $P^B_{d,max}$ = 1.2 MW. These charging/discharging power capacities are also indicated in Figure 4.4. The probability $P_{MF}(t)$ is within the range of [-1.2 MW, 2.8 MW] was determined using the method of Section 4.3.1 and it yielded p_B = 0.968. It shows that the BESS has the probability of 0.968 to successfully buffer $P_{MF}(t)$. Thus p_B is higher than the set minimum $p_{B,\min}$ of 0.95 and hence, this combination of the charging/discharging power capacities is acceptable. Furthermore, the optimum power and energy capacities $P_{B,r}$ and $E_{B,r}$ of the BESS corresponding to the minimum c_B were found to be 2.8 MW and 34.224 MWh, with the minimum c_B of US\$$7.26\times10^6$.

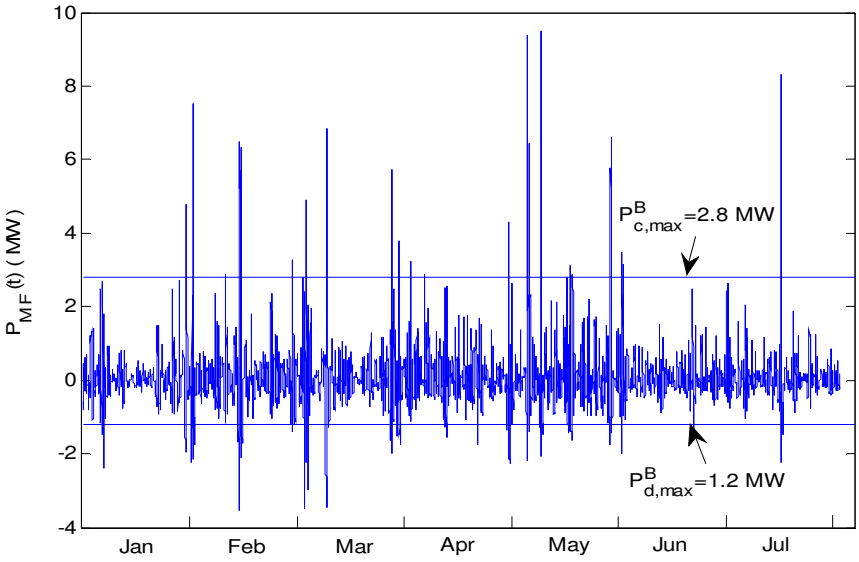

Figure 4.4. $P_{MF}(t)$ over the months of Jan-July 2007.

Again, by following the design procedure of Section 4.3, the optimal rated $P_{S,r}$ and $E_{S,r}$ of the SC at minimum c_S were determined to be 0.408 MW and 0.28 MWh respectively. The minimum c_S is US\$$5.42\times10^5$. The optimum $P^S_{c,max}$= 0.408 MW and $P^S_{d,max}$= 0.392 MW and the probability $P_{HF}(t)$ is within the range of [-0.392 MW, 0.408 MW] was found to be 0.9957.

Table 4.1 Parametric values of a, b, c and d used in calculating c_B and c_S

a(US$/MW)	b (US$/MWh)	c (US$/MW)	d (US$/MWh)
150×10^3	200×10^3	300×10^3	500×10^3

Therefore, the probability that the BSHESS can successfully buffer the high- and mid-frequency fluctuations is 0.968×0.9957 or 0.964.

4.4.3 Outcome of power smoothing by the designed BSHESS

The designed BSHESS was then used to effect the power smoothing function of the recorded $P_w(t)$ shown in Figure 3.8. An expanded view of $P_w(t)$, SC power $P_S(t)$, BESS power $P_B(t)$ and the smoothed power $P_L(t)$ of the 1st week of Jan 2007 is shown in Figure 4.5. $P_B(t)$ is to track $P_{B,ref}(t)$ which was obtained based on (4.4) while similar expression was used to calculate $P_S(t)$. The charging and discharging power limits $P^B_{c,max}$, $P^B_{d,max}$, $P^S_{c,max}$ and $P^S_{d,max}$ are also indicated in the figure. As $P_w(t)$ fluctuates, the BSHESS acts to buffer the perturbations as indicated by the power flows $P_S(t)$ and $P_B(t)$. As expected, the perturbations in $P_S(t)$ are more rapid than that in $P_B(t)$. Compared with $P_w(t)$, $P_L(t)$ has become significantly smoother except when the perturbations in $P_w(t)$ were so intense over certain periods within days 5 and 6 that the BESS and/or the SC had reached their respective charging/discharging power limits. These are clearly illustrated on the even more detailed plot of $P_w(t)$, $P_S(t)$, $P_B(t)$ and $P_L(t)$ shown in Figure 4.6. The total interval during which the BSHESS was not able to smooth $P_w(t)$ is approximately some 1.84% of the time in the week, a level which is consistent with the predicted probability of 0.964 the BSHESS is able to smooth the wind power.

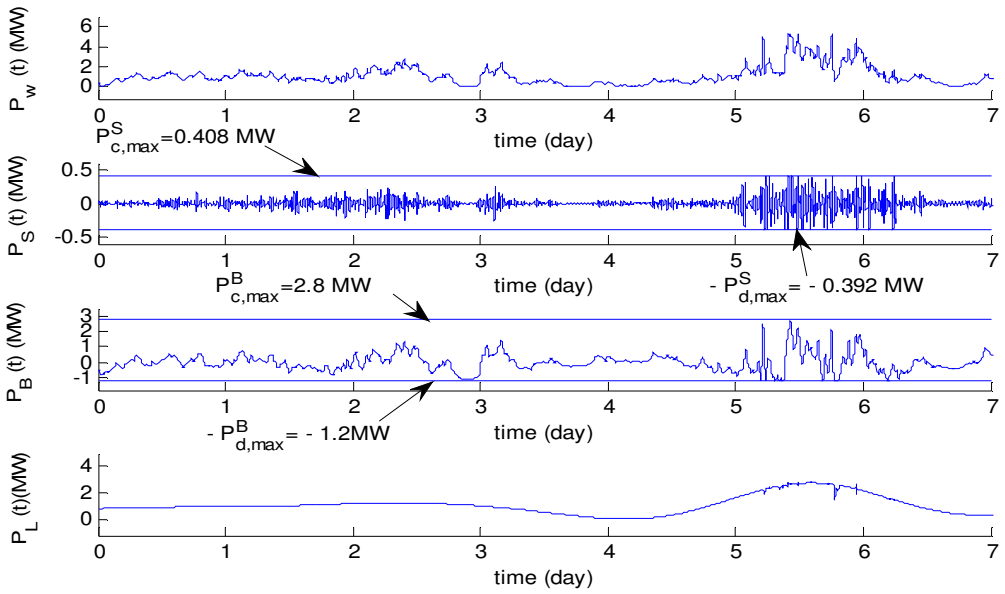

Figure 4.5. Expanded view of $P_w(t)$, $P_S(t)$, $P_B(t)$ and $P_L(t)$ over the first week of Jan 2007, $p_{B,min}$ = 0.95, $p_{S,min}$ = 0.995.

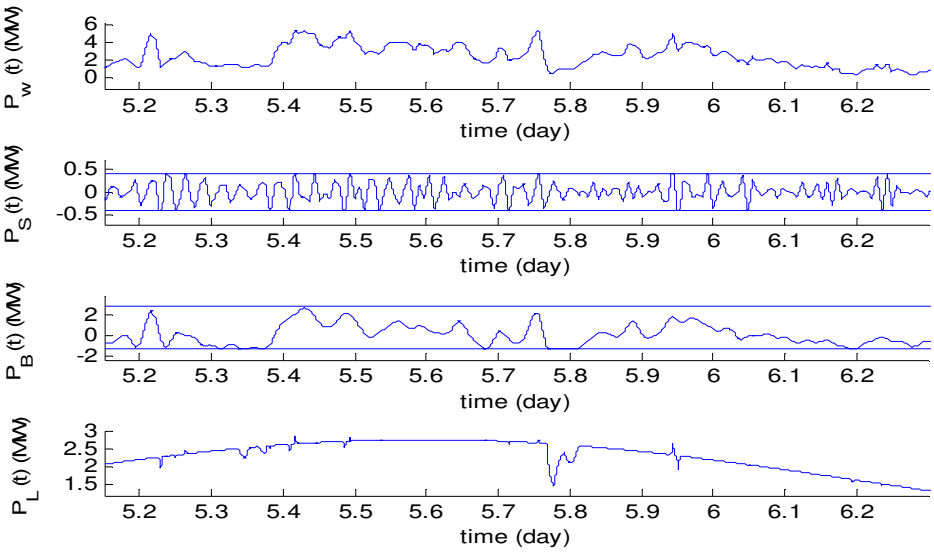

Figure 4.6. Expanded view of $P_w(t)$, $P_S(t)$, $P_B(t)$ and $P_L(t)$ over days 5-6 of the first week of Jan 2007, $p_{B,min}$ = 0.95, $p_{S,min}$ = 0.995.

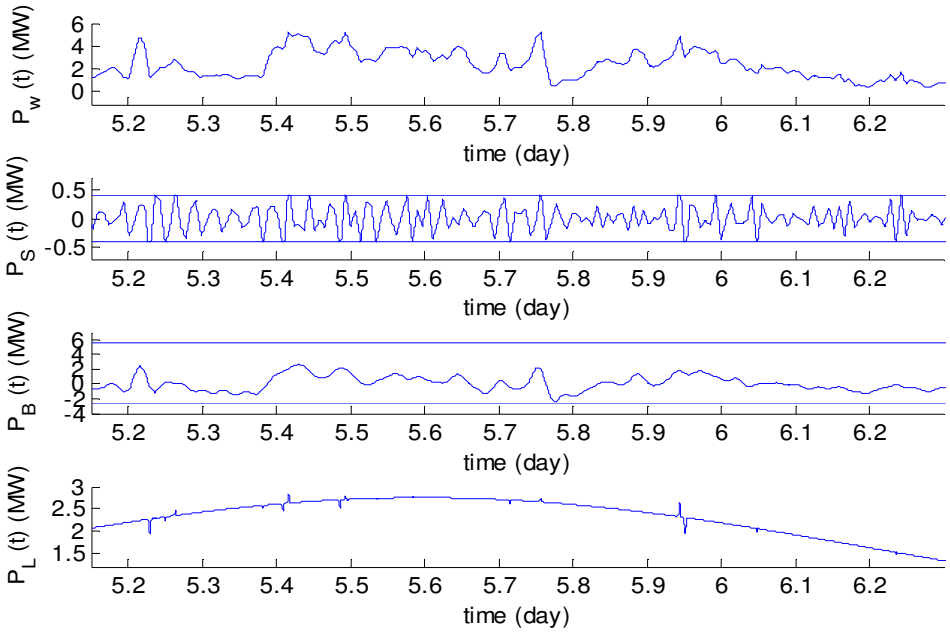

Figure 4.7 Expanded view of $P_w(t)$, $P_S(t)$, $P_B(t)$ and $P_L(t)$ over days 5-6 of the first week of Jan 2007, $p_{B,\min} = 0.99$, $p_{S,min} = 0.995$.

As a comparison, suppose $p_{B,\min}$ is increased to 0.99 while $p_{S,\min}$ remains unchanged. The optimum power and energy capacities $P_{B,r}$ and $E_{B,r}$ of the BESS were found to have increased to 5.5 MW and 34.414 MWh and the minimum c_B is now US\$7.71×10^6. The optimum $P^B_{c,max}$ and $P^B_{d,max}$ are 5.5 MW and 2.5 MW respectively. Using the method of Section 4.3.1, the BESS was found to have the probability of 0.9955 to successfully buffer $P_{MF}(t)$. Therefore, the probability that the BSHESS can successfully buffer the high and mid-frequency fluctuations is now higher at 0.9955×0.9957 or 0.9912. This is achieved with an increase in the cost c_B of the BESS, as can be seen from Table 4.2. Expanded view of days 5-6 plots of $P_w(t)$, $P_S(t)$, $P_B(t)$ and $P_L(t)$ for $p_{B,\min}$=0.99 is shown in Figure 4.7. It can be readily seen that with the increase in $P^B_{c,max}$ and $P^B_{d,max}$, the resulting $P_L(t)$ becomes significantly smoother than that shown in Figure 4.6. The total interval during which the BSHESS is not able to completely smoothen $P_w(t)$ was determined to be approximately 0.58% of the time in

the 1st week of Jan 2007. The out-of-range level is again in line with the predicted probability of 0.9912 the BSHESS is able to smooth the wind power.

Table 4.2: Comparison of the Optimum BESS Capacities Designed for $p_{B,min} = 0.95$ and $p_{B,min} = 0.99$: $p_{S,min} = 0.995$ for both cases

$p_{B,\min}$	p_B	$P^B_{c,max}$	$P^B_{d,max}$	$P_{B,r}$	$E_{B,r}$	Minimum c_B
0.95	0.968	2.8MW	1.2MW	2.8MW	34.224MWh	US$7.26×10^6
0.99	0.9955	5.5 MW	2.5 MW	5.5 MW	34.414 MWh	US$7.71×10^6

The example of this section shows the BSHESS design problem becomes one of specifying the acceptable minimum probabilities $p_{B,\min}$ and $p_{S,\min}$ the BSHESS is expected to successfully smoothen the wind power. The outcome shall be the power and energy capacities of the SC and BESS corresponding to the least-cost BSHESS.

4.4.4 Verification of the effectiveness of the designed BSHESS

Notwithstanding the encouraging results shown earlier, it will be prudent to verify whether the determined cutoff frequencies of the filters and the determined power and energy capacities of the BSHESS are suitable over the longer-term. The verification in this section is through examining the outcome of the smoothing of $P_w(t)$ measured in Jan 2011 at the wind-farm, using firstly the designed filters and the designed BSHESS for $p_{B,\min}$=0.95 and $p_{S,\min}$ = 0.995 and based on the Jan-Jul 2007 wind data wherein f_u=4.38 × 10^{-4} Hz, f_l = 6.74 × 10^{-6} Hz, $P^B_{c,max}$= 2.8 MW, $P^B_{d,max}$= 1.2 MW, $P^S_{c,max}$= 0.408 MW and $P^S_{d,max}$ =0.392 MW, as determined in the previous sub-section. When the designed BSHESS was applied to $P_w(t)$ measured in Jan 2011, the probability $P_{MF}(t)$ is within the range of [-1.2 MW, 2.8 MW] was found to be only 0.9311, a level which is lower than the specified $p_{B,\min}$ of 0.95. It would appear the mid-frequency wind power perturbations in Jan 2011 are more severe than that over the Jan-July

2007 period. A larger power capacity BESS is called for if p_B is to meet the specified level of 0.95. Concurrently, with the designed HPF and the SC charging and discharging power capacities of 0.408 MW and 0.392 MW respectively, the probability the SC is capable of buffering the $P_{HF}(t)$ is 0.9953 which marginally meets the specified probability level $p_{S,\min}$ of 0.995. Using (4.7) and (4.9), the energy capacities of the BESS and SC needed for the month of Jan 2011 were found to be 28.94 MWh and 0.139 MWh respectively. Both energy capacities are well within the designed BESS and SC energy capacities based on the Jan-Jul 2007 wind data.

$P_w(t)$, and the expanded first week sample plot of $P_S(t)$, $P_B(t)$ and the smoothed power $P_L(t)$ are shown in Figure 4.8 and Figure 4.9. Not surprisingly, $P_L(t)$ is again much smoother than $P_w(t)$ in most instances except between days 3 and 4 when the charging and discharging power limits of the BSHESS have been breached, as shown in Figure 4.10. Based on the obtained results, the probability of such violations was estimated to be 0.0388 in the first week of Jan 2011.

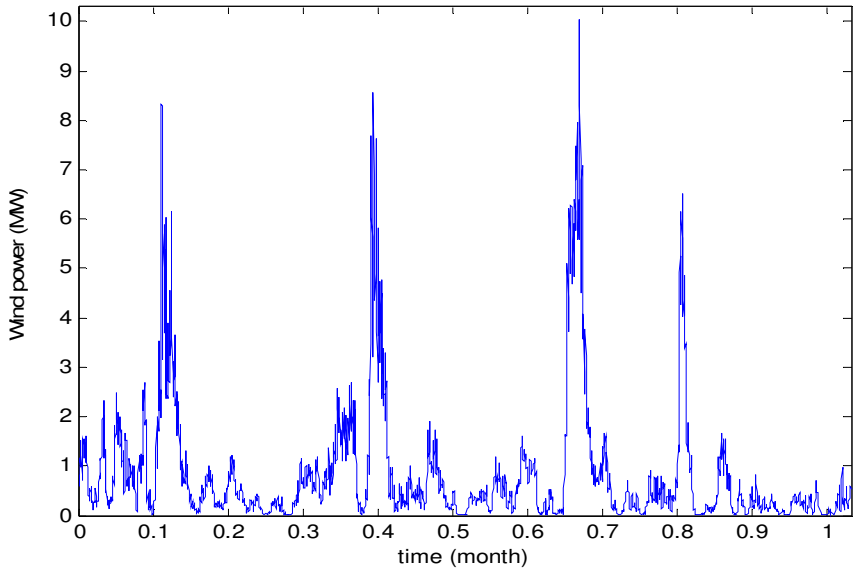

Figure 4.8. $P_w(t)$ over Jan 2011

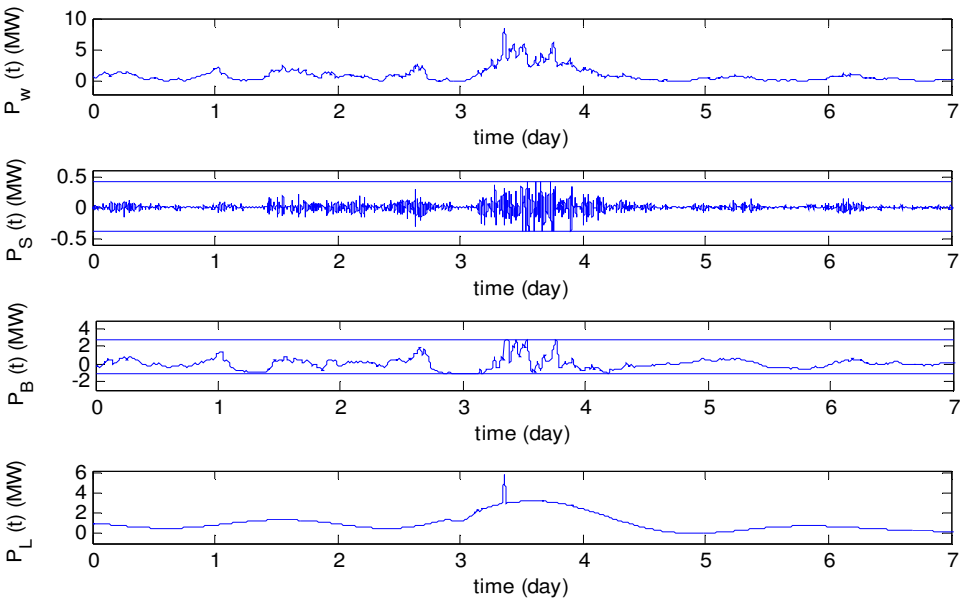

Figure 4.9. Expanded view of 1-week plots of $P_w(t)$, $P_S(t)$, $P_B(t)$ and $P_L(t)$

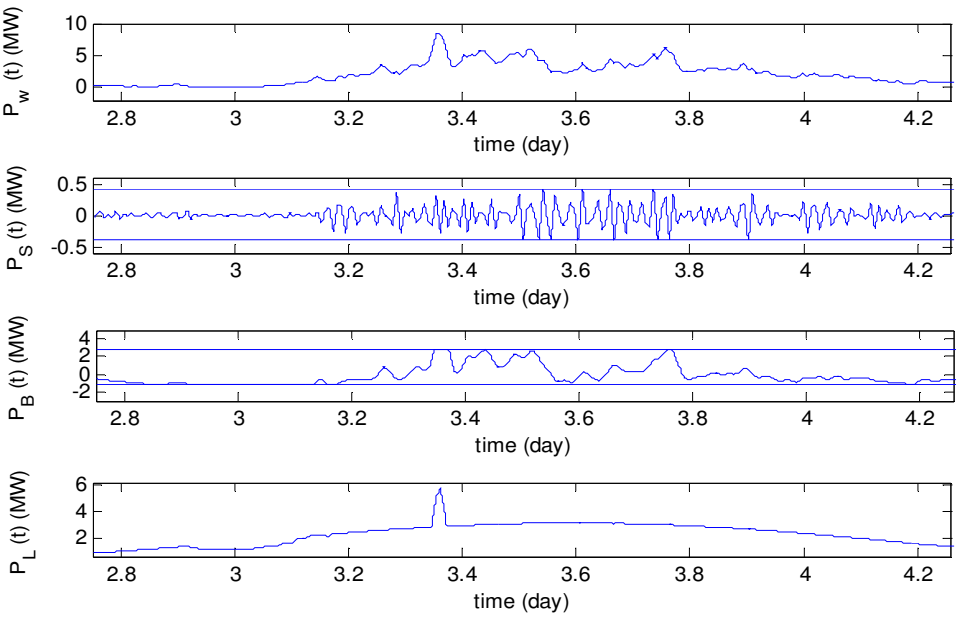

Figure 4.10. Expanded view of days 3-4 plots of $P_w(t)$, $P_S(t)$, $P_B(t)$ and $P_L(t)$.

Suppose the BESS power capacities $P^B_{c,max}$ and $P^B_{d,max}$ were increased to 5.5 MW and 2.5 MW respectively, the BESS power capacities as were determined using the Jan-Jul 2007 wind data and for $p_{B,\min} = 0.99$. The probability $P_{MF}(t)$ of the Jan 2011 wind power is within the range of [-2.5 MW, 5.5 MW] was found to be 0.99982, a level which meets the specified probability level of 0.99. Recall the probability the SC are capable of buffering $P_{HF}(t)$ is shown to be 0.9953. Therefore, the BSHESS would be able to buffer the high-frequency and mid-frequency fluctuations of $P_W(t)$ of Jan 2011 with the probability of 0.99982×0.9953 or 0.9951.

4.5 Conclusions

The use of a BSHESS for reducing wind power fluctuations has been examined. The BESS, in conjunction with the BPF, acts to buffer the mid-frequency variations of the wind power while the SC and the HPF perform to remove the high-frequency wind power perturbations. Furthermore, a statistical method has been developed to determine the power and energy capacities of the BSHESS so that the cost of the BSHESS is minimized while the BSHESS is able to smoothen the wind power to meet specified probability level. The proposed approach has been applied to the design of a BSHESS of an existing wind farm and the designed BSHESS is shown to be able to achieve wind power smoothing to a satisfactory level. Specifically at the design stage, the historical wind power data recorded between Jan to July 2007 was used to determine the cutoff frequencies of the filters and storage capacities of the BSHESS. Then in order to verify whether the determined cutoff frequencies of the filters and the determined power and energy capacities of the BSHESS are suitable over the longer-term, the wind power smoothing scheme was implemented with the designed filters and BSHESS to smooth $P_w(t)$ measured in Jan 2011. The outcome is that the designed filters and BSHESS are able to smooth $P_w(t)$ to meet the desired probability level. The designed BSHESS seems to be suitable for the two different periods.

CHAPTER 5. Determination of the Storage Capacity of Pumped-Hydroelectric Storage for Dispatch Planning of Large-scale Wind Power

In Section 3.2, a conceptual energy storage scheme has been described to achieve power quality enhancement and dispatch planning objectives for large-scale wind power generation. The high- and mid-frequency components of the wind power are buffered by SC and battery banks respectively using the respective HPF and BPF designed according to the method shown in Section 3.3. It results in the smoothening of the wind power. The capacity of the SC and BESS required to mitigate the wind power fluctuations can be determined based on the statistical method described in Chapter 4. It is also shown in Section 3.2 that the low-frequency wind power components are extracted by a LPF. The low-frequency wind power components are to be used to realize the dispatch planning of the wind power, as stated in Section 3.2, although the detail of the dispatch planning method is not described. The focus of this chapter is to fill this gap by explaining in detail a proposed method to dispatch planning for wind power. The method would allow wind power generator to participate in short-term energy markets. The dispatch is to be realized by utilizing the buffering actions offered by a PHS, the operation of which will be governed by a developed power flows control strategy. Finally, the required capacity of the PHS to meet the wind power dispatchability objective shall be determined using a proposed statistical method.

Accordingly, this chapter is organized as follows. Section 5.1 contains some preliminary considerations in the formulation of the dispatch planning task and an explanation on why PHS has been selected as the preferred form of the ESS. The

development of the new approach to wind power dispatch planning is shown in Section 5.2. Based on the developed power flow control strategy for the PHS, a statistical method is proposed in this section to determine the PHS capacity with the view to meet the dispatchability objective at specified probability level. Using data obtained from an existing wind farm, an example is given in Section 5.3 to illustrate the application of the proposed dispatch planning approach.

5.1 Some Preliminary Considerations

5.1.1 The Relevance of low-frequency intrinsic mode and residue functions of wind power to dispatch planning

In this chapter, it is assumed that wind power generators are to participate in a competitive energy market. The generation from the wind farms are to be included in short-term dispatch planning of the grid system to which the farms are interconnected. To meet the same short-term dispatch requirements as that demanded on the conventional generators, the wind farm operators will have to submit their dispatch bids to the grid operator typically a day ahead. The dispatch bids would consist of the wind farms' output power specified at regular interval of ΔT, with ΔT in the order of 15 – 60 minutes. However, as explained in Section 3.3.1, analysis of typical wind farm output power indicate the presence of oscillating wind power components having periods much shorter than ΔT. So over each ΔT, these relatively high frequency oscillating power components will not contribute significantly toward the net export of energy to the grid. In the dispatch planning of the wind farms, these high frequency wind power components do not need to be considered in the present focus on dispatch planning. Instead, the high-frequency components can be suitably buffered by fast response energy storage devices to enhance the quality of the power supply, a topic as considered in Chapter 4.

On the other hand, the remaining lower frequency oscillating wind power components with periods comparable or larger than ΔT will be considered in the dispatch planning of the wind farms. Since the variations of the low-frequency wind power components would be slower compared to those in the higher frequency components, accurate forecast of the low-frequency wind power components for the purpose of short-term dispatch planning can be more readily obtained. To be able to do so is a distinct advantage over the other dispatch planning approaches described in the current literature, as reviewed in Section 2.3.2.

For the short-term dispatch planning as envisaged under the scenario depicted in Figure 3.1, the concern of the grid operator is the total amount of wind power that can be committed a day or so ahead. Accordingly, in this chapter, the aggregate of $P_{w,i}(t)$ from the n groups of wind generators are denoted as $P_w(t)$ in Figure 5.1, where

$$P_w(t) = \sum_{i=1}^{n} P_{w,i}(t) \tag{5.1}$$

In the present investigation, $P_w(t)$ then forms the input to the LPF to generate the signal corresponding to the low-frequency components signal $P_L(t)$. The LPF is included in the control loop for wind power dispatch as shown in the figure. The cutoff frequency of the LPF can be determined based on the method described in Section 3.3, using the results of EMD analysis on $P_w(t)$ and the developed concept of minimum overlap energy. The filter determines which of the IMFs $c_i(t)$ and the residue function $r_n(t)$ of $P_w(t)$ are to be included in $P_L(t)$. The setting of the cut-off frequency of the filter is crucial in ensuring the success of the scheme. The details of the EMD analysis are in Section 3.3.

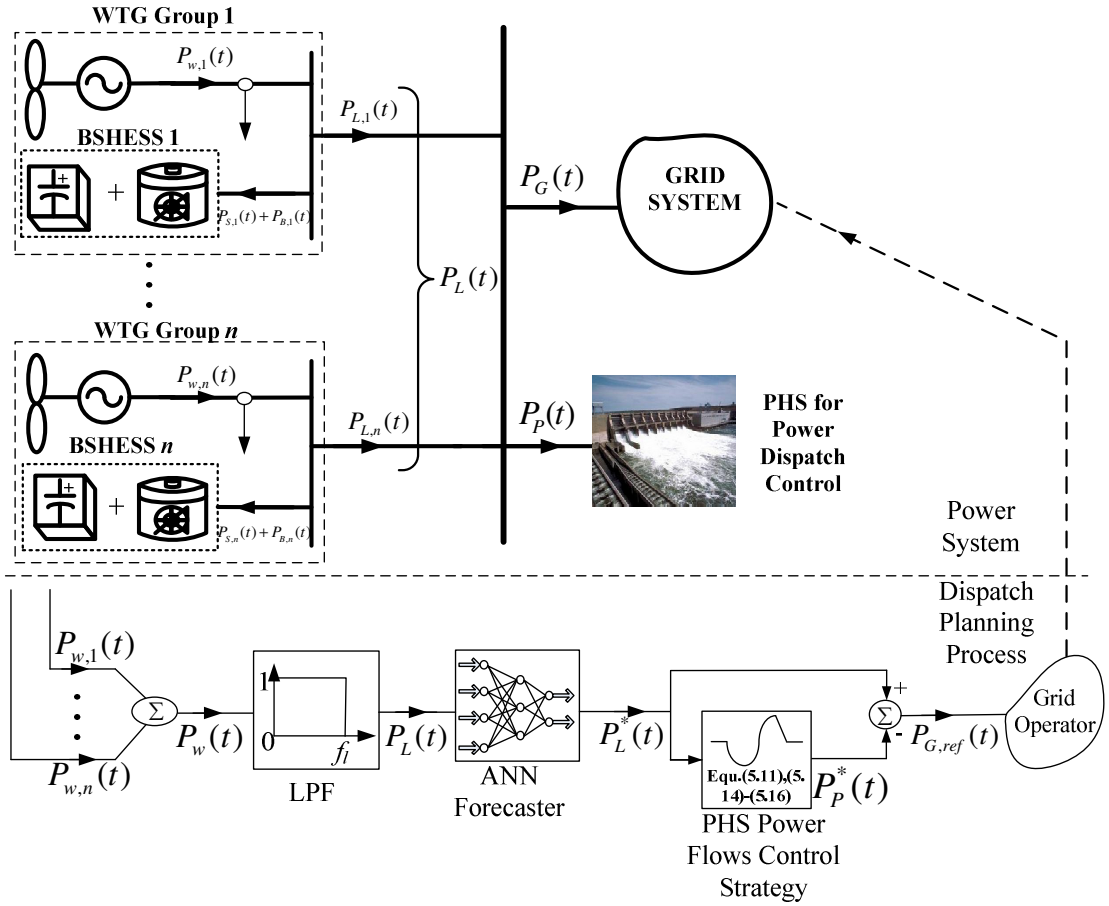

Figure 5.1. A conceptual large-area wind power generation incorporated with a hierarchical ESS scheme: BSHESS for power smoothing and the PHS for dispatch planning.

In the power system section of Figure 5.1, $P_L(t)$ is shown as the net power flows to the grid and to a PHS installation. While the selection of the PHS and its functions shall be explained in greater detail shortly, it will be instructive to study closely the characteristics of $P_L(t)$, as example of which is shown in Figure 5.2. As can be seen, in most instances, the fluctuating $P_L(t)$ assumes positive values although there are isolated instances of negative $P_L(t)$. Negative $P_L(t)$ only occurs rarely. Hence, the area under the positive portion of $P_L(t)$, which corresponds to the situation of energy export from the wind generators, is larger than that under the negative portion of $P_L(t)$: the aggregated wind generation is a net exporter of energy. This is as expected. Indeed, in the absence of the PHS and for those instances when $P_L(t)$ is positive and is known,

one could even treat $P_L(t)$ as the short-term wind generation dispatch bids committed to the grid, provided $P_L(t)$ can meet with the smoothness criteria as stipulated in grid-code such as [137]. However, the negative portion of $P_L(t)$ would then necessitate power import from the grid system. If the imported energy is produced by the burning of fossil fuels and since the purpose of introducing the renewable source is to reduce the dependency on such conventional generation, the importation of power from the grid is deemed undesirable. Hence, power import from the grid is not allowed in this investigation and accordingly, one obtains the following strategy for the dispatch power $P_G(t)$:

$$P_G(t) = P_L(t) - P_P(t) \quad when\ P_L(t) > 0 \tag{5.2}$$

$$\left.\begin{array}{l} P_G(t) = 0 \\ P_P(t) = P_L(t) \end{array}\right\} \quad when\ P_L(t) \le 0 \tag{5.3}$$

Equation (5.2) follows from the power balance requirement whereas under the strategy (5.3), the importation of power from the grid is prevented when $P_L(t)$ becomes negative: $P_G(t)$ is set to zero and the PHS will act as a source. The PHS will then discharge so that $P_P(t) = P_L(t)$. Equation (5.2) and (5.3) therefore forms the basis of the planning of the dispatch $P_G(t)$, the details of which shall be described in Section 5.2.

An important outcome of adopting the strategy (5.2) and (5.3) follows from the observation alluded to earlier in that the amount of energy contained in a negative $P_L(t)$ event tends to be small in comparison to the energy exported from the WTG. Since the PHS will only discharge in respond to the occurrence of a negative $P_L(t)$, the PHS will be buffering a relatively small amount of energy in comparison to that harnessed from the wind. Hence the strategy (5.2) and (5.3) will only require the installation of a PHS of modest storage capacity.

5.1.2 Selection of PHS for Dispatch Planning

Having explained the characteristics of $P_L(t)$, the role of the PHS in wind power dispatch planning shall be elaborated next. Among the various types of ESS, the ESS with the most appropriate attributes is to be selected to effect the strategy expressed by (5.2) and (5.3). The low-frequency wind power components $P_L(t)$ are slow-varying. They tend to be of larger magnitudes than the high-frequency wind power components. Considering the capacity of each of the n groups of the WTG can be up to 100 MW, $P_L(t)$ could reach several hundred MW or higher. Moreover, the net amount of the energy in the wind power $P_w(t)$ is contained in $P_L(t)$. The design of the needed ESS is pertaining to the management of virtually all the energy contained in the wind. To smooth out these low-frequencies power components, the large-scale storage PHS would be more suitable. This is because PHS has slower response characteristics and it is a large-capacity centralized storage facility. Moreover, the PHS is more economically viable, in terms of $/MWh, to handle power level of such a scale and to sustain it over several hours [78]. Also, the PHS is based on well-established and highly reliable motor-generator technology. In view of the relatively slow variations observed in $P_L(t)$, the MG set can readily respond and regulate $P_P(t)$ to effect the strategy (5.2) and (5.3). PHS is therefore selected as the energy buffering medium to facilitate the large-scale wind power dispatch scheme shown in Figure 5.1.

Also with regard to the PHS, the water level in the PHS reservoir reflects the amount of stored energy in the ESS. When the water level is at the maximum designed height, the PHS is considered to be at the maximum stored energy state and its *SOC* is 1. Conversely, when the water level drops to the minimum designed height, the *SOC* of the PHS is 1-$d_{P,max}$ where $d_{P,max}$ denotes the maximum allowable depth of discharge. In practice however, to prevent the PHS from being over-discharged or over-charged, a small positive tolerant ε is included in the permissible *SOC* operating range, i.e. the SOC of the PHS is allowed to vary within the more realistic range of [1- $d_{P,max}$+ε, 1-ε].

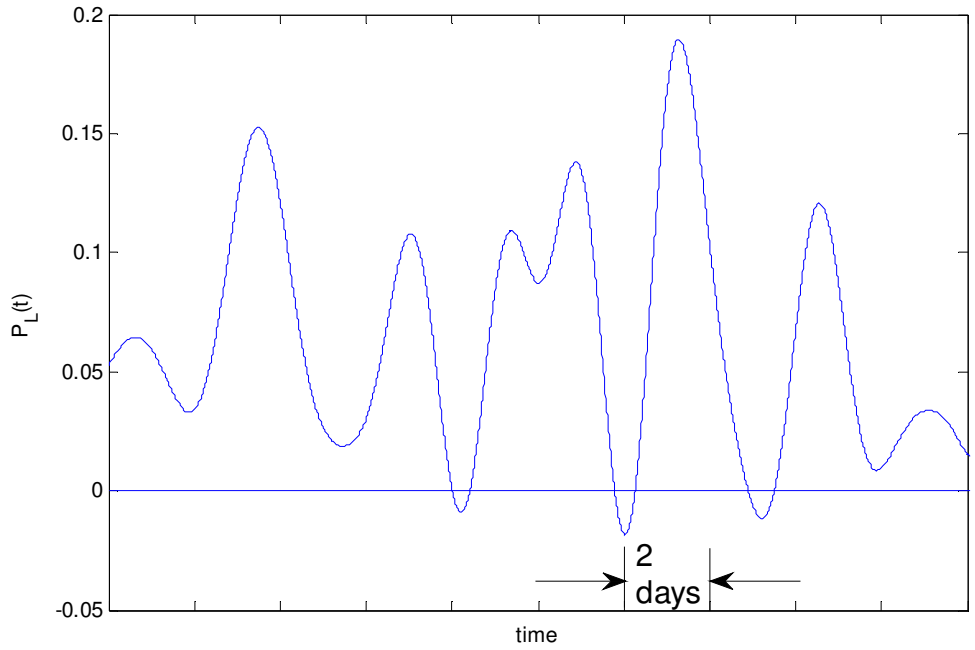

Figure 5.2. An example of the low-frequency wind power component $P_L(t)$: $P_L(t)$ expressed in puMW.

5.2 Determination of Short-Term Dispatch

Section 5.1.1 explains $P_G(t)$ is governed by (5.2) and (5.3) and the role of the PHS is to act as a source during instances of negative $P_L(t)$. In the planning process, $P_{w,i}(t)$ are measured and aggregated to form $P_w(t)$. $P_w(t)$ is then fed into the LPF. The output of the filter is the required low-frequency component $P_L(t)$ of $P_w(t)$. The generated $P_L(t)$ will form the input to the remaining blocks in the dispatch planning loop. Next the development of a power flows control strategy on $P_P(t)$ which is necessary in the realization of a reliable dispatch plan shall be described.

Of the various existing forms of power market, the one adopted herewith to develop the dispatch plan is as follows. As explained in Section 2.3, the dispatch plan is to be submitted to the grid operator up to a day ahead, and the plan contains wind power

generation schedules specified at the regular interval ΔT. The wind farm operators may revise and re-submit the bids once every *s* hours. However, the operators would only be allowed to revise the dispatch schedule for the period beyond the m^{th} hour from the time of re-submitting the bids [146, 147]. Typically, $s = 1$ and $m = 2$. Since the dispatch planning considered involves only the low-frequency component $P_L(t)$ of $P_w(t)$, and the commitment of the wind farms output power several hours ahead, it calls for the forecasting of $P_L(t)$. This is shown next.

5.2.1 Forecast of the low-frequency wind power

With the LPF constructed in the manner as described in the previous section, $P_L(t)$ is generated in real-time from the measured $P_w(t)$. As $P_L(t)$ shall only contain the low-frequency components of $P_w(t)$ which have periods much longer than *s*, the forecasted $P_L(t)$ is not expected to be much different from that predicted *s* hours earlier. Hence, over each updating period *s*, it will be a much easier task to obtain accurate forecast of $P_L(t)$ for the short-term dispatch planning, in comparison to the approaches shown in [112] in which the whole $P_w(t)$ has to be forecasted.

In the literatures, the approach to wind forecasting can be based on either physical models or statistical models. Physical models, containing numerical weather prediction (NWP), utilize meteorological information such as temperature, moisture and pressure to forecast wind velocity [148-152]. The disadvantage of NWP models is that it is rather complex due to the heavy computational duty. Statistical methods are based on the analysis of large amount of historical wind data. Traditional statistical techniques include autoregressive (AR), moving average (MA), autoregressive moving average (ARMA) [153], autoregressive integrated moving average (ARIMA) and the Kalman filters [150, 152]. Newer statistical methods use the artificial intelligence (AI) including Artificial Neural Network (ANN) [154-159], fuzzy logic

systems [160, 161], support vector machines [162], learning approach [163] and some hybrid methods [164, 165].

The above methods can be used to forecast the wind power directly or to predict the wind speeds first and transform them to wind power [166]. Also, the physical and statistical approaches are usually hybridized to improve the prediction accuracy [167]. In a hybrid method, physical method is often the first step and the forecast results are utilized as the input for the statistical methods such as ANN, ARMA.

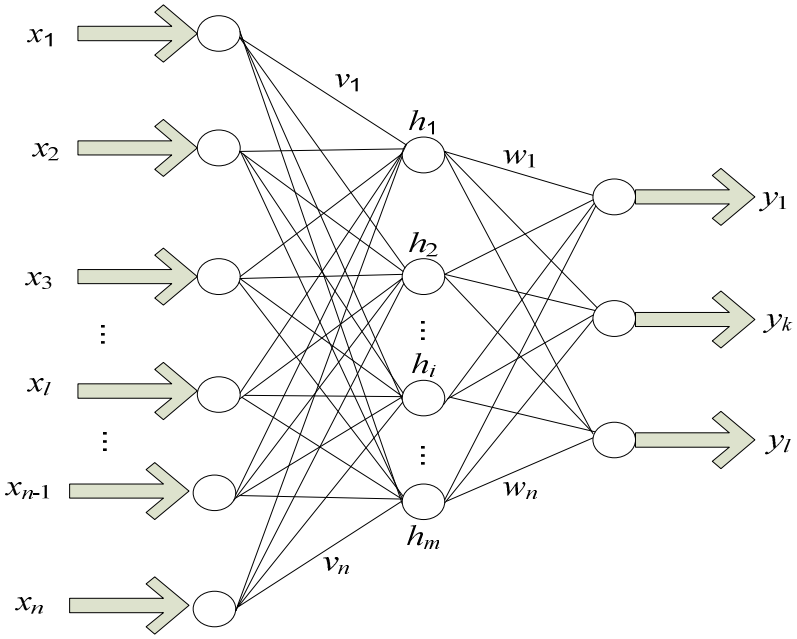

Figure 5.3. Structure of the three-layer BP network

For the problem in hand, denote the forecast of $P_L(t)$ as $P_L^*(t)$. Any one of the above forecasting methods could be used to obtain $P_L^*(t)$ based on $P_L(t)$. Indeed, selected forecasting techniques had been applied to obtain $P_L^*(t)$, and the back-propagation ANN technique was found to perform most satisfactorily in terms of accuracy and solution time. ANN is preferred over other methods because a neural network helps when it is highly complex to formulate an algorithmic solution and also where there is a need to pick out the structure from the existing data. It has good performance when

dealing with raw data. It is fault-tolerant, that is, it is able to handle noisy and incomplete data. It has strong ability to learn from experience and excellent training ability. It is able to deal with non-linear problems and once trained, it can assist in prediction and generalization at high speed. Interested readers may refer to [156] for a general description on ANN. For completeness, it will be sufficient to include in this section a brief introduction to the ANN technique.

ANN is one of the most popular methods in recent years. It was derived from the idea of human neurons and the technique simulates the abilities of neural network of human beings using a large number of artificial neurons. The back-propagation (BP) neural network is one of the most widely used ANNs due to its ease of implementation [168]. Typically, a BP network uses a multilayered feed-forward topology. Figure 5.3 shows the structure of a three-layer BP network where the three layers are denoted as the input, hidden and output layers [169]. Each layer is consisted of a number of neurons. In the figure, the input variable set is denoted by $X = [x_1, x_2,\ldots, x_n]^T$, the hidden variables by $H' = [h_1, h_2,\ldots, h_m]^T$ and the output variables by $Y = [y_1, y_2,\ldots, y_l]^T$. The weight matrix connecting the input and hidden layers and that connecting the hidden and output layers are denoted by $V = [v_1, v_2,\ldots, v_n]^T$ and $W = [w_1, w_2,\ldots, w_n]^T$, respectively.

In the general ANN approach, it involves the training of the network, the purpose of which is to obtain the weights of each of the connections [170].

Mathematically, for the hidden layer,

$$h_j = f(n_j),\ j = 1,2,...,m \tag{5.4}$$

$$n_j = \sum_{j=1}^{n} v_{ij} x_j + b,\ j = 1,2,...,m. \tag{5.5}$$

Similarly, for the output layer,

$$y_k = f(n_k), k = 1,2,...,l \tag{5.6}$$

$$n_k = \sum_{j=1}^{m} w_{jk} h_j + \beta, k = 1,2,...,l \tag{5.7}$$

A transfer function of the neurons often selected is the sigmoid function:

$$f(\mu) = \frac{1}{1+e^{-\mu}} \tag{5.8}$$

Data preprocessing is critical when sigmoid function is applied because the value of this type of function is in the range from 0 to 1 or from -1 to 1. Therefore, the input parameters should be normalized beforehand. The inverse process is needed to convert the output of the network back to the correct range.

To decide on the proper number of hidden layer neurons, "trial-and-error" method can be used. One can start by a small number of layers and increase it by one each time. The process stops when the forecasting error starts to increase or no significant improvement is observed.

Briefly, the construction of the ANN model involves the use of historical data of $P_L(t)$ for the setting up and the training of the neural network. The ANN model developed in this study consists of the input, hidden and output layers. The numbers of neurons in the layers are 20, 10 and 1 respectively. The time step is set to 1 hour so as to satisfy typical power market rule with regard to the frequency of updating power dispatch. After the ANN model has been successfully trained, the well-trained neural network can then be used in the dispatch planning process to yield $P_L^*(t)$ using real-time generated $P_L(t)$ as input in the following way. Firstly the hourly power data $P_L(t)$ of the immediate past 20 hours forms the 20 inputs of the model. The output (one

output) is the forecasted power for the next hour. It is denoted herewith as the 1st forecast data. The model can then be used to forecast the power of the 2nd hour (called the 2nd forecast data) using the 1st forecasted data and the immediate past 19 hourly power as inputs. This can be repeated to generate a series of forecast for (say) the next 24 hours. At the end of the first hour, the actual value of the wind power would be known. It can then be used to replace the 1st forecast data. The forecast for the 2nd and 3rd data can be updated using the actual 1st hour power instead of the 1st forecast data. So in this way, the forecast is updated at every hour.

Typically, the solution time required to generate $P_L^*(t)$ is about 15s using a processor of Intel(R) Core(TM)2 Quad CPU Q9400 @ 2.67GHz. The solution time is short compared to the bid re-submission interval of s hours. Hence, there is ample time for the ANN forecaster to generate $P_L^*(t)$ in time for the bids re-submission.

Next and as shown in Figure 5.1, with the forecast $P_L^*(t)$ as input, the "PHS Power Flows Control Strategy" block determines the estimated PHS output power reference $P_P^*(t)$. The determination of the dispatch reference $P_{G,ref}(t)$ then follows, as described next.

5.2.2 Determination of the dispatch reference

From (5.2) and (5.3) and by treating the forecast $P_L^*(t)$ as the reference for $P_L(t)$, one obtains

$$P_{G,ref}(t) = P_L^*(t) - P_P^*(t) \qquad when\ P_L^*(t) > 0 \tag{5.9}$$

$$\left.\begin{aligned} P_{G,ref}(t) &= 0 \\ P_P^*(t) &= P_L^*(t) \end{aligned}\right\} \quad when\ \ P_L^*(t) \le 0 \tag{5.10}$$

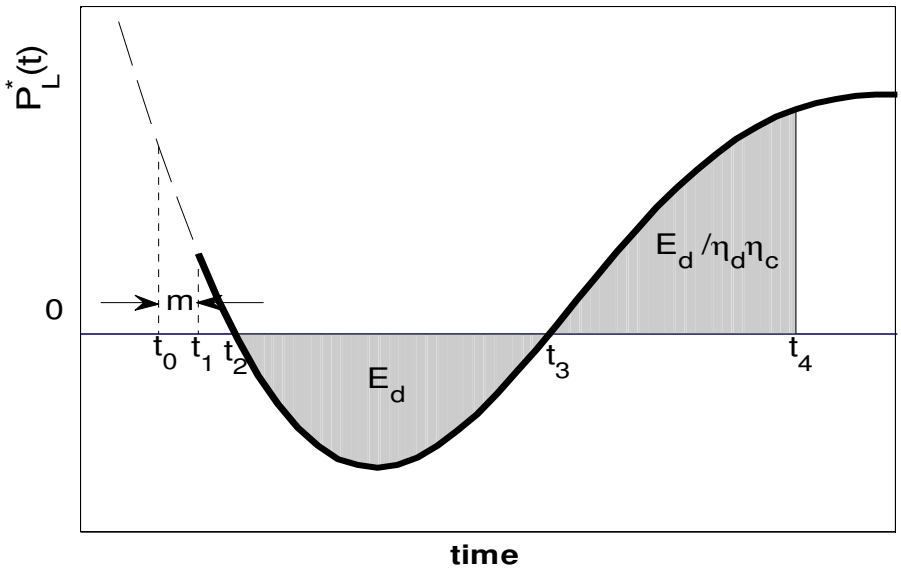

(a)

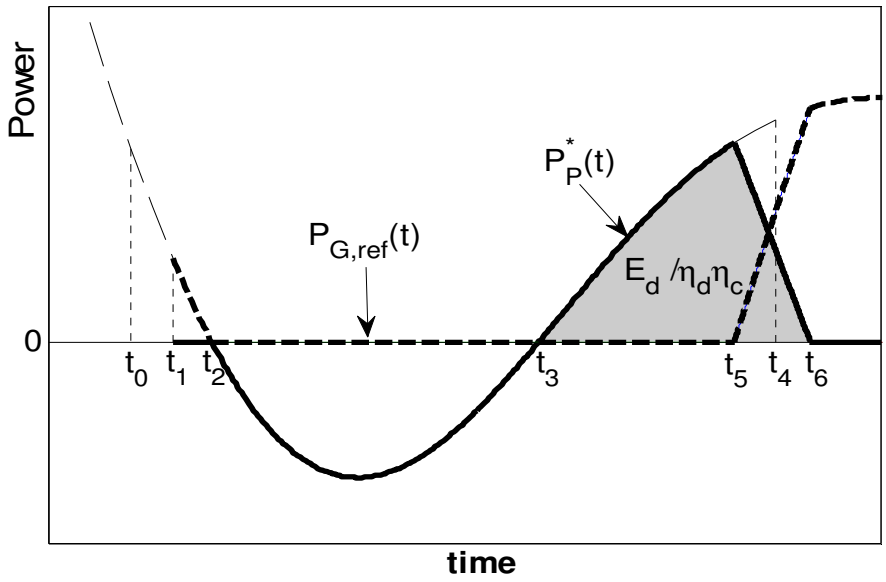

(b)

Figure 5.4 (a) $P_L^*(t)$ determined at t_0; (b) Strategized $P_P^*(t)$ and $P_{G,ref}(t)$ for $t \geq t_1$

So from (5.9) when $P_L^*(t) > 0$, in order to generate the reference $P_{G,ref}(t)$ in the planning of the dispatch $P_G(t)$, $P_P^*(t)$ has to be determined since $P_L^*(t)$ is known from the output of the LPF. The method to determine $P_P^*(t)$ shall now be explained. At time t_0, suppose the wind power generation operators are to provide the dispatch bids for the subsequent hours. Also at t_0, suppose the ANN forecaster generates the forecast $P_L^*(t)$ shown in Figure 5.4(a). However, in line with the adopted market rules explained earlier, $P_{G,ref}(t)$ in the immediate m hours must retain the bid values submitted before t_0. Therefore at t_0, the operators are to submit bids for the t_1^{th} hour and beyond, where $t_1 = t_0 + m$.

Within the interval $t_1 \leq t \leq t_2$, Figure 5.4(a) shows that $P_L^*(t) \geq 0$, i.e., there is a predicted net outflow of power from the direction of the n groups of the WTG. As will be shown later, the SOC of the PHS will be at the maximum level of $1 - \varepsilon$ at this stage of the PHS operations. Thus it is necessary to export all the outflow power to the grid:

$$\left.\begin{aligned} P_{G,ref}(t) &= P_L^*(t) \\ P_P^*(t) &= 0 \end{aligned}\right\} \quad for\ t_1 \leq t \leq t_2 \tag{5.11}$$

At $t = t_2$, however, Figure 5.4(a) shows that $P_L^*(t) = 0$. Since the *SOC* of the PHS can be tracked in real-time, thus the *SOC* of the PHS at t_0 is known and that at t_2 can be estimated as

$$\begin{aligned} SOC(t_2) = SOC(t_0) &+ \frac{1}{E_{P,r}} \int_{t_0}^{t_1} (P_L^*(t) - P_{G,ref}(t))dt \\ &+ \frac{1}{E_{P,r}} \int_{t_1}^{t_2} (P_L^*(t) - P_{G,ref}(t))dt \end{aligned} \tag{5.12}$$

In (5.12), $E_{P,r}$ denotes the rated energy storage capacity of the PHS and $P_L^*(t)$ is the forecast made at t_0. Also in (5.12) and as alluded to earlier, over the m-hours interval $t_0 \leq t \leq t_1$, $P_{G,ref}(t)$ is set equal to the forecast $P_L^*(t)$ made before t_0. However $P_L^*(t)$ generated at t_0 inevitably differs from that made before t_0. Thus, the PHS acts to

compensate for the difference. This is reflected in the expected change in the SOC, as reflected by the 2nd term on the RHS of (5.12). On the other hand, from (5.11), over the interval $t_1 \leq t \leq t_2$, $P_{G,ref}(t) = P_L^*(t)$ or $P_P^*(t) = 0$. Hence, the 3rd term on the RHS of (5.12) will be zero.

Next, within the interval $t_2 \leq t \leq t_3$, a new situation has occurred as $P_L^*(t)$ is negative: there is a predicted net inflow of power toward the n groups of the WTG. To prevent the importation of power from the grid as indicated by (5.3), so $P_{G,ref}(t)$ is set to zero as shown in (5.10). The forecasted shortfall in the power, i.e. the negative $P_L^*(t)$, is to be supplied by the PHS and the PHS is called upon to discharge. The amount of the discharged energy is equaled to E_d/η_d, where η_d is the efficiency of the PHS discharging process. E_d is the energy equaled to the shaded area shown in Figure 5.4(a). E_d can be readily determined since $P_L^*(t)$ is known. At the end of the discharging process at t_3, $SOC(t_3)$ of the PHS can be estimated as

$$SOC(t_3) = SOC(t_2) - E_d / (\eta_d E_{P,r}) \tag{5.13}$$

Following the negative $P_L^*(t)$ event and beyond t_3, $P_L^*(t)$ returns to positive values and there would be once more a net outflow of power from the direction of the groups of the WTG. Since the PHS has been discharging over the interval $t_2 \leq t \leq t_3$, $SOC(t_3)$ will be less than $1-\varepsilon$. So instead of exporting $P_L^*(t)$ to the grid, it will be prudent to direct all of $P_L^*(t)$ to re-charge the PHS so that the PHS can reach the fully charged state, i.e. SOC = $1-\varepsilon$, in the shortest possible time. In Figure 5.4(b) and at $t = t_5$, the PHS is expected to be almost fully charged and it will then be desirable to institute a smooth ramping-down charging strategy. This is to be accomplished at a rate in compliance of the maximum allowable power ramp rate stipulated in grid-code such as [137] and/or that permissible for the safe ramping down operation of the PHS, whichever is applicable. This maximum allowable power ramp rate is denoted as γ_{max}. It is proposed herewith that $P_P^*(t)$ is to ramp down at the constant rate γ_{max}. The time t_5 can be calculated as follows. With the known $P_L^*(t)$, numerically one can determine the

value of t_4 such that the positive shaded area bounded by $P_L^*(t)$ and between t_3 and t_4 in Figure 5.4(a) is $E_d/\eta_d\eta_c$ where η_c is the efficiency of the PHS charging process. At the precise instance t_4, the SOC of the PHS will then be equaled to that at t_2. Again by numerical means, one can readily determine the time t_5 when the charging process should start to ramp down at the maximum rate of γ_{max} such that by the time t_6, the SOC of the PHS is 1-ε. The shaded area in Figure 5.4(b) shown bounded by $P_P^*(t)$ for $t_3 \leq t \leq t_6$ would be exactly the charging energy $E_d/\eta_d\eta_c$. The PHS charging process can then terminate and the PHS shall be ready for the next round of discharging-charging cycle.

In view of the above, thus over the interval $t_2 \leq t \leq t_5$, set

$$\left.\begin{aligned} P_P^*(t) &= P_L^*(t) \\ P_{G,ref}(t) &= 0 \end{aligned}\right\} \; for\; t_2 \leq t \leq t_5 \tag{5.14}$$

Starting from t_5, $P_{G,ref}$ (t) is to follow the linear power ramp-up curve as shown in Figure 5.4(b). Hence,

$$\left.\begin{aligned} P_P^*(t) &= P_P^*(t_5) - \gamma_{\max}(t - t_5) \\ P_{G,ref}(t) &= P_L^*(t) - P_P^*(t) \end{aligned}\right\} \; for\; t_5 \leq t \leq t_6 \tag{5.15}$$

After t_6, all the WTG output power is exported to the grid. Thus, set

$$\left.\begin{aligned} P_{G,ref}(t) &= P_L^*(t) \\ P_P^*(t) &= 0 \end{aligned}\right\} \; for\; t \geq t_6 \tag{5.16}$$

The process of (5.16) is maintained until the next instance when $P_L^*(t)$ becomes negative again and the discharging-charging cycle of the PHS is repeated. Thus, prior to the PHS discharging, the SOC of the PHS is at the maximum level of 1 – ε which is precisely the state of the PHS when deriving(5.11).

In summary, the estimated PHS output power reference $P_P^*(t)$ and the dispatch power reference $P_{G,ref}(t)$ for $t \geq t_1$ are governed by (5.11), (5.14), (5.15) and (5.16). $P_P^*(t)$ is shown in the form of the solid line while that of $P_{G,ref}(t)$ is indicated by the dashed-line in Figure 5.4(b). The "PHS Power Flows Control Strategy" block of Figure 5.1 effects this PHS discharging-charging strategy. As fresh $P_L(t)$ becomes available at the output of the LPF, $P_L^*(t)$ can be readily computed within the dispatch bids re-submission interval s. The "Dispatch Planning Process" loop can therefore generate and update the dispatch reference $P_{G,ref}(t)$ in time to meet the power market requirements.

5.2.3 Role of PHS in Increasing the Robustness of Dispatch Plan

Being the forecast of $P_L(t)$, $P_L^*(t)$ does contain errors. The error is un-avoidable and yet, it is desirable to minimize its impact on the dispatch bids $P_{G,ref}(t)$. Let the forecast error in $P_L^*(t)$ be $e(t)$, i.e.,

$$e(t) = P_L(t) - P_L^*(t) \tag{5.17}$$

Substituting $P_L^*(t)$ from (5.17) into (5.9) and (5.10) and in order to maintain $P_{G,ref}(t)$ at the same values as that determined using the forecast $P_L^*(t)$, the actual PHS power $P_P(t)$ is given by

$$P_P(t)=P_P^*(t) + e(t) \tag{5.18}$$

Thus another role of the PHS is to compensate for the errors in $P_L^*(t)$ so that $P_{G,ref}(t)$ can maintain at the values determined from $P_L^*(t)$ using (5.9) and (5.10). So apart from the primary function of the PHS in providing power when $P_L(t)$ becomes negative, the PHS also buffers the forecast errors in $P_L^*(t)$ and can thus play the role in increasing the robustness of the dispatch reference $P_{G,ref}(t)$.

$P_L^*(t)$ provides the information to determine $P_P^*(t)$ and whence $P_{G,ref}(t)$. The accuracy of the forecasts tend to degrade as the time horizon of the forecasts increases. Thus regular update of $P_L^*(t)$ is necessary so as to improve on the credibility of the dispatch plan $P_{G,ref}(t)$. It is for this reason that in this investigation, $P_L^*(t)$ is updated hourly, i.e. $s = 1$, and $P_{G,ref}(t)$ beyond the immediate 2 hours will be refreshed once the update in $P_L^*(t)$ is available.

5.2.4 Determination of PHS storage capacities

In this section, a statistical approach is suggested as a possible way to determine the power and energy capacities of the PHS necessary to achieve the dispatch planning objective.

Having determined the cutoff frequency of the LPF in Section 3.3, and with known historical $P_w(t)$ as input to the filter, the low-frequency components $P_L(t)$ of the wind power can be obtained. It is assumed that the forecast error in $P_L(t)$ is negligible and the actual $P_L(t)$ is used when designing the capacities of the PHS. From the power flows control strategy for the PHS described in Section 5.2.2 , the power flows to the PHS $P_P(t)$ can be obtained based on the known $P_L(t)$ over the complete study period of T_s days. Then take the absolute values of $P_P(t)$ and construct its CDF. Figure 5.5 shows an example of the CDF which shows that the maximum value of $|P_P(t)|$ is 0.08959 puMW which corresponds to the CDF of 1. One could therefore specify the PHS power capacity $P_{P,r}$ as 0.08959 puMW. With this power capacity, the PHS can be expected to buffer completely the low-frequency power fluctuations by the proposed power flows control strategy, provided the energy capacity of the PHS is also sufficiently large. Unfortunately $P_{P,r}$ so determined may be so large that the PHS is uneconomical.

The proposed statistical approach seeks to obtain a lower PHS power capacity such that the probability $|P_P(t)|$ is within the PHS power capacities is at a pre-specified level of p_P. Mathematically, to buffer the low-frequency wind power using the PHS, this design task can be expressed as the determination of $P_{P,r}$ such that

$$P\left\{\left|P_P(t)\right| \le P_{P,r}\right\} = p_P \tag{5.19}$$

In other words, the PHS can successfully satisfy the power demand with the probability of p_P. Using Figure 5.5 to illustrate the above concept, suppose p_P is set to be 0.995. From the figure, the power capacity of the PHS is $P_{P,r}$ = 0.074 puMW. Whence, $P_P(t)$ is expected to be outside the range [-0.074 puMW, 0.074 puMW] with the probability of 0.005. When $P_P(t)$ is outside the PHS power limits, the un-buffered power shall flows to the grid. With a judicious choice of p_P, however, one could arrive at an acceptable probability level for such circumstance while still maintaining a viable PHS design.

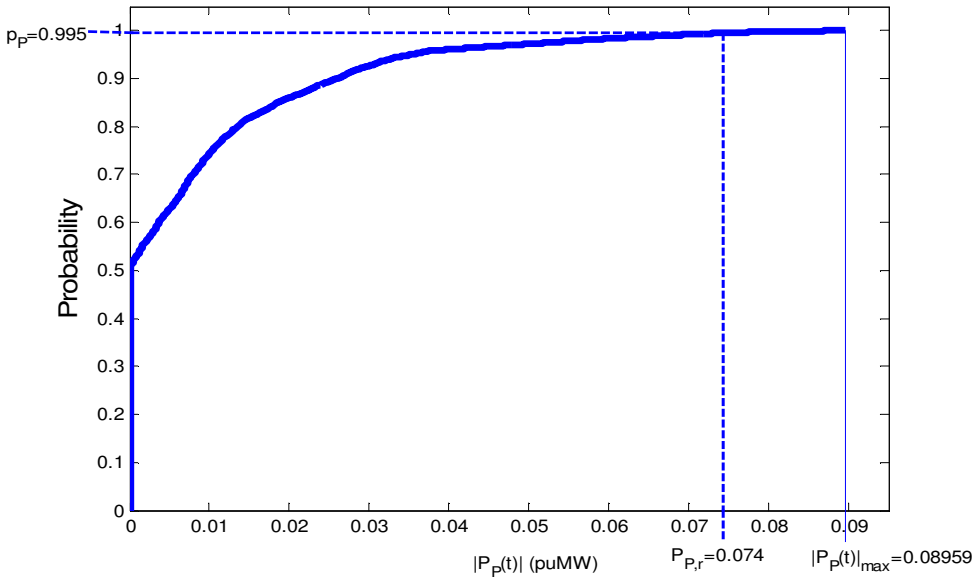

Figure 5.5. CDF of $|P_P(t)|$ showing $P_{P,r}$ is 0.074 puMW when p_P=0.995

The energy capacity of the PHS can also be calculated using the method similar to that described in Section 4.3.2, as follows. With known $P_P(t)$, the change in the stored energy level in the PHS ($\Delta E_P(t)$) is obtained by integrating $P_P(t)$ with respect to time, i.e.

$$\Delta E_P(t) = \int_0^t P_P(\tau) \cdot d\tau \tag{5.20}$$

The maximum and minimum values of $\Delta E_P(t)$, denoted as $\Delta E_{P,\max}$ and $\Delta E_{P,\min}$ respectively, can then be obtained over T_S. As the PHS must not operate below its maximum DoD $d_{P,\max}$, thus the rated energy capacity of the PHS is

$$E_{P,r} = \frac{\Delta E_{P,\max} - \Delta E_{P,\min}}{d_{P,\max}} \tag{5.21}$$

5.3 Illustrative Example

The proposed dispatch planning method will be illustrated, using the same 7-month of the aggregated output power $P_w(t)$ shown in Section 4.4.3. The data was recorded between Jan to July 2007 at a wind-farm in Jiangsu Province, China.

5.3.1 Design of the Dispatch Planning Process Loop

In Section 3.3, following an EMD analysis of the recorded $P_w(t)$, 24 IMFs and the residue function were obtained and a sample of which is as shown in Figure 3.4(b). Based on the IMF and the search procedure described in Section 3.3, it was subsequently found that the cutoff frequency of the LPF to achieve minimum overlap energy is 6.74×10^{-6} Hz. The designed LPF was then applied to obtain $P_L(t)$. The sample of the wind power $P_w(t)$, which is also considered in Sections 3.4 and 4.4, and the obtained $P_L(t)$ are shown in Figure 5.6. In Figure 3.4(b), recall the IMFs $c_1(t)$ and

$c_g(t)$ are components of the high- and mid-frequency wind power while $c_k(t)$, $c_m(t)$ and $r_n(t)$ are the components of $P_L(t)$. From the corresponding $\Delta E_i(t)$ plots shown in Figure 3.4(c), it can be easily established that $\Delta E_i(t)$ of the higher frequency component of $P_w(t)$ is clearly very small compared with that shown in the low-frequency components. Indeed, one can readily calculate the total amount of energy contained in $P_w(t)$ by integrating $P_w(t)$ with respect to time and compare it with that contained in $P_L(t)$. The respective values are 76.146 puMWh and 76.075 puMWh. The difference of 0.071 puMWh amounts to about 0.09% of the total harnessed wind power over the sample period. It therefore indicates that over the period, the net amount of the energy in the wind is contained in $P_L(t)$. The design of the PHS is therefore pertaining to the management of virtually all the energy contained in the wind. Thus the focus of dispatch planning is on the low-frequency $P_L(t)$ and it is a reasonable approach.

Next, the initial 6.5 months of $P_L(t)$ was used to set up and train the ANN model. In order to assess the performance of the ANN forecaster, the trained model was utilized to obtain $P_L^*(t)$ for the last 0.5 months of July 2007. Figure 5.7 shows the comparison between the forecast $P_L^*(t)$ and the actual $P_L(t)$: The mean absolute error of the forecast is 1.67% over the period. The ANN model is considered to have forecasted $P_L(t)$ to an acceptable level of accuracy.

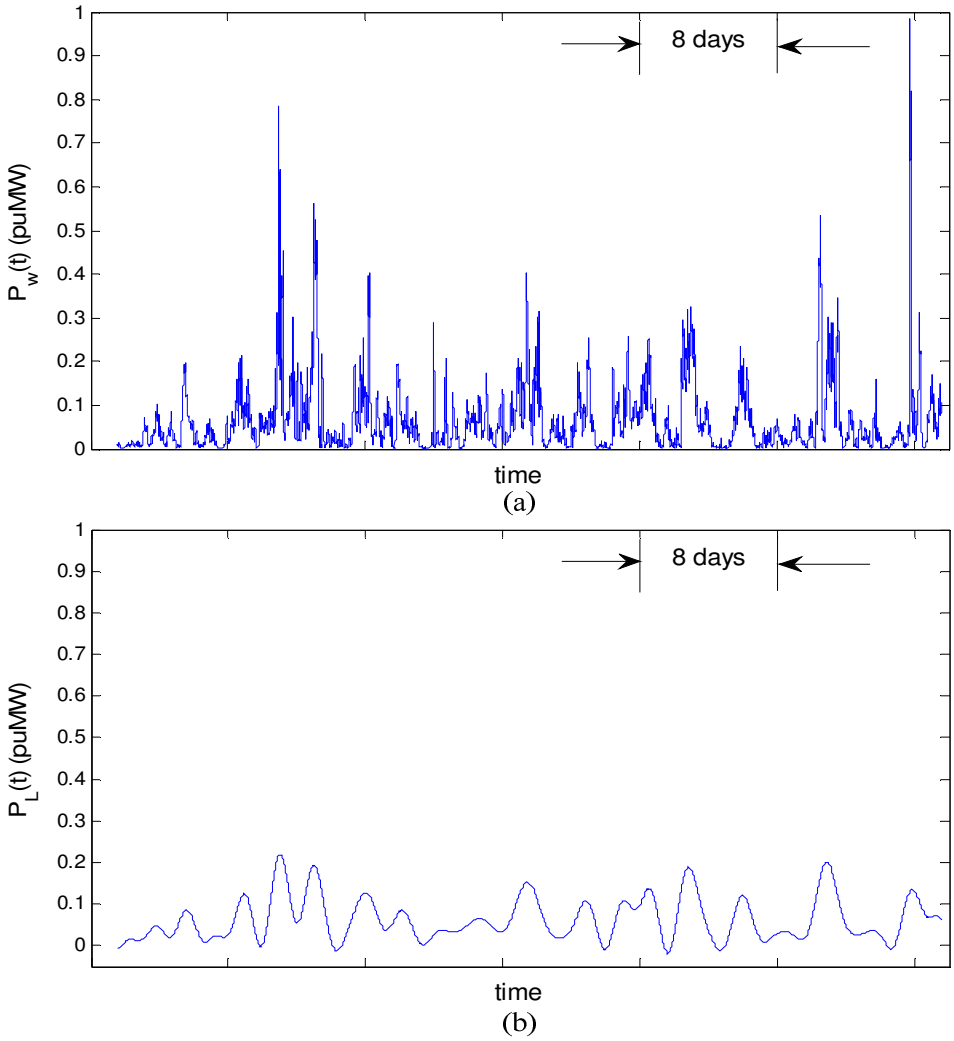

Figure 5.6. (a) A sample of wind power $P_w(t)$; (b) The corresponding $P_L(t)$ extracted from $P_w(t)$ using the designed LPF.

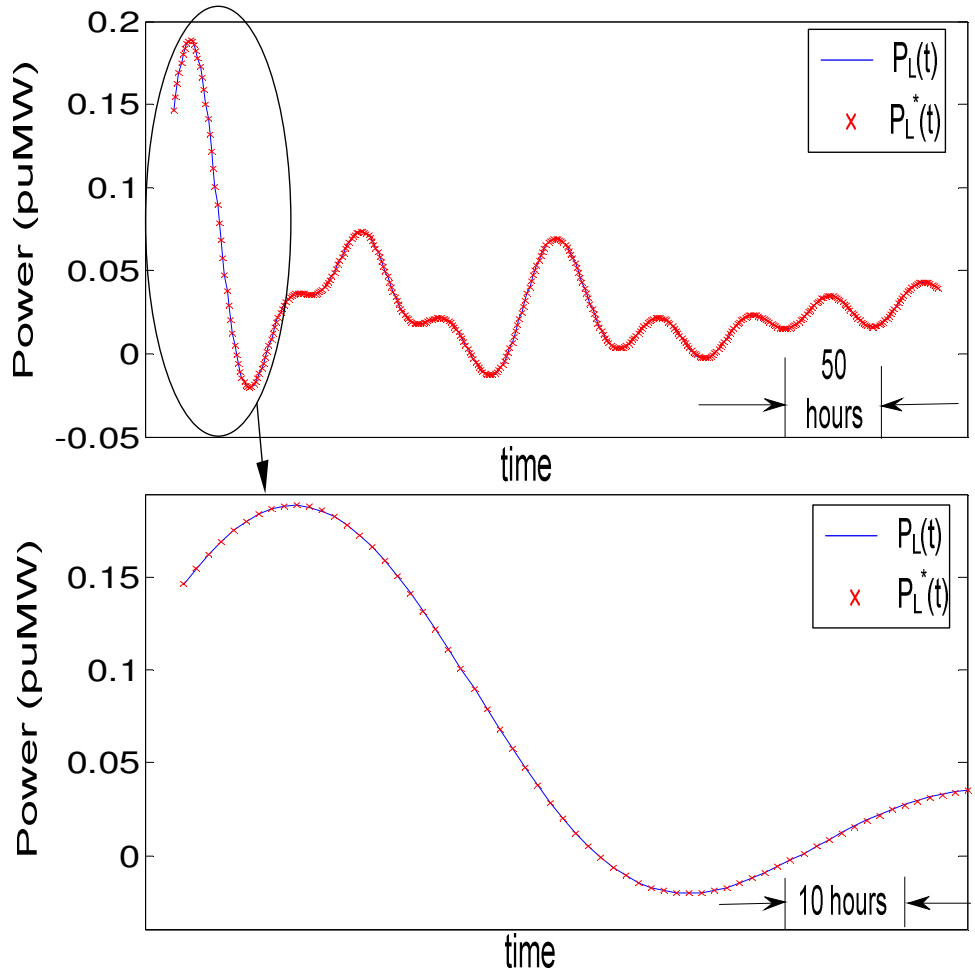

Figure 5.7. Comparison of $P_L(t)$ and $P_L^*(t)$ over the last 0.5 months of July 2007 and the expanded plot over the first 3 days of the period: Forecast updated hourly.

Over this 0.5 months period, negative $P_L^*(t)$ occurs on three occasions and are of durations 15.8, 19.4 and 10.4 hours. As indicated by (5.9) and (5.10), the PHS is to export power when $P_L^*(t)$ is negative. The discharging interval of the PHS corresponds to the duration of the negative $P_L^*(t)$ and are well within the typical periods in which the PHS can be expected to operate satisfactorily. It verifies the PHS is a suitable energy storage medium for the wind power dispatch planning scenario..

5.3.2 Determination of PHS storage capacities

The first 6.5-month of the $P_L(t)$ segment was used to determine the power and energy capacities of the PHS based on the method described in Section 5.2.4. From the power flows control strategy for the PHS described in Section 5.2.2, the power flows at the terminals of the PHS $P_P(t)$ can be obtained based on the known $P_L(t)$ over the 6.5 months. The obtained $P_P(t)$ is as shown in Figure 5.8(a). An expanded view showing one discharging-charging cycle of the PHS is also shown in Figure 5.8(b).

The CDF of $|P_P(t)|$ is shown in Figure 5.5. It shows that if the PHS is to successfully meet the power flows control strategy of Section 5.2.2 with the probability of 0.995, i.e. p_P=0.995, the required PHS power capacity $P_{P,r}$ is 0.074 puMW. This is a very modest level of power capacity, in comparison of the high degree of variability seen in $P_w(t)$ on Figure 5.6(a). The reason for this is because the high- and mid-frequency components of the wind power have been filtered out to be buffered by the BSHESS, as described in Chapter 4. The magnitude of the remaining low-frequency components of $P_w(t)$, shown in Figure 5.6(b), are of much reduced range. Furthermore, negative $P_L(t)$ assumes even lower values than the positive $P_L(t)$. Hence, $P_{P,r}$ is expected to be rather low, as shown.

With known $P_P(t)$, the change in the stored energy level in the PHS ($\Delta E_P(t)$) is obtained by integrating $P_P(t)$ with respect to time. The maximum and minimum values $\Delta E_{P,\max}$ and $\Delta E_{P,\min}$ can then be obtained over the 6.5 months. The maximum DoD $d_{P,max}$ of the PHS is assumed to be 0.8. The corresponding energy rating can be calculated using (5.21) and it yielded $E_{P,r}$=0.43 puMWh.

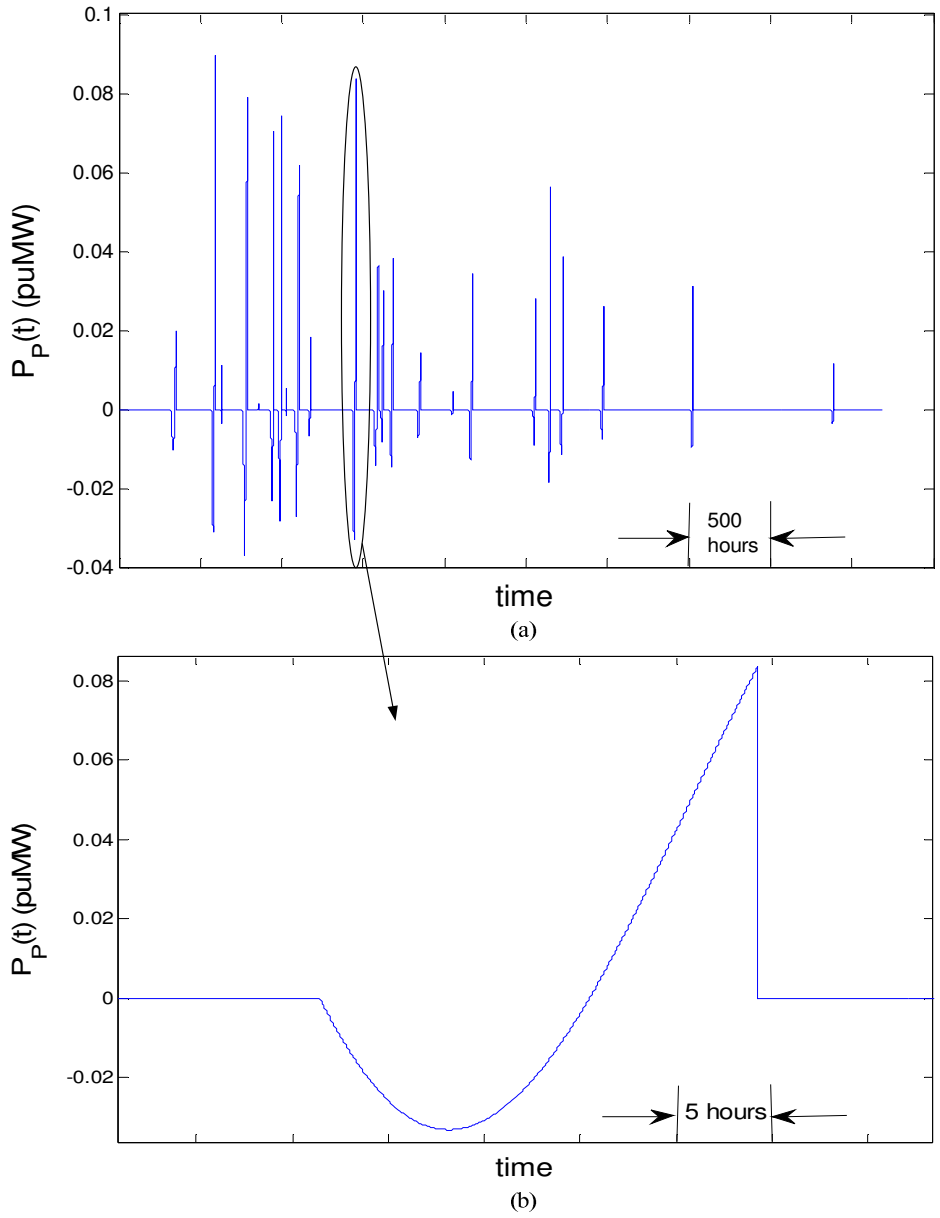

Figure 5.8. (a) $P_P(t)$ over 6.5 months; (b) Expanded view showing one discharging-charging cycle of the PHS

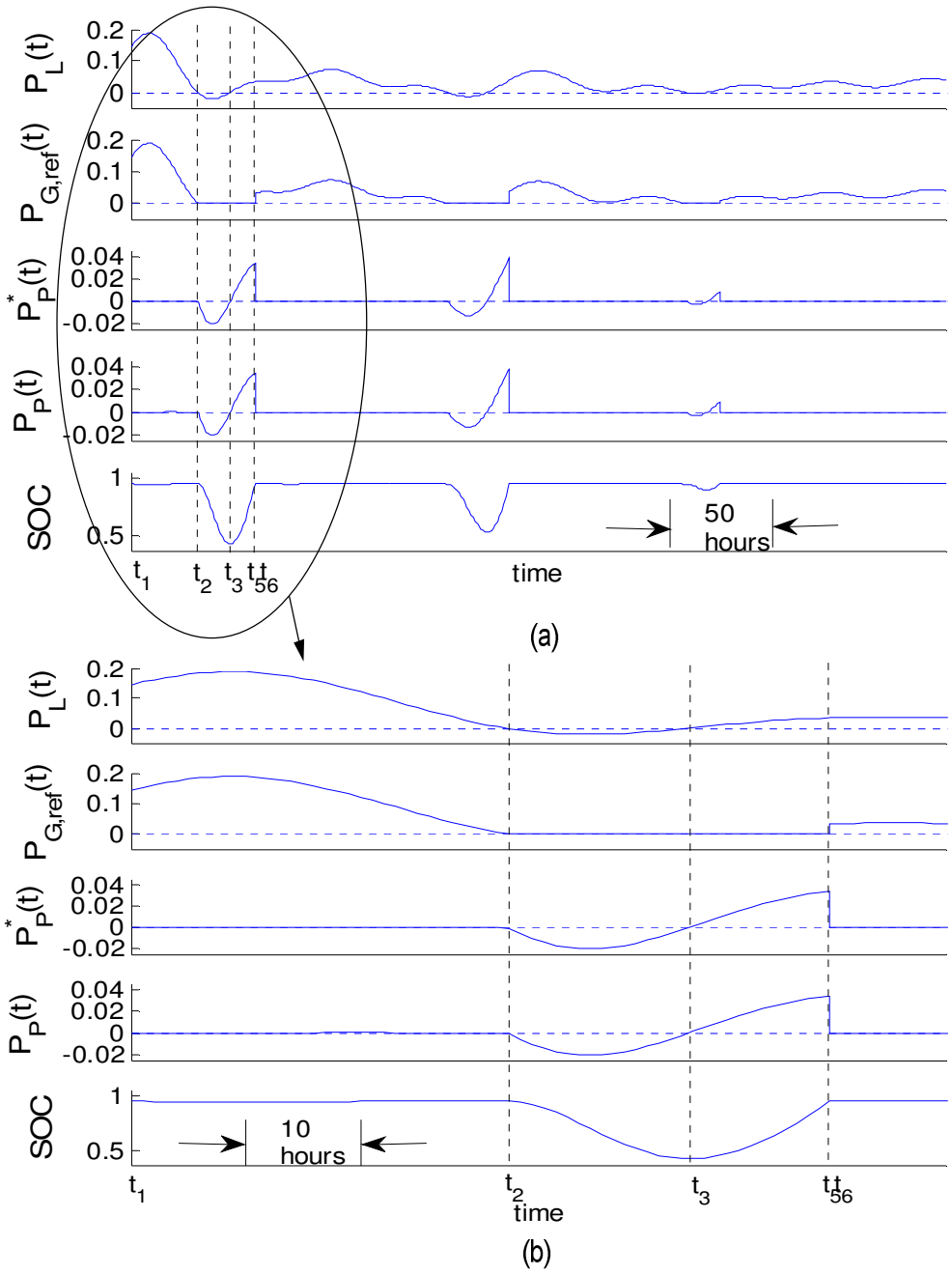

Figure 5.9. Outcome of the dispatch planning of the last 0.5 months of July 2007: (a) $P_L(t)$, $P_{G,ref}(t)$, $P_P^*(t)$, $P_P(t)$ (all expressed in puMW) and the *SOC* of the PHS; (b) Expanded view of the first 3-day of the plots shown in (a).

5.3.3 Outcome of the Dispatch Planning Process

With $P_L^*(t)$ so determined, the dispatch planning of the wind farm for the last 0.5 months of July 2007 can be carried out by following the PHS power flows control strategy described in Section 5.2.2. The obtained $P_{G,ref}(t)$ is as shown in Figure 5.9(a). Also shown is $P_L(t)$. Although $P_L(t)$ does assume negative values over certain intervals, however, with the help of the PHS, the dispatch bids submitted to the grid operator $P_{G,ref}(t)$ are always positive, i.e. there would be no power import from the grid. The actual PHS output power, $P_P(t)$, was obtained by subtracting $P_{G,ref}(t)$ from $P_L(t)$. The PHS is seen to undergo three distinct discharging-charging cycles over the 0.5-months period.

It would be instructive to examine the expanded view of the 3-day plots of $P_L(t)$, $P_{G,ref}(t)$, $P_P^*(t)$, $P_P(t)$ and the *SOC* of the PHS shown in Figure 5.9(b). Within the interval $t_1 \leq t \leq t_2$, $P_L(t)$ is positive and this net power is to be exported to the grid. Indeed, $P_{G,ref}(t)$ shows the export is taking place. However, $P_{G,ref}(t)$ is determined based on the forecast $P_L^*(t)$ and as shown on Figure 5.7, $P_L^*(t)$ differs slightly from $P_L(t)$. The power difference is buffered by the PHS, a role as explained in Section 5.2.3. PHS output power flows $P_P(t)$ are at relatively low level and are difficult to decipher from Figure 5.9(b). Subsequently over the interval $t_2 \leq t \leq t_3$, $P_L(t)$ is negative. Based on the dispatch planning strategy (5.14), there shall be no power export to the grid over this interval. Instead, the PHS discharges to support the wind farm-BSHESS. Hence, over this period, $P_P^*(t) = P_L^*(t)$ and as the PHS discharges, its *SOC* is seen to decrease, as expected. At $t = t_3$, $P_L(t)$ is observed to revert back to the positive directional flow. Instead of exporting $P_L(t)$ to the grid, the proposed dispatch planning strategy is to replenish the discharged energy of the PHS first so that the re-charged PHS will have the ability to provide the buffer power when the subsequent negative $P_L(t)$ occurs. Accordingly, the PHS is charged and its *SOC* increases from $t = t_3$ until $t = t_6$ when the PHS is fully charged, as indicated by its SOC of close to $1 - \varepsilon$ or 0.95.

Beyond t_6, as the PHS is fully charged and since $P_L(t)$ is positive, almost all of $P_L(t)$ would be exported to the grid in the form of the positive $P_{G,ref}(t)$. Only a small amount of $P_P(t)$ would be used to buffer the forecast error in $P_L^*(t)$, as explained earlier. The above process repeats itself subsequently.

With $\varepsilon = 0.05$, the SOC of the PHS is therefore allowed to operate within the range of [0.25, 0.95]. As can be seen in Figure 5.9, the SOC of the PHS is indeed within this range. It shows that the energy capacity of the PHS assumed earlier is adequate.

5.3.4 Comparison of the Dispatch Planning Approaches

An additional study has also been made into the dispatch planning strategy proposed in [109] and adopting it for the PHS. The aim is to compare the short-term dispatch schedules obtained using this strategy with that shown on Figure 5.9. For a reasonable comparison, the same PHS rated energy storage capacity $E_{P,r}$ of 0.43 puMWh has been assumed in this study. The same forecast $P_L^*(t)$ of Figure 5.7 was also used to determine $P_{G,ref}(t)$. However, in adopting the method of [109], $P_{G,ref}(t)$ is to assume either the maximum or the minimum value of $P_L^*(t)$, depending on whether the PHS is to undergo a discharging or charging process respectively. The PHS only changes its operating when the PHS is either fully charged or discharged. By applying this strategy, the results of Figure 5.10 was obtained for the same 3-day period shown in Figure 5.9(b).

Figure 5.10 shows that over the 3-day period, the PHS has undergone 3 complete charge-discharge cycles. Each of the cycles utilizes fully the PHS allowable charge-discharge energy of $(d_{P,max} - 2\varepsilon)E_{P,r}$ or 0.301 puMWh. In comparison, Figure 5.9(b) shows that the PHS has undergone only 1 charge-discharge cycle over the same period based on the present proposed strategy. It also involves the much lower charge-discharge energy level of about 0.21 puMWh. Thus one can expect a longer PHS

lifetime if the strategy proposed in the present work is adopted because of the less number of operating cycles. The much larger discharging-charging energy is involved in the approach of [109] because the resulting dispatch scheme requires the PHS to deal with both the positive as well as the negative $P_L^*(t)$.

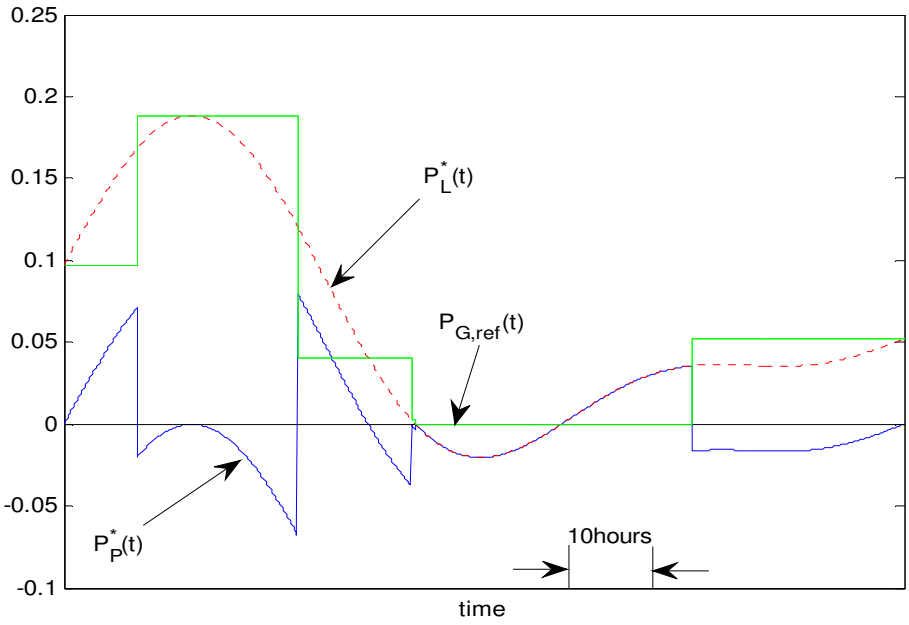

Figure 5.10. $P_{G,ref}(t)$ based on the dispatch strategy proposed in [109].

5.4 Conclusions

A method for dispatch planning has been proposed by focusing on the low-frequency components of the wind power extracted by a LPF. The output of the filter is then used in a developed ANN model to produce forecast of the low-frequency wind power components. By controlling the power flows of a PHS according to the developed strategy shown in the chapter, short-term dispatch planning can be achieved. The power and energy capacities of the PHS have been determined using a statistical

method. The proposed approach to dispatch planning has been demonstrated on the historical data of an existing wind farm.

As a result of adopting the proposed dispatch strategy, the PHS can be expected to undertake the energy buffering role infrequently, and the required PHS energy storage capacity is modest in comparison to the level of the harnessed energy from the wind. This is because the PHS is concerned with the provision of the power during periods of negative $P_L(t)$. The magnitudes of $P_L(t)$ are much lower than that observed in the variations of $P_w(t)$ which contain the high- and mid-frequency components. Hence, the proposed method has resulted in a much more realistic PHS design.

CHAPTER 6. Conclusions and Recommendations

6.1 Conclusions

The use of ESS for wind power smoothing and wind power dispatch has been studied in this thesis.

Chapter 2 focuses on the impacts of the perturbing wind power on grid systems by firstly explain the probability distributions of wind speed and wind power. The statistical models are to characterize the fluctuating nature of wind. Wind power perturbations may cause some problems such as voltage instability and frequency deviations, with the result that wind power generation is often considered non-dispatchable. Conventional method to mitigate the negative impacts is through the power regulation of other on-line generators but at the expense of costly reserve margin to be carried by the grid. This is a major impediment to the successful large-scale integration of wind power generation into grid systems, unless viable techniques to lessen the fluctuations can be found. Proper coordination of the control actions of WTG with that of the ESS can provide a solution for smoothing wind power and enhancing the dispatchability of wind generation in electricity markets. There are several storage options for wind energy applications. A review of some common ESS and their various characteristics are compared in the chapter.

In consideration of the above, Chapter 3 proposes a large-scale wind generation-ESS scheme so as to achieve the objectives of smoothing and dispatching the wind power. A battery-supercapacitor energy storage system is used for buffering the mid- and high-frequency wind power fluctuations, while a PHS is utilized to deal with the low-frequency components of the wind power in order to achieve the dispatch planning.

The scheme uses HPF, BPF and LPF to obtain the high-, mid- and low-frequency wind power components. By utilizing the EMD technique and the developed concept of minimum overlap energy, a new method to determine the cutoff frequencies of the three filters is described. In this way, the high-, mid- and low-frequency bands of the fluctuating wind power have been obtained to the extent that the SC, BESS and PHS can maximize the amount of energy they can deal with, with the least amount of cross-coupling between the three ESS.

With the cutoff frequencies of the filters determined, the battery-supercapacitor energy storage system for wind power smoothing is further examined in Chapter 4. In particular, the BSHESS power flows control scheme is shown. Furthermore, a statistical method has been developed to determine the power and energy capacities of the BSHESS so that the cost of the BSHESS is minimized while the BSHESS is able to smoothen the wind power to meet specified probability level. The method differs from the deterministic approach proposed by other researchers. The proposed approach has been applied to the design of a BSHESS of an existing wind farm and the designed BSHESS is shown to be able to achieve wind power smoothing to a satisfactory level.

After the high- and mid-frequency wind power perturbations have been removed by the BSHESS, the remaining low-frequency oscillating components is focused on for dispatch planning. A method to carry out dispatch planning has been proposed in Chapter 5. Specifically, the output of the LPF is used in a developed ANN model to produce forecast of the low-frequency wind power components. By controlling the power flows of a PHS according to the developed strategy shown in Chapter 5, short-term dispatch planning can be achieved. A statistical method is also presented to determine the power and energy capacities of the PHS. The proposed approach to dispatch planning has been illustrated on an existing wind farm.

6.2 Recommendations for Future Works

Notwithstanding of the progress made so far, the following areas are suggested for further investigations.

1. **Dynamic model of system**

   The more detailed model of the proposed grid-connected wind generation-ESS scheme should be established to assess its dynamic performance. The power smoothing and dispatching capability of proposed scheme can then be examined dynamically by considering the possible interactions between the ESS and the WTG. Also the effects of filters' cutoff frequencies and the ESS storage capacities can also be studied in greater detail. In the model, the power quality enhancement and the power dispatch is integrated into a combined operational scheme. Thus the two different aspects of network functions, i.e. power quality and power/energy management, could result in a faster inner power quality control loop and an outer but slower power dispatch control loop. The coordination of the control actions and the different ESS mediums which cater for their respective functions can be investigated.

2. **Voltage quality of point-of-common coupling (PCC)**

   In Figure 3.3, the voltage quality at the PCC remains to be investigated. Under both uncertain generation and demand scenario, maintaining voltage quality in network is a significant concern to ensure the proper operation of the power system. Reactive power flows from grid, WTG and ESS can be determined to ensure acceptable voltage quality in the system so that the magnitude of the voltage at PCC is controlled to remain acceptable level. An effective control method has to be developed to control the reactive power flows. Therefore,

another loop for reactive power control would have to be included to the dynamical model of the system.

3. Mixed renewable power generation

Thus far the study has only focused on wind generation. A fruitful area would be to investigate a mixed renewable power generation scenario, e.g. a mixed solar-wind generation. The different sources could complement each other. For example, instances of strong wind may coincide with that of low or no solar irradiation conditions, and vice versa. Thus one can expect the degree of variability of the mixed renewable generation system to be lower than that of a wind generation system. As a result, the capacity of the ESS required to achieve power smoothing and renewable power dispatchability will be correspondingly lower. This will make the harnessing of RE for electricity production an even more viable proposition.

Author's Publications

- M. T. Li, S. S. Choi, Y. Yuan, C. C. Sun and Jiyun Zhao, "Design of Battery-Supercapacitor Energy Storage System for Wind Power Smoothing Using Minimum Overlap Energy Concept and Statistical Technique", IET Generation, Transmission & Distribution, Submitted.

- M. T. Li, S. S. Choi, Y. Yuan, C. C. Sun and Jiyun Zhao, "Dispatch Planning for Large-scale Wind Power-Pumped Hydroelectric Scheme Based on Low-frequency Intrinsic Mode and Residue Functions", Revise to re-submit.

- M. T. Li, S. S. Choi, K. J. Tseng, Y. Yuan and C. C. Sun, "Design of energy storage scheme for the smoothing and dispatch planning of large-scale wind power generation," *5th International Conference on Electric Utility Deregulation and Restructuring and Power Technologies (DRPT)*, Changsha, 2015, pp. 2113-2119.

- S.S. Choi, K.W. Wee and M.T. Li, "Roles of Energy Storage in the Dispatch Planning of Large-scale Wind Power," *2017 international conference on sustainable energy engineering (ICSEE 2017)*, Perth, Australia, Accepted.

Bibliographies

[1] S. Chu and A. Majumdar, "Opportunities and challenges for a sustainable energy future," *nature,* vol. 488, no. 7411, pp. 294-303, 2012.

[2] I. Dincer, "Renewable energy and sustainable development: a crucial review," *Renewable and Sustainable Energy Reviews,* vol. 4, no. 2, pp. 157-175, 2000.

[3] *International Energy Agency in World Energy Outlook 2011*. Available: http://www.worldenergyoutlook.org/

[4] J. Goldemberg, "Ethanol for a sustainable energy future," *Science,* vol. 315, no. 5813, pp. 808-810, 2007.

[5] L. Freris and D. Infield, *Renewable energy in power systems*: John Wiley & Sons, 2008.

[6] A. D. Şahin, "Progress and recent trends in wind energy," *Progress in energy and combustion science,* vol. 30, no. 5, pp. 501-543, 2004.

[7] T. Ackermann, *Wind power in power systems*: Chichester, UK: John Wiley & Sons, 2005.

[8] A. Hepbasli, "A key review on exergetic analysis and assessment of renewable energy resources for a sustainable future," *Renewable and Sustainable Energy Reviews,* vol. 12, no. 3, pp. 593-661, 2008.

[9] O. Alnatheer, "The potential contribution of renewable energy to electricity supply in Saudi Arabia," *Energy Policy,* vol. 33, no. 18, pp. 2298-2312, 2005.

[10] J. M. Huacuz, "The road to green power in Mexico—reflections on the prospects for the large-scale and sustainable implementation of renewable energy," *Energy Policy,* vol. 33, no. 16, pp. 2087-2099, 2005.

[11] R. Duke, R. Williams and A. Payne, "Accelerating residential PV expansion: demand analysis for competitive electricity markets," *Energy Policy,* vol. 33, no. 15, pp. 1912-1929, 2005.

[12] G. M. Montes, M. d. M. S. López, M. d. C. R. Gámez and A. M. Ondina, "An overview of renewable energy in Spain. The small hydro-power case," *Renewable and Sustainable Energy Reviews,* vol. 9, no. 5, pp. 521-534, 2005.

[13] J. Kaldellis, D. Vlachou and G. Korbakis, "Techno-economic evaluation of small hydro power plants in Greece: a complete sensitivity analysis," *Energy Policy,* vol. 33, no. 15, pp. 1969-1985, 2005.

[14] C. K. N. Cavaliero and E. P. Da Silva, "Electricity generation: regulatory mechanisms to incentive renewable alternative energy sources in Brazil," *Energy policy,* vol. 33, no. 13, pp. 1745-1752, 2005.

[15] M. A. El-Sayed, "Solar supported steam production for power generation in Egypt," *Energy Policy,* vol. 33, no. 10, pp. 1251-1259, 2005.

[16] E. Gnansounou, A. Dauriat and C. Wyman, "Refining sweet sorghum to ethanol and sugar: economic trade-offs in the context of North China," *Bioresource Technology,* vol. 96, no. 9, pp. 985-1002, 2005.

[17] H. Lund, "Renewable energy strategies for sustainable development," *Energy,* vol. 32, no. 6, pp. 912-919, 2007.

[18] *REN21-The Renewable Energy Policy Network for the 21st Century . Renewables 2011-Global Status Report.* Available: http://www.ren21.net/Portals/97/documents/GSR/REN21_GSR2011.pdf.

[19] B. V. Mathiesen, H. Lund and K. Karlsson, "100% Renewable energy systems, climate mitigation and economic growth," *Applied Energy,* vol. 88, no. 2, pp. 488-501, 2011.

[20] D. Y. Leung and Y. Yang, "Wind energy development and its environmental impact: A review," *Renewable and Sustainable Energy Reviews,* vol. 16, no. 1, pp. 1031-1039, 2012.

[21] G. de Carmoy, "The USA faces the energy challenge," *Energy Policy,* vol. 6, no. 1, pp. 36-52, 1978.

[22] R. L. Thomas and W. H. Robbins, "Large wind-turbine projects in the United States wind energy program," *Journal of Wind Engineering and Industrial Aerodynamics,* vol. 5, no. 3, pp. 323-335, 1980.

[23] P. Gipe, "Wind energy comes of age California and Denmark," *Energy Policy,* vol. 19, no. 8, pp. 756-767, 1991.

[24] J. K. Kaldellis and D. Zafirakis, "The wind energy (r) evolution: A short review of a long history," *Renewable Energy,* vol. 36, no. 7, pp. 1887-1901, 2011.

[25] T. Ackermann and L. Söder, "An overview of wind energy-status 2002," *Renewable and sustainable energy reviews,* vol. 6, no. 1, pp. 67-127, 2002.

[26] A. Hepbasli and O. Ozgener, "A review on the development of wind energy in Turkey," *Renewable and Sustainable Energy Reviews,* vol. 8, no. 3, pp. 257-276, 2004.

[27] J. Xu, D. He and X. Zhao, "Status and prospects of Chinese wind energy," *Energy,* vol. 35, no. 11, pp. 4439-4444, 2010.

[28] B. K. Sahu, M. Hiloidhari and D. C. Baruah, "Global trend in wind power with special focus on the top five wind power producing countries," *Renewable and Sustainable Energy Reviews,* vol. 19, pp. 348-359, March 2013.

[29] S. Gsänger, "World Wind Energy Report 2010," *World Wind Energy Association,* 2010.

[30] S. Santoso, M. F. F. MCGRANAGHAN, R. C. Dugan and H. W. Beaty, "Electrical power systems quality," *Recherche,* vol. 67, p. 02, 2012.

[31] T. Kousksou, P. Bruel, A. Jamil, T. El Rhafiki and Y. Zeraouli, "Energy storage: Applications and challenges," *Solar Energy Materials and Solar Cells,* vol. 120, pp. 59-80, 2014.

[32] F. Díaz-González, A. Sumper, O. Gomis-Bellmunt and R. Villafáfila-Robles, "A review of energy storage technologies for wind power applications," *Renewable and Sustainable Energy Reviews,* vol. 16, no. 4, pp. 2154-2171, May. 2012.

[33] S. Koohi-Kamali, V. Tyagi, N. Rahim, N. Panwar and H. Mokhlis, "Emergence of energy storage technologies as the solution for reliable operation of smart power systems: a review," *Renewable and Sustainable Energy Reviews,* vol. 25, pp. 135-165, 2013.

[34] Q. Jiang, Y. Gong and H. Wang, "A battery energy storage system dual-layer control strategy for mitigating wind farm fluctuations," *IEEE Trans. Power Syst.,* vol. 28, no. 3, pp. 3263-3273, 2013.

[35] L. Journal of Power ElectronicsHansang, S. Byoung Yoon, H. Sangchul, J. Seyong, P. Byungjun and J. Gilsoo, "Compensation for the Power Fluctuation of the Large Scale Wind Farm Using Hybrid Energy Storage Applications," *IEEE Trans. Appl. Supercond.,* vol. 22, no. 3, pp. 5701904-5701904, Jun. 2012.

[36] J. Garcia-Gonzalez, R. M. R. de la Muela, L. M. Santos and A. M. Gonzalez, "Stochastic Joint Optimization of Wind Generation and

Pumped-Storage Units in an Electricity Market," *IEEE Trans. Power Syst.,* vol. 23, no. 2, pp. 460-468, 2008.

[37] R. Jiang, J. Wang and Y. Guan, "Robust unit commitment with wind power and pumped storage hydro," *IEEE Trans. Power Syst.,* vol. 27, no. 2, pp. 800-810, 2012.

[38] X. Y. Wang, D. M. Vilathgamuwa and S. S. Choi, "Buffer scheme with battery energy storage capability for enhancement of network transient stability and load ride-through," *Journal of Power Sources,* vol. 179, no. 2, pp. 819-829, 2008.

[39] F. Liu, S. Mei, D. Xia, Y. Ma, X. Jiang and Q. Lu, "Experimental evaluation of nonlinear robust control for SMES to improve the transient stability of power systems," *IEEE Trans. Energy Convers.,* vol. 19, no. 4, pp. 774-782, 2004.

[40] H. T. Le, S. Santoso and T. Q. Nguyen, "Augmenting wind power penetration and grid voltage stability limits using ESS: application design, sizing, and a case study," *IEEE Trans. Power Syst.,* vol. 27, no. 1, pp. 161-171, 2012.

[41] P. Mercier, R. Cherkaoui and A. Oudalov, "Optimizing a Battery Energy Storage System for Frequency Control Application in an Isolated Power System," *IEEE Trans. Power Syst.,* vol. 24, no. 3, pp. 1469-1477, 2009.

[42] T. K. Brekken, A. Yokochi, A. Von Jouanne, Z. Z. Yen, H. M. Hapke and D. A. Halamay, "Optimal energy storage sizing and control for wind power applications," *IEEE Trans. Sustain. Energy,* vol. 2, no. 1, pp. 69-77, 2011.

[43] Y. Iijima, Y. Sakanaka, N. Kawakami, M. Fukuhara, K. Ogawa, M. Bando, *et al.*, "Development and field experiences of NAS battery inverter for

power stabilization of a 51 MW wind farm," presented at the 2010 International Power Electronics Conference (IPEC), 2010.

[44] P. A. Lynn, *Onshore and offshore wind energy : an introduction*: Chichester, West Sussex : Wiley, 2012.

[45] T. Burton, D. Sharpe, N. Jenkins and E. Bossanyi, *Wind energy handbook*: John Wiley & Sons, 2001.

[46] P. Jain, *Wind energy engineering*: New York : McGraw-Hill, 2011.

[47] M. Sathyajith, *Wind energy: fundamentals, resource analysis and economics*: Springer Science & Business Media, 2006.

[48] J. P. Hennessey Jr, "Some aspects of wind power statistics," *Journal of applied meteorology,* vol. 16, no. 2, pp. 119-128, 1977.

[49] S. M. s. PT, "The estimation of parameters of the Weibull wind speed distribution for wind energy utilization purposes," *Wind Engineering,* vol. 3, no. 2, pp. 132-145, 1979.

[50] J. Carta, P. Ramirez and S. Velázquez, "A review of wind speed probability distributions used in wind energy analysis: Case studies in the Canary Islands," *Renewable and Sustainable Energy Reviews,* vol. 13, no. 5, pp. 933-955, 2009.

[51] M. Chinchilla, S. Arnaltes and J. C. Burgos, "Control of permanent-magnet generators applied to variable-speed wind-energy systems connected to the grid," *IEEE Trans. Energy Convers.,* vol. 21, no. 1, pp. 130-135, 2006.

[52] M. E. Haque, M. Negnevitsky and K. M. Muttaqi, "A Novel Control Strategy for a Variable-Speed Wind Turbine With a Permanent-Magnet

Synchronous Generator," *IEEE Trans. Ind Appl,* vol. 46, no. 1, pp. 331-339, 2010.

[53] Z. Shao, T. King-Jet, D. M. Vilathgamuwa, T. D. Nguyen and W. Xiao-Yu, "Design of a Robust Grid Interface System for PMSG-Based Wind Turbine Generators," *IEEE Trans. Ind. Electron.,* vol. 58, no. 1, pp. 316-328, 2011.

[54] A. Leon-Garcia, *Probability, statistics, and random processes for electrical engineering*: Upper Saddle River, NJ : Pearson/Prentice Hall., 2008.

[55] P. Z. Peebles, *Probability, random variables, and random signal principles*: New York, NY : McGraw Hill, 4th ed., 2001.

[56] L. Xian and X. Wilsun, "Minimum Emission Dispatch Constrained by Stochastic Wind Power Availability and Cost," *IEEE Trans. Power Syst.,* vol. 25, no. 3, pp. 1705-1713, 2010.

[57] R. C. Dugan, M. F. McGranaghan and H. W. Beaty, "Electrical power systems quality," *New York, NY: McGraw-Hill,| c1996,* vol. 1, 1996.

[58] M. Ammar and G. Joos, "A Short-Term Energy Storage System for Voltage Quality Improvement in Distributed Wind Power," *IEEE Trans. Energy Convers.,* vol. 29, no. 4, pp. 997-1007, 2014.

[59] A. Arulampalam, M. Barnes, N. Jenkins and J. B. Ekanayake, "Power quality and stability improvement of a wind farm using STATCOM supported with hybrid battery energy storage," *Generation, Transmission and Distribution, IEE Proceedings-,* vol. 153, no. 6, pp. 701-710, 2006.

[60] S. W. Mohod and M. V. Aware, "A STATCOM-Control Scheme for Grid Connected Wind Energy System for Power Quality Improvement," *Systems Journal, IEEE,* vol. 4, no. 3, pp. 346-352, 2010.

[61] T. Aigner, S. Jaehnert, G. L. Doorman and T. Gjengedal, "The Effect of Large-Scale Wind Power on System Balancing in Northern Europe," *IEEE Trans. Sustain. Energy,* vol. 3, no. 4, pp. 751-759, 2012.

[62] D. D. Banham-Hall, G. A. Taylor, C. A. Smith and M. R. Irving, "Flow Batteries for Enhancing Wind Power Integration," *IEEE Trans. Power Syst.,* vol. 27, no. 3, pp. 1690-1697, 2012.

[63] H. Bevrani and P. R. Daneshmand, "Fuzzy Logic-Based Load-Frequency Control Concerning High Penetration of Wind Turbines," *Systems Journal, IEEE,* vol. 6, no. 1, pp. 173-180, 2012.

[64] Y. Z. Sun, Z. S. Zhang, G. J. Li and J. Lin, "Review on frequency control of power systems with wind power penetration," presented at the 2010 International Conference on Power System Technology (POWERCON), 2010.

[65] P. Kundur, N. J. Balu and M. G. Lauby, *Power system stability and control* vol. 7: McGraw-hill New York, 1994.

[66] J. Machowski, J. W. Bialek and J. R. Bumby, *Power system dynamics : stability and control*: Chichester, U.K. : Wiley. 2nd ed., 2008.

[67] Y. G. Rebours, D. S. Kirschen, M. Trotignon and S. Rossignol, "A survey of frequency and voltage control ancillary services--Part I: technical features," *IEEE Trans. Power Syst.,* no. 1, p. 350, 2007.

[68] H. Bevrani and T. Hiyama, *Intelligent automatic generation control*: Boca Raton : CRC Press., 2011.

[69] T. Ackermann, *Wind power in power systems.* : Chichester, West Sussex ; Hoboken, N.J. : Wiley., 2012.

[70] H. Holttinen, "Hourly wind power variations and their impact on the Nordic power system operation," *Licenciate Thesis,* 2003.

[71] R. Zavadil, "2006 Minnesota Wind Integration Study," *Enernex Corp.,* vol. I, Nov. 30, 2006.

[72] G. Koeppel and M. Korpås, "Improving the network infeed accuracy of non-dispatchable generators with energy storage devices," *Electric Power Systems Research,* vol. 78, no. 12, pp. 2024-2036, 2008.

[73] M. U. Usama, D. Kelle and T. Baldwin, "Utilizing spinning reserves as energy storage for renewable energy integration," presented at the Power Systems Conference (PSC), Clemson University, 2014.

[74] M. Black and G. Strbac, "Value of storage in providing balancing services for electricity generation systems with high wind penetration," *Journal of Power Sources,* no. 2, p. 949, 2006.

[75] A. M. Howlader, N. Urasaki, A. Yona, T. Senjyu and A. Y. Saber, "A review of output power smoothing methods for wind energy conversion systems," *Renewable and Sustainable Energy Reviews,* vol. 26, pp. 135-146, 2013.

[76] X. Luo, J. Wang, M. Dooner and J. Clarke, "Overview of current development in electrical energy storage technologies and the application potential in power system operation," *Applied Energy,* vol. 137, pp. 511-536, 2015.

[77] S. Sundararagavan and E. Baker, "Evaluating energy storage technologies for wind power integration," *Solar Energy,* vol. 86, no. 9, pp. 2707-2717, 2012.

[78] H. Chen, T. N. Cong, W. Yang, C. Tan, Y. Li and Y. Ding, "Progress in electrical energy storage system: A critical review," *Progress in Natural Science,* vol. 19, no. 3, pp. 291-312, 2009.

[79] C. Abbey and G. Joos, "Supercapacitor Energy Storage for Wind Energy Applications," *IEEE Trans. Ind Appl,* vol. 43, no. 3, pp. 769-776, 2007.

[80] N. Thanh Hai and L. Dong-Choon, "Advanced Fault Ride-Through Technique for PMSG Wind Turbine Systems Using Line-Side Converter as STATCOM," *IEEE Trans. Ind. Electron.,* vol. 60, no. 7, pp. 2842-2850, 2013.

[81] S. M. Muyeen, H. M. Hasanien and J. Tamura, "Reduction of frequency fluctuation for wind farm connected power systems by an adaptive artificial neural network controlled energy capacitor system," *Renewable Power Generation, IET,* vol. 6, no. 4, pp. 226-235, 2012.

[82] T. Kinjo, T. Senjyu, N. Urasaki and H. Fujita, "Output levelling of renewable energy by electric double-layer capacitor applied for energy storage system," *IEEE Trans. Energy Convers.,* vol. 21, no. 1, pp. 221-227, 2006.

[83] S. M. Muyeen, S. Shishido, M. H. Ali, R. Takahashi, T. Murata and J. Tamura, "Application of energy capacitor system to wind power generation," *Wind Energy,* vol. 11, no. 4, pp. 335-350, 2008.

[84] S. M. Muyeen, R. Takahashi, T. Murata and J. Tamura, "Integration of an Energy Capacitor System With a Variable-Speed Wind Generator," *IEEE Trans. Energy Convers.,* vol. 24, no. 3, pp. 740-749, 2009.

[85] S. D. G. Jayasinghe, D. M. Vilathgamuwa and U. K. Madawala, "A Dual Inverter-Based Supercapacitor Direct Integration Scheme for Wind Energy

Conversion Systems," *IEEE Trans. Ind Appl,* vol. 49, no. 3, pp. 1023-1030, 2013.

[86] X. Y. Wang, D. Mahinda Vilathgamuwa and S. S. Choi, "Determination of battery storage capacity in energy buffer for wind farm," *IEEE Trans. Energy Convers.,* vol. 23, no. 3, pp. 868-878, 2008.

[87] J. Zeng, B. Zhang, C. Mao and Y. Wang, "Use of battery energy storage system to improve the power quality and stability of wind farms," presented at the International Conference on Power System Technology, 2006.

[88] K. Li, H. Xu, Q. Ma and J. Zhao, "Hierarchy control of power quality for wind–battery energy storage system," *IET Power Electronics,* vol. 7, no. 8, pp. 2123-2132, 2014.

[89] B. Parkhideh, J. Zeng, S. Baek, S. Bhattacharya, M. Baran and A. Q. Huang, "Improved wind farm's power availability by battery energy storage systems: Modeling and control," presented at the Industrial Electronics, IECON, 34th Annual Conference of IEEE, 2008.

[90] X. Li, "Fuzzy adaptive Kalman filter for wind power output smoothing with battery energy storage system," *Renewable Power Generation, IET,* vol. 6, no. 5, pp. 340-347, 2012.

[91] M. Khalid and A. Savkin, "A model predictive control approach to the problem of wind power smoothing with controlled battery storage," *Renewable Energy,* vol. 35, no. 7, pp. 1520-1526, 2010.

[92] Q. Jiang and H. Hong, "Wavelet-Based Capacity Configuration and Coordinated Control of Hybrid Energy Storage System for Smoothing Out Wind Power Fluctuations," *IEEE Trans. Power Syst.,* vol. 28, no. 2, pp. 1363-1372, 2013.

[93] N. E. Huang, Z. Shen, S. R. Long, M. C. Wu, H. H. Shih, Q. Zheng, *et al.*, "The empirical mode decomposition and the Hilbert spectrum for nonlinear and non-stationary time series analysis," *Proceedings of the Royal Society of London. Series A: Mathematical, Physical and Engineering Sciences,* vol. 454, no. 1971, pp. 903-995, 1998.

[94] A. Esmaili, B. Novakovic, A. Nasiri and O. Abdel-Baqi, "A Hybrid System of Li-Ion Capacitors and Flow Battery for Dynamic Wind Energy Support," *IEEE Trans. Ind Appl,* vol. 49, no. 4, pp. 1649-1657, 2013.

[95] H. Zhou, T. Bhattacharya, D. Tran, T. S. T. Siew and A. M. Khambadkone, "Composite energy storage system involving battery and ultracapacitor with dynamic energy management in microgrid applications," *IEEE Trans. Power Electron.,* vol. 26, no. 3, pp. 923-930, Mar. 2011.

[96] W. Li, G. Joós and J. Bélanger, "Real-time simulation of a wind turbine generator coupled with a battery supercapacitor energy storage system," *IEEE Trans. Ind. Electron.,* vol. 57, no. 4, pp. 1137-1145, Apr. 2010.

[97] T. Gee, F. Robinson and R. Dunn, "Analysis of battery lifetime extension in a small-scale wind-energy system using supercapacitors," *IEEE Trans. Energy Convers.,* vol. 28, no. 1, pp. 24-33, Mar. 2013.

[98] K. W. Wee, S. S. Choi and D. M. Vilathgamuwa, "Design of a Least-Cost Battery-Supercapacitor Energy Storage System for Realizing Dispatchable Wind Power," *IEEE Trans. Sustain. Energy,* vol. 4, no. 3, pp. 1-11, Jul. 2013.

[99] J. M. Loring, "Wind energy planning in England, Wales and Denmark: Factors influencing project success," *Energy policy,* vol. 35, no. 4, pp. 2648-2660, 2007.

[100] N. Zouros, G. Contaxis and J. Kabouris, "Decision support tool to evaluate alternative policies regulating wind integration into autonomous energy systems," *Energy Policy,* vol. 33, no. 12, pp. 1541-1555, 2005.

[101] R. Saidur, M. Islam, N. Rahim and K. Solangi, "A review on global wind energy policy," *Renewable and Sustainable Energy Reviews,* vol. 14, no. 7, pp. 1744-1762, 2010.

[102] A. Ciarreta, C. Gutiérrez-Hita and S. Nasirov, "Renewable energy sources in the Spanish electricity market: Instruments and effects," *Renewable and Sustainable Energy Reviews,* vol. 15, no. 5, pp. 2510-2519, 2011.

[103] F. Yong, M. Shahidehpour and L. Zuyi, "Security-Constrained Unit Commitment With AC Constraints*," *IEEE Trans. Power Syst.,* vol. 20, no. 3, pp. 1538-1550, 2005.

[104] P. Jain, *Wind energy engineering*: McGraw Hill Professional, 2010.

[105] J. Matevosyan and L. Soder, "Minimization of imbalance cost trading wind power on the short-term power market," *IEEE Trans. Power Syst.,* vol. 21, no. 3, pp. 1396-1404, 2006.

[106] T. Gul and T. Stenzel, "Variability of wind power and other renewables: management options and strategies," *International Energy Agency, Paris, France,* 2005.

[107] M. E. Khodayar, L. Abreu and M. Shahidehpour, "Transmission-constrained intrahour coordination of wind and pumped-storage hydro units," *IET Generation, Transmission & Distribution,* vol. 7, no. 7, pp. 755-765, 2013.

[108] J. P. Deane, E. J. McKeogh and B. P. O. Gallachoir, "Derivation of Intertemporal Targets for Large Pumped Hydro Energy Storage With

Stochastic Optimization," *IEEE Trans. Power Syst.,* vol. 28, no. 3, pp. 2147-2155, 2013.

[109] Q. Li, S. S. Choi, Y. Yuan and D. L. Yao, "On the Determination of Battery Energy Storage Capacity and Short-Term Power Dispatch of a Wind Farm," *IEEE Trans. Sustain. Energy,* vol. 2, no. 2, pp. 148-158, 2011.

[110] D. L. Yao, S. S. Choi, K. J. Tseng and T. T. Lie, "Determination of short-term power dispatch schedule for a wind farm incorporated with dual-battery energy storage scheme," *IEEE Trans. Sustain. Energy,* vol. 3, no. 1, pp. 74-84, 2012.

[111] D. L. Yao, S. S. Choi, K. J. Tseng and T. T. Lie, "A Statistical Approach to the Design of a Dispatchable Wind Power-Battery Energy Storage System," *IEEE Trans. Energy Convers.,* vol. 24, no. 4, pp. 916-925, 2009.

[112] F. Luo, K. Meng, Z. Y. Dong, Y. Zheng, Y. Chen and K. P. Wong, "Coordinated Operational Planning for Wind Farm With Battery Energy Storage System," *IEEE Trans. Sustain. Energy,* vol. 6, no. 1, pp. 253-262, 2015.

[113] L. Meng, F. L. Quilumba and L. Wei-Jen, "Dispatch Scheduling for a Wind Farm With Hybrid Energy Storage Based on Wind and LMP Forecasting," *IEEE Trans. Ind Appl,* vol. 51, no. 3, pp. 1970-1977, 2015.

[114] A. Khatamianfar, M. Khalid, A. V. Savkin and V. G. Agelidis, "Improving wind farm dispatch in the Australian electricity market with battery energy storage using model predictive control," *IEEE Trans. Sustain. Energy,* vol. 4, no. 3, pp. 745-755, 2013.

[115] E. D. Castronuovo and J. A. Peas Lopes, "On the optimization of the daily operation of a wind-hydro power plant," *IEEE Trans. Power Syst.,* vol. 19, no. 3, pp. 1599-1606, 2004.

[116] J. M. Angarita and J. G. Usaola, "Combining hydro-generation and wind energy: biddings and operation on electricity spot markets," *Electric Power Systems Research,* vol. 77, no. 5, pp. 393-400, 2007.

[117] Y. V. Makarov, P. Du, M. C. W. Kintner-Meyer, C. Jin and H. F. Illian, "Sizing Energy Storage to Accommodate High Penetration of Variable Energy Resources," *IEEE Trans. Sustain. Energy,* vol. 3, no. 1, pp. 34-40, Jan. 2012.

[118] C. Abbey, K. Strunz and G. Joos, "A Knowledge-Based Approach for Control of Two-Level Energy Storage for Wind Energy Systems," *IEEE Trans. Energy Convers.,* vol. 24, no. 2, pp. 539-547, 2009.

[119] S. Carr, G. C. Premier, A. J. Guwy, R. M. Dinsdale and J. Maddy, "Energy storage for active network management on electricity distribution networks with wind power," *Renewable Power Generation, IET,* vol. 8, no. 3, pp. 249-259, 2014.

[120] L. Ha Thu, S. Santoso and N. Thang Quang, "Augmenting Wind Power Penetration and Grid Voltage Stability Limits Using ESS: Application Design, Sizing, and a Case Study," *IEEE Trans. Power Syst.,* vol. 27, no. 1, pp. 161-171, 2012.

[121] P. Wang, Z. Gao and B. Lina, "Operational Adequacy Studies of Power Systems With Wind Farms and Energy Storages," *IEEE Trans. Power Syst.,* vol. 27, no. 4, pp. 2377-2384, 2012.

[122] S. C. Smith, P. K. Sen and B. Kroposki, "Advancement of energy storage devices and applications in electrical power system," presented at the

Power and Energy Society General Meeting - Conversion and Delivery of Electrical Energy in the 21st Century, 2008 IEEE, 2008.

[123] T. Mahlia, T. Saktisahdan, A. Jannifar, M. Hasan and H. Matseelar, "A review of available methods and development on energy storage; technology update," *Renewable and Sustainable Energy Reviews,* vol. 33, pp. 532-545, 2014.

[124] R. B. Schainker, "Executive overview: energy storage options for a sustainable energy future," presented at the Power Engineering Society General Meeting, IEEE, 2004.

[125] N. Koshizuka, F. Ishikawa, H. Nasu, M. Murakami, K. Matsunaga, S. Saito*, et al.*, "Progress of superconducting bearing technologies for flywheel energy storage systems," *Physica C: Superconductivity,* vol. 386, pp. 444-450, 2003.

[126] M. Beaudin, H. Zareipour, A. Schellenberglabe and W. Rosehart, "Energy storage for mitigating the variability of renewable electricity sources: An updated review," *Energy for Sustainable Development,* vol. 14, no. 4, pp. 302-314, 2010.

[127] P. F. Ribeiro, B. K. Johnson, M. L. Crow, A. Arsoy and Y. Liu, "Energy storage systems for advanced power applications," *Proceedings of the IEEE,* vol. 89, no. 12, pp. 1744-1756, 2001.

[128] H. McCrabb, S. Snyder and E. J. Taylor, "An Electrochemical Etching Process for Flow Battery Structures to Improve Performance and Reduce Manufacturing Cost," presented at the Electrochemical Society, 2014.

[129] A. Z. Weber, M. M. Mench, J. P. Meyers, P. N. Ross, J. T. Gostick and Q. Liu, "Redox flow batteries: a review," *Journal of Applied Electrochemistry,* vol. 41, no. 10, pp. 1137-1164, 2011.

[130] C. Schoppe, "Wind and pumped-hydro power storage: Determining optimal commitment policies with knowledge gradient non-parametric estimation," Princeton University, 2010.

[131] R. A. Huggins, *Energy Storage.*: Boston, MA : Springer Science+Business Media, LLC, 2010.

[132] RWE power. ADELE - Adiabatic compressed-air energy storage (CAES) for electricity supply. [Online]. Available: http://www.rwe.com/web/cms/en/365478/rwe/innovation/projects-technologies/energy-storage/project-adele/

[133] LightSail Energy Ltd. We store energy in compressed air. [Online]. Available: http://www.lightsail.com/

[134] R. Madlener and J. Latz, "Economics of centralized and decentralized compressed air energy storage for enhanced grid integration of wind power," *Applied Energy,* vol. 101, pp. 299-309, 2013.

[135] S. Vazquez, S. M. Lukic, E. Galvan, L. G. Franquelo and J. M. Carrasco, "Energy Storage Systems for Transport and Grid Applications," *IEEE Trans. Ind. Electron.,* vol. 57, no. 12, pp. 3881-3895, 2010.

[136] John JS. Texas to host 317MWof compressed air energy storage - After a long wait, a second big CAES project gets underway in the U.S. Published 9th July 2013. [Online]. Available: http://www.greentechmedia.com/articles/read/texas-calls-for-317mw-of-compressed-air-energy-storage2

[137] State Grid of China, Instructions for wind farm to connect to the power grid of the state grid of China [Online]. Available: http://wenku.baidu.com/view/f03739330b4c2e3f57276328.html?re=view

[138] L. Pei, H. Banakar, P.-K. Keung, H. G. Far and O. Boon-Teck, "Macromodel of Spatial Smoothing in Wind Farms," *IEEE Trans. Energy Convers.,* vol. 22, no. 1, pp. 119-128, 2007.

[139] A. Uehara, A. Pratap, T. Goya, T. Senjyu, A. Yona, N. Urasaki*, et al.*, "A Coordinated Control Method to Smooth Wind Power Fluctuations of a PMSG-Based WECS," *IEEE Trans. Energy Convers.,* vol. 26, no. 2, pp. 550-558, 2011.

[140] M. Pedram, N. Chang, Y. Kim and Y. Wang, "Hybrid electrical energy storage systems," in *Low-Power Electronics and Design (ISLPED), 2010 ACM/IEEE International Symposium on*, 2010, pp. 363-368.

[141] Y. Wang, X. Lin, Y. Kim, Q. Xie, M. Pedram and N. Chang, "Single-Source, Single-Destination Charge Migration in Hybrid Electrical Energy Storage Systems," *IEEE Transactions on Very Large Scale Integration (VLSI) Systems,* vol. 22, no. 12, pp. 2752-2765, 2014.

[142] Q. Xie, Y. Wang, Y. Kim, M. Pedram and N. Chang, "Charge Allocation in Hybrid Electrical Energy Storage Systems," *IEEE Transactions on Computer-Aided Design of Integrated Circuits and Systems,* vol. 32, no. 7, pp. 1003-1016, 2013.

[143] H. Jia, Y. Mu and Y. Qi, "A statistical model to determine the capacity of battery–supercapacitor hybrid energy storage system in autonomous microgrid," *International Journal of Electrical Power & Energy Systems,* vol. 54, pp. 516-524, Jan. 2014.

[144] P. Poonpun and W. T. Jewell, "Analysis of the Cost per Kilowatt Hour to Store Electricity," *IEEE Trans. Energy Convers.,* vol. 23, no. 2, pp. 529-534, Jun. 2008.

[145] J. K. Lina and H. M. James, "Digital Filtering," in *Digital Signal Processing Fundamentals*, ed: CRC Press, 1998, pp. 11-1 to 11-86.

[146] E. Ela, M. Milligan and B. Kirby, "Operating Reserves and Variable Generation," *NREL/TP-5500-51928,* August 2011.

[147] G. N. Bathurst, J. Weatherill and G. Strbac, "Trading wind generation in short term energy markets," *IEEE Trans. Power Syst.,* vol. 17, no. 3, pp. 782-789, 2002.

[148] L. Landberg, G. Giebel, H. A. Nielsen, T. Nielsen and H. Madsen, "Short ‐ term Prediction—An Overview," *Wind Energy,* vol. 6, no. 3, pp. 273-280, 2003.

[149] J. Apt and P. Jaramillo, *Variable renewable energy and the electricity grid*: Hilton Park, Abingon, Oxon ; New York : RFF Press, 2014.

[150] M. Lei, L. Shiyan, J. Chuanwen, L. Hongling and Z. Yan, "A review on the forecasting of wind speed and generated power," *Renewable and Sustainable Energy Reviews,* vol. 13, no. 4, pp. 915-920, 2009.

[151] K. Dragoon, *Valuing wind generation on integrated power systems*: Amsterdam ; New York : William Andrew/Elsevier, 2010.

[152] A. M. Foley, P. G. Leahy, A. Marvuglia and E. J. McKeogh, "Current methods and advances in forecasting of wind power generation," *Renewable Energy,* vol. 37, no. 1, pp. 1-8, 2012.

[153] J. L. Torres, A. Garcia, M. De Blas and A. De Francisco, "Forecast of hourly average wind speed with ARMA models in Navarre (Spain)," *Solar Energy,* vol. 79, no. 1, pp. 65-77, 2005.

[154] T. G. Barbounis, J. B. Theocharis, M. C. Alexiadis and P. S. Dokopoulos, "Long-term wind speed and power forecasting using local recurrent neural

network models," *IEEE Trans. Energy Convers.,* vol. 21, no. 1, pp. 273-284, 2006.

[155] G. N. Kariniotakis, G. S. Stavrakakis and E. F. Nogaret, "Wind power forecasting using advanced neural networks models," *IEEE Trans. Energy Convers.,* vol. 11, no. 4, pp. 762-767, 1996.

[156] K. Methaprayoon, C. Yingvivatanapong, L. W. Jen and R. Liao, "An Integration of ANN Wind Power Estimation Into Unit Commitment Considering the Forecasting Uncertainty," *IEEE Trans. Ind Appl,* vol. 43, no. 6, pp. 1441-1448, 2007.

[157] H. B. Azad, S. Mekhilef and V. G. Ganapathy, "Long-Term Wind Speed Forecasting and General Pattern Recognition Using Neural Networks," *IEEE Trans. Sustain. Energy,* vol. 5, no. 2, pp. 546-553, 2014.

[158] K. Bhaskar and S. N. Singh, "AWNN-Assisted Wind Power Forecasting Using Feed-Forward Neural Network," *IEEE Trans. Sustain. Energy,* vol. 3, no. 2, pp. 306-315, 2012.

[159] Q. Hao, D. Srinivasan and A. Khosravi, "Short-Term Load and Wind Power Forecasting Using Neural Network-Based Prediction Intervals," *IEEE Trans. Neural Netw. Learn. Syst.,* vol. 25, no. 2, pp. 303-315, 2014.

[160] I. G. Damousis and P. Dokopoulos, "A fuzzy expert system for the forecasting of wind speed and power generation in wind farms," presented at the Power Industry Computer Applications (PICA), 2001. Innovative Computing for Power - Electric Energy Meets the Market. 22nd IEEE Power Engineering Society International Conference on, 2001.

[161] I. G. Damousis, M. C. Alexiadis, J. B. Theocharis and P. S. Dokopoulos, "A fuzzy model for wind speed prediction and power generation in wind

parks using spatial correlation," *IEEE Trans. Energy Convers.,* vol. 19, no. 2, pp. 352-361, 2004.

[162] M. Mohandes, T. Halawani, S. Rehman and A. A. Hussain, "Support vector machines for wind speed prediction," *Renewable Energy,* vol. 29, no. 6, pp. 939-947, 2004.

[163] T. H. M. El-Fouly, E. F. El-Saadany and M. M. A. Salama, "Grey predictor for wind energy conversion systems output power prediction," *IEEE Trans. Power Syst.,* vol. 21, no. 3, pp. 1450-1452, 2006.

[164] M. Negnevitsky, P. Johnson and S. Santoso, "Short term wind power forecasting using hybrid intelligent systems," presented at the IEEE Power Engineering Society General Meeting, 2007.

[165] P. Pinson and G. N. Kariniotakis, "Wind power forecasting using fuzzy neural networks enhanced with on-line prediction risk assessment," presented at the Power Tech Conference Proceedings, 2003 IEEE Bologna, 2003.

[166] M. Khalid and A. V. Savkin, "A Method for Short-Term Wind Power Prediction With Multiple Observation Points," *IEEE Trans. Power Syst.,* vol. 27, no. 2, pp. 579-586, 2012.

[167] G. Boyle, *Renewable electricity and the grid: the challenge of variability*: Earthscan, 2012.

[168] M. Gupta, Jin, L., Homma, N., "Multilayered Feedforward Neural Networks (MFNNs) and Backpropagation Learning Algorithms " in *Static and Dynamic Neural Networks:From Fundamentals to Advanced Theory* 1ed: Wiley-IEEE Press, 2003, pp. 103-170.

[169] A. Sfetsos, "A comparison of various forecasting techniques applied to mean hourly wind speed time series," *Renewable energy,* vol. 21, no. 1, pp. 23-35, 2000.

[170] S. Han, Y. Liu and Y. Yang, "Taboo search algorithm based ANN model for wind speed prediction," presented at the 2nd IEEE Conference on Industrial Electronics and Applications (ICIEA), 2007.